Mechanics and Physics of Contact Interfaces

V A Yastrebov

Habilitation à Diriger des Recherches

Mechanics and Physics of Contact Interfaces

Vladislav A. Yastrebov

MINES Paris, PSL University
Centre des matériaux, CNRS UMR 7633
Evry, France

Sorbonne University
November 12, 2021

Habilitation à Diriger des Recherches

Mechanics and Physics of Contact Interfaces

Dr. Vladislav A. Yastrebov

MINES ParisTech, PSL University
CNRS UMR 7633, Centre des matériaux
Evry / Paris, France

July 2, 2021

Defended publicly on November 12, 2021 at MINES ParisTech, Paris, France.

Defense committee

Res. Dir. Marie-Christine Baietto	president
Prof. Basile Audoly	reviewer
Prof. Valentin Popov	reviewer
Prof. Stanislaw Stupkiewicz	reviewer
Res. Dir. Samuel Forest	examinator
Prof. Djimédo Kondo	examinator
Res. Dir. Benoît Roman	examinator

full online version

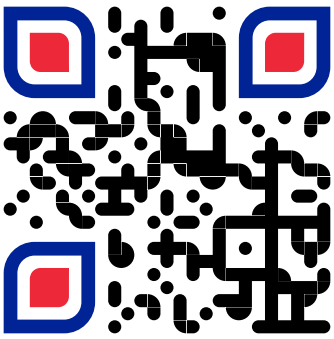

HDR.yastrebov.FR

Foreword

This "document" (or rather an interactive online source) gathers together my major and minor scientific results as well as ideas and preliminary results for the future research. The document spans a period of approximately 10 years starting on March 25, 2011, when I defended my PhD thesis entitled "Computational Contact Mechanics: geometry, detection and resolution techniques" and ending on July 2, 2021. All the descriptions I provide here are supposed to be as concise as possible and most of them are focused on novel and interesting results only, the mentioned papers do not reduce only to the reported results. At the same time, the "document" is crafted to be simple to navigate through, therefore the reader is invited to go through it online rather than in a rigid [pdf]. The flexible online source of the document allows to easily navigate through different parts, provides a fast access to cited references and also to animated figures and videos.

The central topic of my research is the *mechanical contact of solids*. However, the derivatives of my research might seem to expand way beyond this research domain; the study of annihilation of elastic waves in asymmetric materials (Sec. 1.5.1), construction of microstructure of cemented carbides (Sec. 1.3.5) or the study on the origins of glacial earthquakes ((Sec. 1.6) might seem to be irrelevant to mechanical contact at the first glance, but even in these projects the root or the origin lies within the scope of the contact mechanics. However, the main contributions of my research cluster within a small sub-domain of mechanical contact, namely in the contact of solids possessing rough surfaces.

The "document" is split into four parts.

1. **Research results**
   a short note and an illustration is provided for every scientific result, relevant references to our papers and/or presentations are also given.

2. **Ideas**
   a very brief description is provided for some preliminary results and ideas, which I consider interesting but which were not yet fully (or not at all) explored because either the lack of time or resources.

3. **Future research**
   research directions and concrete questions I plan to explore in the future are listed here.

4. **Miscellaneous**
   this part contains some CV-type information about teaching, supervision activities, and some community targeted activities I have been carrying out.

Even though an HDR manuscript is a person-oriented document, I can write it only because there was a join effort of many people behind all the research results reported here. More importantly, I would not be able to reach this stage in my academic career without a strong and kind support of Georges Cailletaud and Boris Evgenievich Melnikov without whom this story would not happen. Thank you very much! All other people interaction with whom was and remains important to me are also acknowledged in the end of the document (Sec. 4.5.4).

Whenever available, a French version is provided. Nevertheless, in all cases the English version is either equivalent or more elaborated than the French one. The style of the whole document is slightly heterogeneous and varies in correlation with the importance of the contribution reported in the section, therefore sometimes the style is a little bit informal.

Vladislav A. Yastrebov
Evry / Paris, France

Contents

Chapter 1

Research results

1.1 Motivation and Scope

My theoretical research is focused on phenomena related to mechanical contact between solids. My research is on the intersection between contact mechanics, tribology and numerical methods. Therefore, I work on computational algorithms related to contact mechanics, mainly using the finite element method. The computational frameworks that we construct with colleagues and students, we employ to understand better the interfacial physics of contact and friction. My first original results in the domain of **computational mechanics** were obtained during my PhD thesis and were related to optimization of detection and geometrical projection techniques, enhancement of interface geometries, and constructing a so-called partial Dirichlet-Neumann approach to handle contact problems. Further in this domain of computational mechanics, we developed a novel framework combining the extended finite element method (X-FEM) with mortar technique which enables us to handle tying, frictional contact and wear over overlapping domains and between boundary-fitted and embedded surfaces. This method is referred as MorteX and benefits from a novel stabilization technique for mixed problems that we developed. Further, we constructed an original monolithic finite element framework to solve problems of interfacial thin fluid flow in contact interface which takes into consideration the possibility of entrapment of fluid/liquid in the pockets surrounded by contact zones.

In **modelling and simulations** that we carry out, the target is set on the improvement of our understanding of micromechanical processes happening in contact interfaces. A part of these studies was carried out using an in-house boundary element method, for which we developed a novel technique for correction of discretization errors. This correction as well as a careful handling of surface representativity permitted us to establish a link between roughness parameters and the growth of the true contact area under the increasing normal load. Notably, we demonstrated the importance of higher-order spectral moments of the roughness for this area growth which were ignored in the most of recent studies. Using additional data and self-consistent homogenized model for transmissivity, a novel empirical law was obtained to link the permeability, pressure and roughness parameters. Using the coupled hydro-mechanical finite element framework that we constructed, we studied the effect of trapped liquids on the transmissivity properties of contact interfaces and obtained several original results including a non-local empirical permeability model and possible escape of the fluid from the trap under the increasing load. Few other contributions related to thermal/electric contact, roughness morphology, elasto-plastic contact were also made.

In other domains of solid mechanics and physics we made some contributions in the following topics: (1) the statics and dynamics of asymmetric materials, (2) dynamics of capsizing icebergs and their interaction with marine ice-sheets, (3) slip stability, slip triggering and arrest in frictional bi-material interfaces, (4) multiscale modelling of hardmetals in drilling applications, (5) material-arc interaction in electric contactors, (6) scale effects in indentation, and a few others.

A summary of other relevant activities is provided below. **Supervion:** I co-supervised (1) 8 PhD candidates, 6 more PhD candidates I supervised at occasional basis, 4 postdocs, and several master students; one of my PhD students received the CSMA PhD award 2020 and the Hirn award 2020 for the

best PhD thesis in tribology. **Teaching:** I created an original 30h master/doctoral level course "Contact Mechanics and Elements of Tribology" and I also teach Continuum Mechanics, Molecular Dynamics and Dynamics of Dislocations. **Institutional and other responsibilities:** I am a member of the CSMA Juniors committee since 2017 and a co-founder and a member of the Board of the new overlay journal JTCAM, which we created in 2017-2020 and launched in the summer 2020. **Scientific production:** 26 peer-reviewed articles, 1 monograph.

1.2 Contact and multi-physics

Involved people:

- Andrei Shvarts (PhD, MINES 2016-2019, now at University of Glasgow),
- Guillaume Anciaux (EPFL),
- Georges Cailletaud (MINES ParisTech),
- Jean-François Molinari (EPFL),
- Andreas Almqvist (Luleå University of Technology),
- Francesc Pérez-Ràfols (PhD, Luleå University of Technology),
- Paul Beguin (PhD student, MINES 2020-now),
- Samuel Forest (MINES ParisTech),
- Vikram Phalke (PhD student, ITN),
- Aurélien Fouque (PhD, MINES/CentraleSupélec 2016-2020, now at Siemens),
- Frederick Sorel Mballa Mballa (postdoc, MINES/CentraleSupélec, 2013-2015, now at Vitrociset),
- Julian Durand (PhD, MINES 2009-2012, now at Areva)

Contact mechanics at the roughness scale represents a holy grail of tribology providing a better understanding of contact, friction, wear, lubrication, sealing, as well as electrical and thermal conductivity at the system scale [1]. We have been working on this subject since the period of my PhD project, when in parallel with my own thesis, I participated in another doctoral study on the rough contact [2], which was as mine, supervised by Georges Cailletaud. My contributions in this field focus on understanding the role of surface roughness in the process of deformation of elastic, elasto-plastic and viscoelastic bodies, as well as on the study of energy and mass transfers through and along contact interfaces. Emphasis is put on elastic contact for which analytical theories exist and which poses many important questions about the limits of surface fractality, the limits of continuous description and the relevance of various topographic parameters. This work requires efficient and precise numerical tools, a thorough statistical analysis, rather large parametric spaces and of course a sharp interpretation. All these elements have been implemented in our studies to draw relevant conclusions.

🇫🇷 **Version française**: La mécanique du contact à l'échelle de la rugosité représente un Graal dans la compréhension du contact, du frottement, de l'usure, de la lubrification, de l'étanchéité, ainsi que de la conductivité électrique et thermique [1]. Je travaille sur ce sujet depuis la période de mon doctorat. C'est en effet dès cette époque que j'ai participé en parallèle de ma propre étude de thèse à une autre étude doctorale sur le sujet [2] , qui était comme la mienne encadrée par mon directeur de thèse Georges Cailletaud. Mes contributions dans ce domaine se focalisent sur la compréhension du rôle de la rugosité dans le processus de déformation des corps élastiques, élasto-plastiques et viscoélastiques, ainsi que sur l'étude des transferts d'énergie et de masse à travers et le long des interfaces de contact. L'accent est mis sur le contact élastique pour lequel des théories analytiques existent et qui pose beaucoup de questions de fond sur les limites de la fractalité des surfaces, sur les limitations de la description continue et sur la pertinence de divers paramètres topographiques. Ce travail nécessite des outils numériques efficaces et précis, une analyse statistique poussée, des espaces paramétriques assez larges et bien entendu une interprétation pointue. Tous ces éléments ont été mis en œuvre dans nos études pour en tirer des conclusions pertinentes.

1.2.1 Wavy surface in contact

We revisited the classic problem of an elastic solid with a two-dimensional wavy surface squeezed against an elastic flat half-space from infinitesimal to full contact [3]. Through extensive numerical calculations using the boundary and the finite element methods as well as using analytic derivations, we discover previously overlooked by Johnson, Greenwood and Higginson [3] transition regimes [4]. These transition (see Fig. 1.1) are seen in the evolution with applied load of the contact area and perimeter, in the mean pressure and in the probability density of contact pressure. They occur close to the percolation of initially separate contact-area spots. In addition, while studying this problem, I was interested by the geometrical characteristics of contact clusters, notably the so-called compactness which can be defined as the ratio of the square root of the area A to the perimeter P:

$$c = \frac{\sqrt{A}}{P},$$

which is maximal for a circle and tends to zero for fractal forms for which the perimeter tends to ∞ for constant area. Finally, using famous differentiation under the integral sign (see Richard Feynman "Surely You're Joking, Mr. Feynman!" Part 2. A different box of tools.), I could found an analytical expression for the probability density of heights of a regular wavy surface $z = 1 + \cos(2\pi x)\cos(2\pi y)$, which turns to be

$$P'(z) = \frac{4}{\pi^2}\frac{\mathrm{F}\left[\arccos(z-1), 1/\sqrt{2z-z^2}\right]}{\sqrt{2z-z^2}}, \text{ for } z \in [0,2]$$

where

$$\mathrm{F}(l,k) = \int_0^l \frac{1}{\sqrt{1-k^2\sin(\phi)}} d\phi$$

is the incomplete elliptic integral of the first kind. The singularity at $z = 1$ is justified by appearance of a saddle point.

Version française Nous avons révisé le problème classique du contact normal entre une surface bi-sinusoïdale et un plan rigide. Numériquement nous avons pu démontrer [4] que la courbe maîtresse proposée par Johnson et al [3] n'est pas tout à fait correcte et qu'elle doit comporter un changement de signe de courbure près du point de percolation des zones de contact associées avec des crêtes différentes. Ce changement rapide provoque une décroissance de pression moyenne de contact même si l'aire de contact ainsi que la force continuent à augmenter (cf. Fig. 1.1).

References

- [4] V.A. Yastrebov, G. Anciaux, J.F. Molinari. "The contact of elastic regular wavy surfaces revisited". Tribology Letters, 56:171-183 (2014). [doi] [arXiv] [pdf]
- Few slides from a presentation I gave at LSMS, EPFL in 2013.
- Presentation of G. Anciaux and myself given by Guillaume at EuroMech "Contact Mechanics and Coupled Problems in Surface Phenomena" conference hold in Lucca, Italy, 30 March - 2 April (2015).

1.2.2 Roughness and its representativity

In [6] we have introduced a Representative Surface Element (RSE) as a part of the reference surface whose height distribution has properties equivalent to those of the reference surface. Of course this definition is only valid in the case of stationary roughness and does not apply in the case of really fractal surfaces [7], for which the rms changes with the change of the scale. Later, in [8, 9] we demonstrated that to represent a periodic rough surface (here, periodicity implies that the spectrum of surfaces is discrete) with Gaussian distribution, the spectrum of the surface must be deprived of largest wavelengths $\lambda_l > L/k_l$, $k_l > 4 \ldots 16$ where L being the period of the surface Fig. 1.2. We have therefore highlighted the importance of the lower cut-off frequencies which have been used in numerical simulations made in the

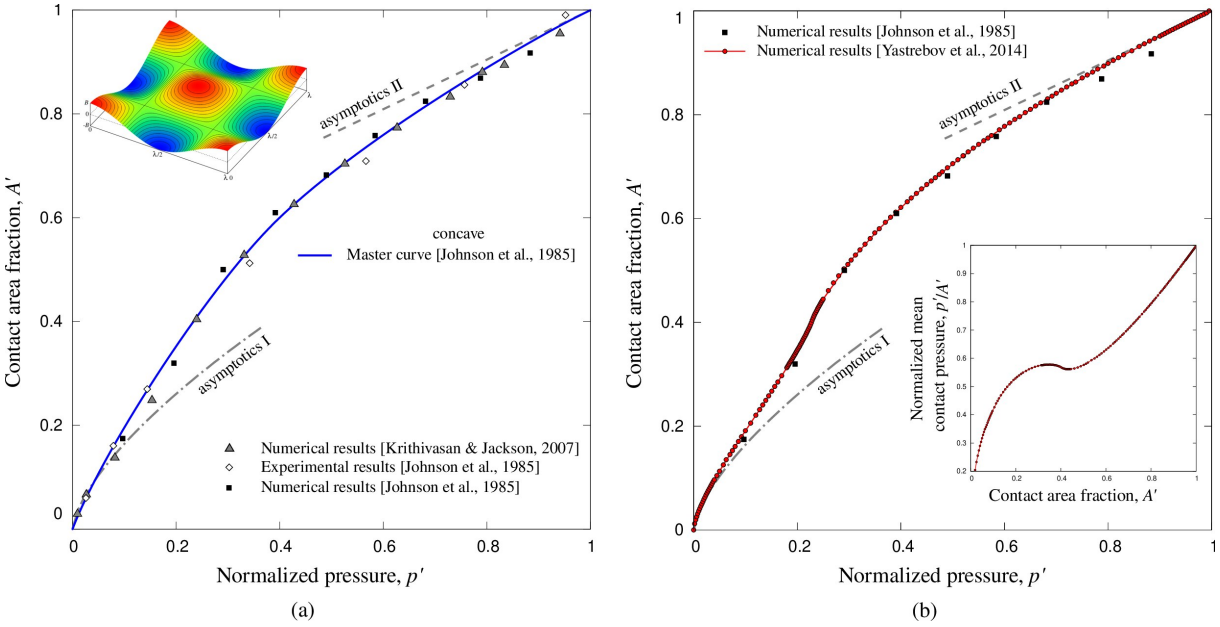

Figure 1.1: Evolution of the contact area A' with the normalized pressure p' for a bi-sinusoidal surface brought in normal contact: (a) results from the literature where the transition was missed by the construction of a master curve [5, 3], (b) results of our simulations capturing the transition near percolation point, in the inset we show that the mean pressure p'/A' can decrease even when the external pressure increases.

Version française: Évolution de l'aire de contact A' avec la pression normalisée p' d'une surface bi-sinusoïdale : (a) résultats de la littérature où une transition intéressante a été manqué par la construction d'une courbe maîtresse [5, 3], (b) notre solution numérique capturant le régime transitoire près de la percolation, dans l'inset on montre que la pression moyenne p'/A' peut diminuer même la pression externe augmente.

community working on theoretical problems of contact between rough surfaces. Considering surfaces without highest wavelengths (or smallest wavenumbers) facilitates reaching convergence in the average response of the rough surface and makes possible the comparison with analytical theories for surfaces with normal height distribution. I believe that this work added more rigor in the digital treatment of the problems of contact between rough surfaces.

Version française: Dans [6] nous avons introduit une Surface Élémentaire Représentative (SER) comme une partie de la surface de référence dont la distribution de hauteurs a des propriétés équivalentes à celles de la surface de référence. Bien entendu cette définition n'est valide que dans le cas de la rugosité stationnaire et ne s'applique pas dans le cas des surfaces réellement fractales [7]. Plus tard, dans [8, 9] nous avons démontré que pour représenter une surface rugueuse périodique (la périodicité implique que le spectre des surfaces est discret) à distribution gaussienne, le spectre de la surface doit être privé des longueurs d'ondes les plus grandes $\lambda_l > L/k_l$, $k_l > 4 \ldots 16$ où L étant la période de la surface Fig. 1.2. Nous avons donc souligné l'importance de la coupure aux basses fréquences qui a été plutôt ignorée dans la communauté travaillant sur des problèmes théoriques du contact entre des surfaces rugueuses. Ce concept influence les résultats mécaniques et facilite la comparaison avec des théories valides pour des surfaces à distribution normale des hauteurs. Je crois que ces travaux ont rajouté plus de rigueur dans le traitement numérique des problèmes de contact entre surfaces rugueuses.

References

- [6] V.A. Yastrebov, J. Durand, H. Proudhon, G. Cailletaud. "Rough surface contact analysis by means of the Finite Element Method and of a new reduced model". Comptes Rendus Mecanique,

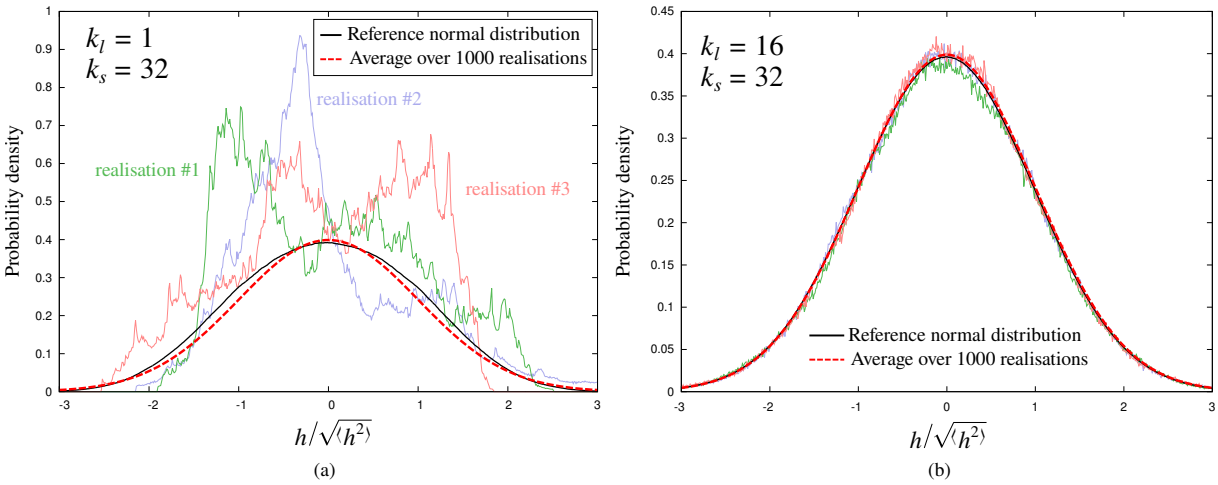

Figure 1.2: Height distribution for the different frequency cutoffs: high frequency cutoff is $L/\lambda_s = 32$ and low frequency cutoffs (a)$L/\lambda_l = 1$, (b) $L/\lambda_l = 16$. Distribution of heights of three random samples and the average calculated over 1000 realizations (dashed line) and a reference normal distribution are shown.

Version française: Distribution de hauteurs pour la coupure haute fréquence $\lambda_s = L/32$ et coupure basse fréquence (a) $\lambda_l = L$, (b) $\lambda_l = L/16$. Distribution de hauteurs des trois échantillons aléatoires et la moyenne calculée sur 1000 réalisations (ligne pointillée) et une distribution normale de référence.

339:473-490 (2011) [doi] [pdf]

- [8] V.A. Yastrebov, G. Anciaux, J.F. Molinari. "Contact between representative rough surfaces". Physical Review E, 86(3):035601 (2012) [doi] [arXiv] [pdf]
- [9] V.A. Yastrebov, G. Anciaux, J.F. Molinari. "From infinitesimal to full contact between rough surfaces : evolution of the contact area". International Journal of Solids and Structures, 52:83-102 (2015) [doi] [arXiv] [pdf]

1.2.3 Contact area evolution and the role of roughness parameters

Despite all the efforts undertaken, we were initially unable to draw strong conclusions from our early numerical studies [8, 9] on how the contact area evolves under increasing pressure $A(p_0)$ for different roughness parameters and such as the Hurst exponent H, the richness of the spectrum $\zeta = \lambda_l/\lambda_s$ (the ratio between the cutoffs, i.e. the longest and the shortest wavelengths) and the standard deviation of the roughness $\sigma = \sqrt{\langle (z-\bar{z})^2 \rangle}$, because the discretization error βPh depends in a non-trivial way on the cutoff parameters λ_l and λ_s. Multi-asperity models suggested that the evolution of the contact area should depend on the Nayak parameter $\alpha = m_0 m_4/m_2^2$, where m_i is the i-th spectral moment of the random isotropic surface [10, 11]. Persson's model [12, 13], which is widely used today, suggested that this evolution should only depend on the second spectral moment m_2 which is nothing more than a half-variance of the gradient of the surface. At the same time, numerical calculations focused on finding the dependence of the contact area on the Hurst exponent H or on a certain fractal dimension of the surface [14, 15, 16, 17] (the term "fractal" is used here even if all the studied surfaces are not really fractals, since they all have cutoffs in their spectra).

Regardless all the technical difficulties, in our recent study [18] which used discretization error compensation Eq. (1.11), we succeeded to go beyond the accuracy of all numerical calculations existing at that time while preserving statistical representativity and relatively large parametric range. We have shown numerically that (1) the dependence of the Hurst exponent H is only an "illusion": in reality within a large studied interval, the contact area does not depend on it, but it does depend on the Nayak parameter. The proof is quite straightforward: consider a function $F(x, y)$ where x and y are not necessarily *independent* parameters; to determine true dependencies, it would be enough to study how F varies with x at fixed y and vice versa within a certain interval $\{x, y\} \in \{\mathcal{X}, \mathcal{Y}\}$, see Fig. 1.3. Moreover, we

succeeded to characterize this dependence analytically and explained all numerical results published by other groups; (2) the revealed dependence on the Nayak's parameter suggests that Persson's approach lacks rigor and should be improved, see also [19, 1].

This result was difficult to reach because the dependence on the Nayak parameter is very weak and can only be observed (using a reasonable number of calculations) with very finely discretized representative surfaces. This discovery would not have been possible without the error compensation technique we have introduced.

Version française: Malgré tous les efforts entrepris, nous n'avons pas pu dans un premier temps tirer de nos études numériques [8, 9] des conclusions définitives sur la façon dont évolue l'aire de contact avec la pression $A(p_0)$ en fonction des paramètres de la rugosité tels que l'exposant de Hurst H, la richesse du spectre $\zeta = \lambda_l/\lambda_s$ (rapport entre la plus grande et la plus petite longueur d'onde) et l'écart type de la rugosité $\sigma = \sqrt{\langle(z-\bar{z})^2\rangle}$, car l'erreur de discrétisation βPh dépend d'une manière non triviale des paramètres de coupure λ_l et λ_s. Des modèles multi-aspérités suggéraient que l'évolution de l'aire de contact devrait dépendre du paramètre de Nayak $\alpha = m_0 m_4/m_2^2$, où m_i est le i-ième moment spectral de la surface aléatoire isotrope [10, 11]. Le modèle de Persson [12, 13], qui est bien répandu aujourd'hui, suggérait que cette évolution ne devrait dépendre que du deuxième moment spectral m_2 qui n'est rien d'autre qu'une demi-variance du gradient de la surface. En même temps, des calculs numériques se focalisaient sur la recherche de la dépendance de l'aire de contact à l'exposant de Hurst H ou à une certaine dimension fractale (ce terme est utilisé même si toutes les surfaces étudiées ne sont pas vraiment fractales, puisqu'elles possèdent toutes des coupures de basse et haute fréquences). de la surface [14, 15, 16, 17].

Dans notre étude récente [18] qui utilisait la compensation de l'erreur de discrétisation Eq. (1.11), nous avons cependant pu aller au-delà de tous les calculs numériques existants en termes de précision, de représentativité statistique et de plage paramétrique considérée. Nous avons démontré numériquement que (1) la dépendance de l'exposant de Hurst H n'est qu'une illusion : en réalité dans un large intervalle étudié, l'aire de contact n'en dépend pas, mais elle dépend du paramètre de Nayak (la preuve est simple : pour une fonction $F(x, y)$ où x et y ne sont pas forcément des paramètres indépendants, pour déterminer de vraies dépendances, il suffit d'étudier comment varie F pour x qui change à y fixé et vice versa dans une plage $\{x, y\} \in \{\mathcal{X}, \mathcal{Y}\}$) (cf. Fig. 1.3). De plus, on a pu caractériser cette dépendance analytiquement pour expliquer tous les résultats numériques précédemment trouvés ; (2) la dépendance du paramètre de Nayak suggère que l'approche de Persson manque de la rigueur et devrait être améliorée [19, 1].

Ce résultat a été difficile à obtenir car la dépendance au paramètre de Nayak est très faible et ne peut être proprement observée (avec un nombre raisonnable de calculs) qu'avec des surfaces représentatives très finement discrétisées. Cette découverte n'aurait été pas possible sans la technique de compensation d'erreur que nous avons introduite.

References

- [18] V.A. Yastrebov, G. Anciaux, J.F. Molinari. "The role of the roughness spectral breadth in elastic contact of rough surfaces". Journal of the Mechanics and Physics of Solids, 107:469-493 (2017) [doi] [arXiv] [pdf]

1.2.4 Scale separation in rough contact

One of important questions of contact mechanics which still remains relevant today is "to what extent can we neglect the effect of roughness in contact on the structural scale"? It is true that often in the study of the contact between rough surfaces, one is satisfied with a very simplified representation of the two infinite surfaces by considering them nominally flat. But what if, instead of this purely theoretical problem, we consider contacting bodies having a shape and a roughness on the top of it? The first thing that comes to mind is that if the effective radius of curvature of the macroscopic shape greatly exceeds the size of the characteristic wavelengths of the roughness $R \gg \lambda_l$ then the so-called *scale separation* presents a valid approximation and the roughness can be considered separately from the shape. Then it would be enough to make macroscopic calculations and to use on a small scale the pressure obtained at each point to find the real contact area or many other characteristics relevant to this small scale. However,

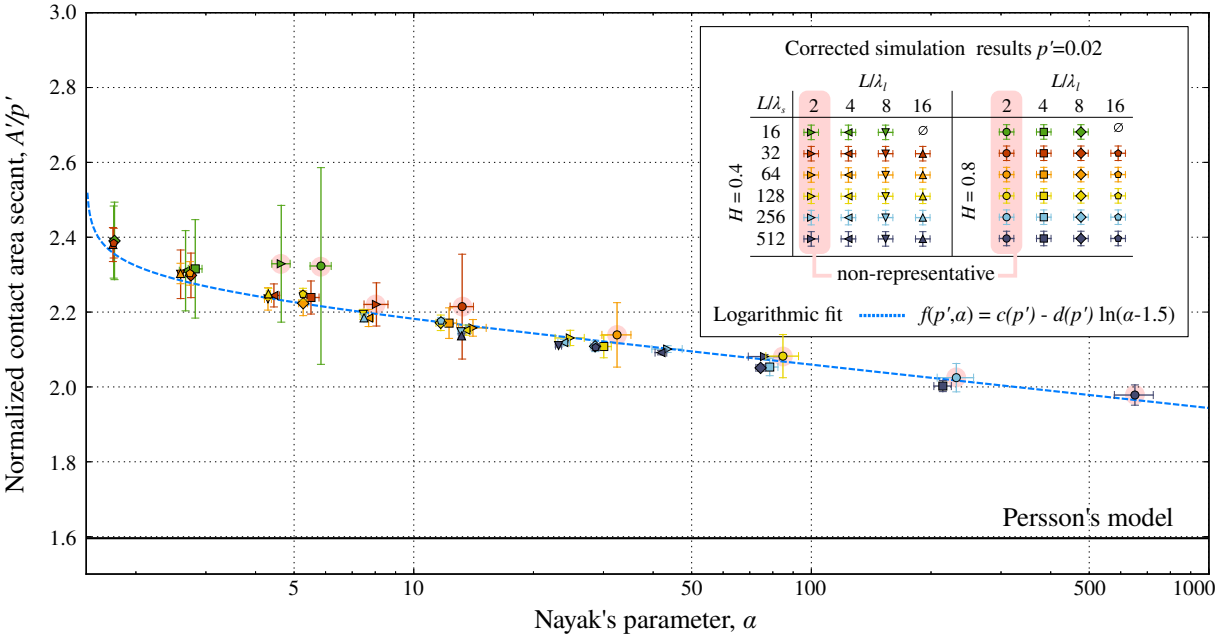

Figure 1.3: The secant of the contact-area–pressure curve A'/p' (or simply, inverse mean pressure) plotted at fixed pressure as a function of Nayak's parameter α and showing a weak logarithmic decrease independent of the Hurst exponents H.

Version française: Le sécant de la courbe aire-de-contact – pression A'/p' tracé en fonction du paramètre de Nayak démontrant une faible dépendance logarithmique.

a slightly more advanced reflection on this *scale separation* adds another characteristic length, it is the radius of the macroscopic contact zone a which can be found in the absence of any roughness. It is then the comparison of the four characteristic lengths $R, a, \lambda_l, \lambda_s$ which determine the separability of the scales in the contact problem. We know from [20] that the effect of roughness is controlled by a dimensionless parameter $\gamma = \sqrt{m_0}R/a^2$: the smaller this parameter, the closer we get to the solution obtained with a smooth contact hypothesis. But what can we say about contact with a significant value of γ?

First, from the pioneer study by Greenwood & Tripp [21] we know that the apparent area of contact between rough bodies can extend much further than the radius predicted by the Hertz theory (see Figs. 1.4,1.5). On the other hand, the Greenwood & Tripp theory is a mean-field theory and does not allow to make a link with fine characteristics of roughness. Among other things, it cannot predict the transition between the contact regime made by the first two asperities which touch each other (deterministic regime) and another regime starting when multiples asperities which touch each other (statistical regime). The most recent attempt to find this missing link was made in [22], but it was unsuccessful due to the fact that the nominal mean pressure $p_0 = N/(\pi a^2)$ used by the cited authors does not make sense for a small contact areas.

We have revised this problem using a deterministic multi-asperity model with elastic interaction between the asperities [23]. As a result, we were able to establish this transition single asperity – multiple asperities. The transition force between the two regimes is given by:

$$N^* = \frac{9}{16c^2} \cdot \frac{\pi^3 (2m_2)^{3/2} E^*}{d^3 \kappa^3 m_4},$$

where $c = \int_0^\infty \int_0^\infty \sqrt{xy} P(x,y)\, dxdy$ has been evaluated numerically for the kernel [24]

$$P(x,y) = \frac{27}{16\sqrt{\pi}} xy|xy| \exp\left[-\frac{3}{16}\left(3x^2 + 3y^2 - 2xy\right)\right],$$

where $d \approx 0.2$ is a constant determined by numerous simulations of random realizations of rough

surfaces. This critical force defines a fairly sharp border between the contact determined by one and more asperities, which is very important for microscopic studies (indentation, nano-tribology, etc.). This study add a small chunk to our knowledge on the separability of scales in microscopic contact established among others by seminal works of Greenwood & Johnson [21, 20] and also by Pastewka & Robbins [22].

Version française: Une des questions importantes de la mécanique du contact qui reste très pertinente aujourd'hui c'est "à quel point peut-on négliger l'effet de la rugosité dans le contact à l'échelle structurelle". Il est vrai que souvent dans l'étude du contact entre des surfaces rugueuses, on se contente d'une représentation très simplifiée des deux surfaces infinies en les considérant nominalement plates. Mais si au lieu de ce problème purement théorique on considère des corps en contact ayant une forme macroscopique et une rugosité en complément ? La première chose qui vient à l'esprit est que si le rayon de courbure effective de la forme macroscopique dépasse largement la taille des longueurs d'onde caractéristiques de la rugosité $R \gg \lambda_l$, les échelles de la forme et de la rugosité peuvent être séparées. Il suffit alors de faire des calculs macroscopiques et d'utiliser à petite échelle la pression obtenue à chaque point pour trouver l'aire de contact réelle ou bien d'autres caractéristiques pertinentes à cette petite échelle. Cependant, une réflexion légèrement plus poussée nous rajoute une autre longueur caractéristique c'est le rayon de la zone de contact macroscopique a qu'on peut trouver en absence de toute rugosité. C'est alors la comparaison des quatre longueurs caractéristiques $R, a, \lambda_l, \lambda_s$ qui détermine la séparabilité des échelles dans le problème de contact. On sait de [20] que l'effet de la rugosité est contrôlé par un paramètre adimensionnel $\gamma = \sqrt{m_0}R/a^2$: plus ce paramètre est petit, plus on s'approche de la solution obtenue avec une hypothèse de contact lisse. Mais que peut-on dire du contact avec une valeur de γ non négligeable ? Premièrement, depuis une étude fort intéressante de Greenwood & Tripp [21], on sait que l'aire apparente du contact entre des corps rugueux peut s'étendre bien plus loin que le rayon prévu par la théorie de Hertz Fig. 1.5. Par contre, cette théorie est de type champs moyens et ne permet pas de faire le lien avec des caractéristiques fines de la rugosité. Entre autres, elle ne peut pas prévoir la transition entre le régime du contact entre les deux premières aspérités qui se touchent (régime déterministe) et l'ensemble des aspérités qui se touchent (régime statistique). Une récente tentative [22] de trouver ce lien manquant n'a pas abouti en raison du fait que la pression moyenne nominale $p_0 = N/(\pi a^2)$ utilisée par les auteurs cités n'a pas de sens pour une faible aire de contact.

Nous avons révisé ce problème en utilisant un modèle multi-aspérités déterministe avec interaction élastique entre les aspérités. Comme résultat, nous avons pu établir le passage entre le régime déterministe du contact entre des premières aspérités et le régime statistique (où l'ensemble des aspérités entrent en contact d'une manière collective). La force de transition entre les deux régimes est donnée par :

$$N^* = \frac{9}{16c^2} \cdot \frac{\pi^3 (2m_2)^{3/2} E^*}{d^3 \kappa^3 m_4},$$

où $c = \int_0^\infty \int_0^\infty \sqrt{xy} P(x,y)\, dxdy$ a été évalué numériquement pour le noyau [24]

$$P(x,y) = \frac{27}{16\sqrt{\pi}} xy|xy| \exp\left[-\frac{3}{16}\left(3x^2 + 3y^2 - 2xy\right)\right],$$

où $d \approx 0.2$ est une constante déterminée par de nombreux calculs sur des réalisations aléatoires des surfaces rugueuses. Cette force critique définit une frontière assez raide entre le contact déterminé par une et plusieurs aspérités, qui est très importante pour les études microscopiques (indentation, nano-tribologie, etc). Cette valeur se rajoute à nos connaissances sur la séparabilité des échelles en contact microscopique établies entre autres dans les travaux de Greenwood & Johnson [21, 20] et Pastewka & Robbins [22] et complète bien le panorama.

References

- [23] V.A. Yastrebov. "The Elastic Contact of Rough Spheres Investigated Using a Deterministic Multi-Asperity Model". Journal of Multiscale Modelling (2019), 10(1):1841002. [doi] [arXiv] [pdf]

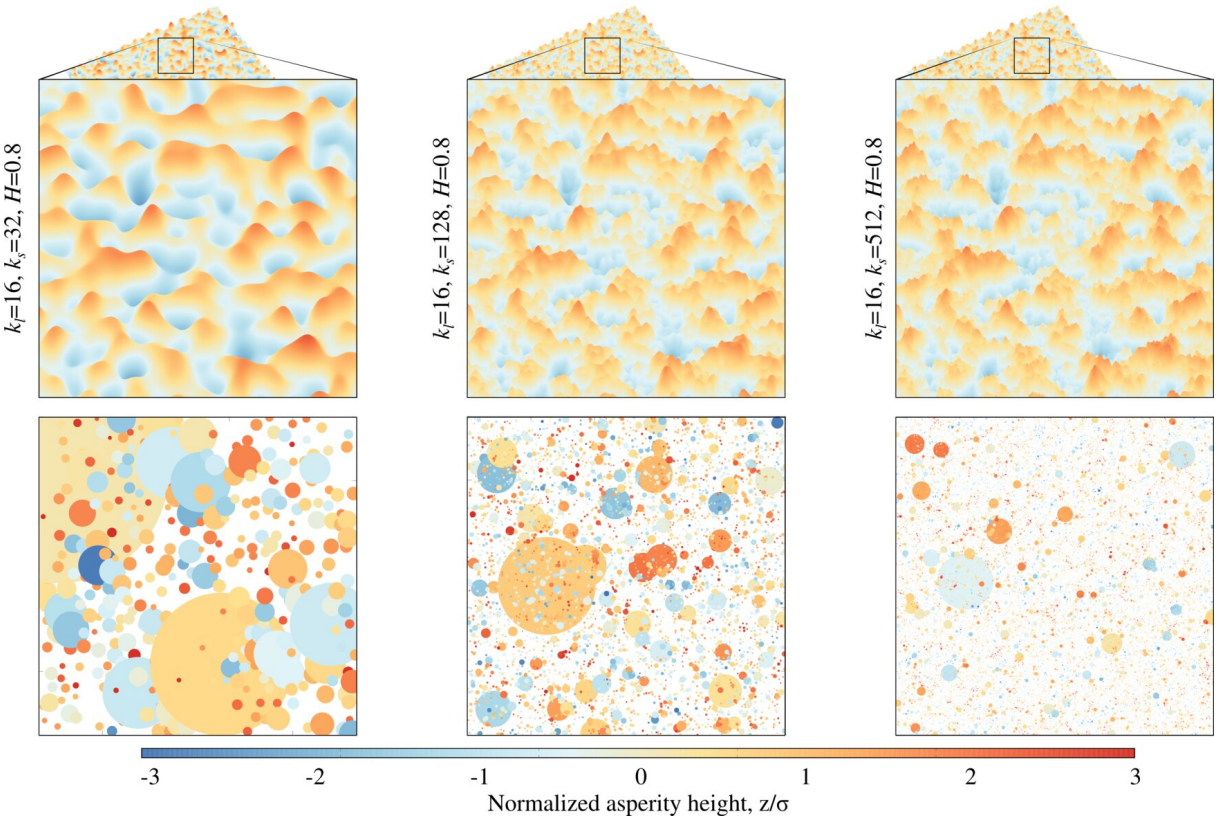

Figure 1.4: Identification of asperities on rough surfaces of different spectral content, the color of asperities corresponds to the vertical position of the summit and the size corresponds to the curvature radius; as could be easily seen from the figure, the higher the upper cutoff frequency $k_s = L/\lambda_s$ is, the sharper the asperity summits are.

1.2.5 Elastic-plastic contact of rough surfaces

When numerical simulations possess several severe non-linearities, the difficulties associated with the numerical treatment of each of them are rather multiplied than simply summed up. It is especially true when the non-linear material behavior is not derived from a potential, but contains internal history variables. Therefore, numerical treatment of elasto-plastic contact of rough surfaces presents serious difficulties in terms of convergence. Therefore, in our in-house finite element suite Z-set we use a special algorithm to split non-linearities: the material non-linearity is not taken into account before the status of contact elements has not converged, which allows in most cases to increase the convergence robustness of the Newton method. The same method can be used with the Partial Dirichlet-Neumann (PDN) method, that I developed during my thesis, which relies on the active-set strategy the inequality contact constraints by equality ones and which operates exclusively on primal variables and nodal reaction forces [25]. These two improvements enabled us to solve complex normal-contact problems between a rigid flat and an elasto-plastic rough surface in large and small deformation formalisms.

From the theoretical point of view, the elasto-plastic contact of rough surfaces is much simpler than elastic one, since it is known that the contact pressure p rapidly saturates at material hardness H, which could be estimated to be $H \approx 2.5 \div 3\ \sigma_Y$, where σ_Y is a certain yield-stress limit (either initial or saturated, depending on the hardening type). Therefore, the simplest elasto-plastic model for the true contact area evolution would be the model in which the area fraction $A' = A/A_0$ is proportional to the nominal pressure p_0:

$$A' = \frac{p_0}{H}.$$

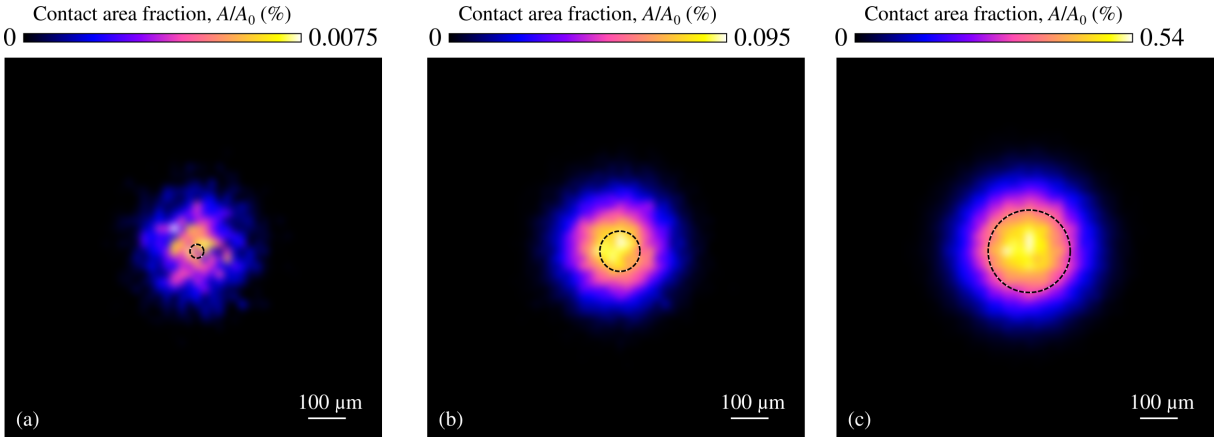

Figure 1.5: Contact between a spherical indenter and a deformable plane with a rough surface: we show the distribution of the contact area averaged over 2000 simulations for three values of the applied force, dashed lines represent the corresponding limits of the contact area predicted by the Hertz theory.

Version française: Contact entre un indenteur sphérique et un plan déformable à surface rugueuse : on montre la distribution de l'aire de contact moyennée sur 2000 simulations pour des trois valeurs de la force appliquée, la ligne pointillée représente la limite du contact prédit par la théorie de Hertz pour des surfaces lisses.

This microscopic model is widely used in many macroscopic empirical laws where the contact area is required. However, this law is valid only for monotonic loading $\dot{p}_0 \geq 0$, which rarely happens in real engineering systems which rather operate under cyclic loading. But even if we assume a monotonic loading, a more accurate plastic law has to take into account the initial elastic deformation of asperities, which would result in an affine function of the area. Finally, under high pressures, which are relevant for machining, metal forming (rolling, drawing, stamping), and other demanding applications, the true contact area saturates at the nominal one, thus giving the following estimation for the contact area:

$$A' = \begin{cases} A'_0 + \dfrac{p_0}{H}, & \text{if } p_0 \leq (1 - A'_0)H \\ 1, & \text{else.} \end{cases}$$

In our studies, with improved finite element algorithms, we could solve a series of elasto-plastic rough contact problems on real geometry [6], solve the viscous flow problem behind [26] and obtain a relatively good agreement with experimental results of Didier Lasseux (see Fig. 1.7). Moreover, we could construct a simple multi-asperity based model, which employs calibrated response of axisymmetric asperities and short range elastic interaction, to obtain quite accurate results, directly comparable with the heavy finite element simulations Fig. 1.8. In addition, in collaboration with Andreas Almqvist, Francesc Pérez-Ràfols and Andrei Shvarts we initiated a study aiming at comparing the boundary-element based method using an empirical algorithm to handle elasto-plasticity (the contact pressure is forced to remain in the interval $p \in [0, H]$) [27] and the accurate finite element analysis. The main objective of this study was to demonstrate the ability of plastic deformations to erase small scale roughness, which would solve the fundamental problem in the elastic contact of rough surface – the necessity to introduce short wavelength cutoff. Regardless promissing results, this study has been remaining in idle state for few years already. Hopefully, it could be restarted soon. Globally, we have not obtained any groundbraking results but we demonstrated the capabilitiy of our computational tools to handle properly elasto-plastic contacts.

Finite element simulation of elasto-plastic contact between a rough Stellite and a saphire plate [26]. Stream lines are coloured in red to highlight flux intensity, the blue-to-orange colour scale represents near surface accumulated plastic strain: the upper panel represents maximal loading, the middle panel shows the moment of separation (the plastic strain remains unchanged whereas the flux becomes more intense). In the lower panel shows comparison of four FE simulations with experimental results of Lasseux's group [28].

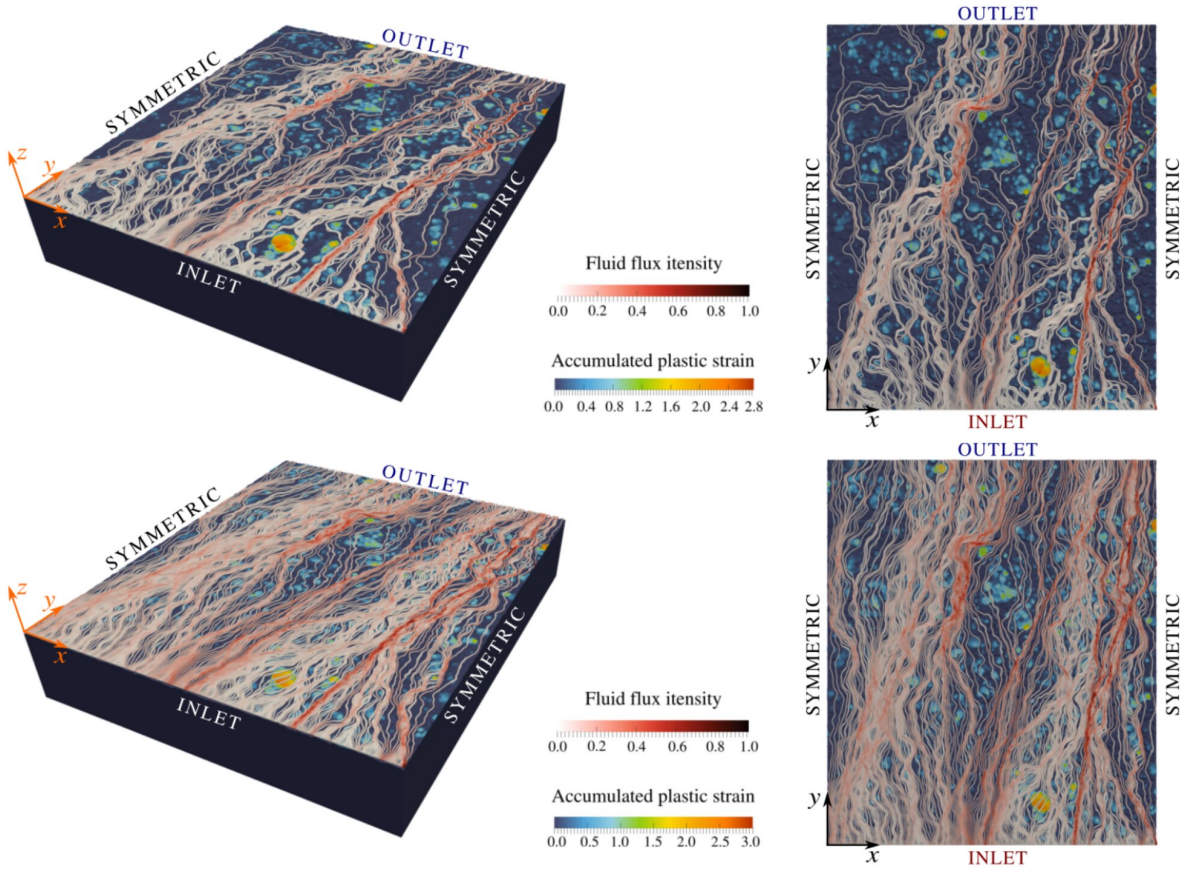

Figure 1.6:

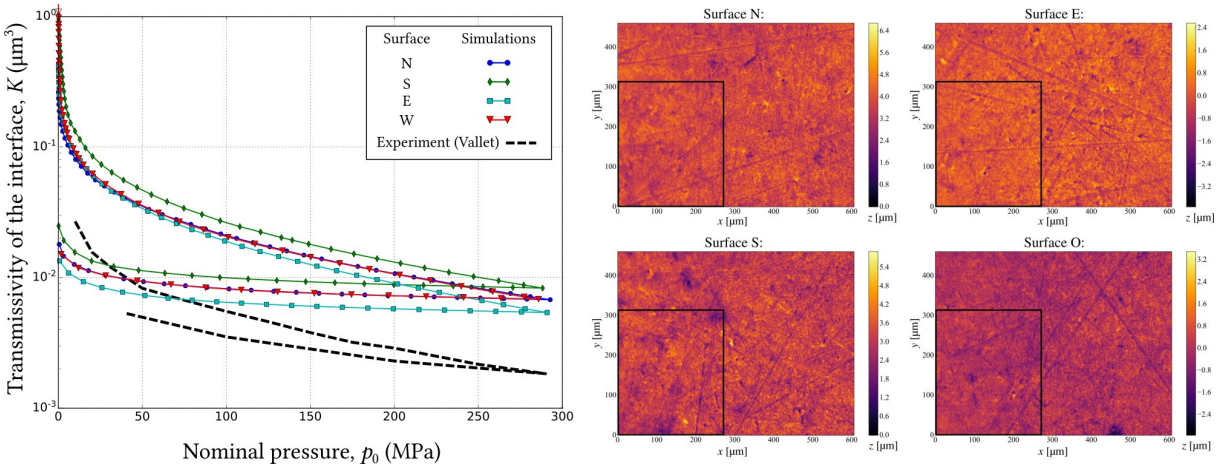

Figure 1.7: Finite element simulation of elasto-plastic contact between a rough Stellite and a saphire plate [26]. Stream lines are coloured in red to highlight flux intensity, the blue-to-orange colour scale represents near surface accumulated plastic strain: the upper panel represents maximal loading, the middle panel shows the moment of separation (the plastic strain remains unchanged whereas the flux becomes more intense). In the lower panel shows comparison of four FE simulations with experimental results of Lasseux's group [28].

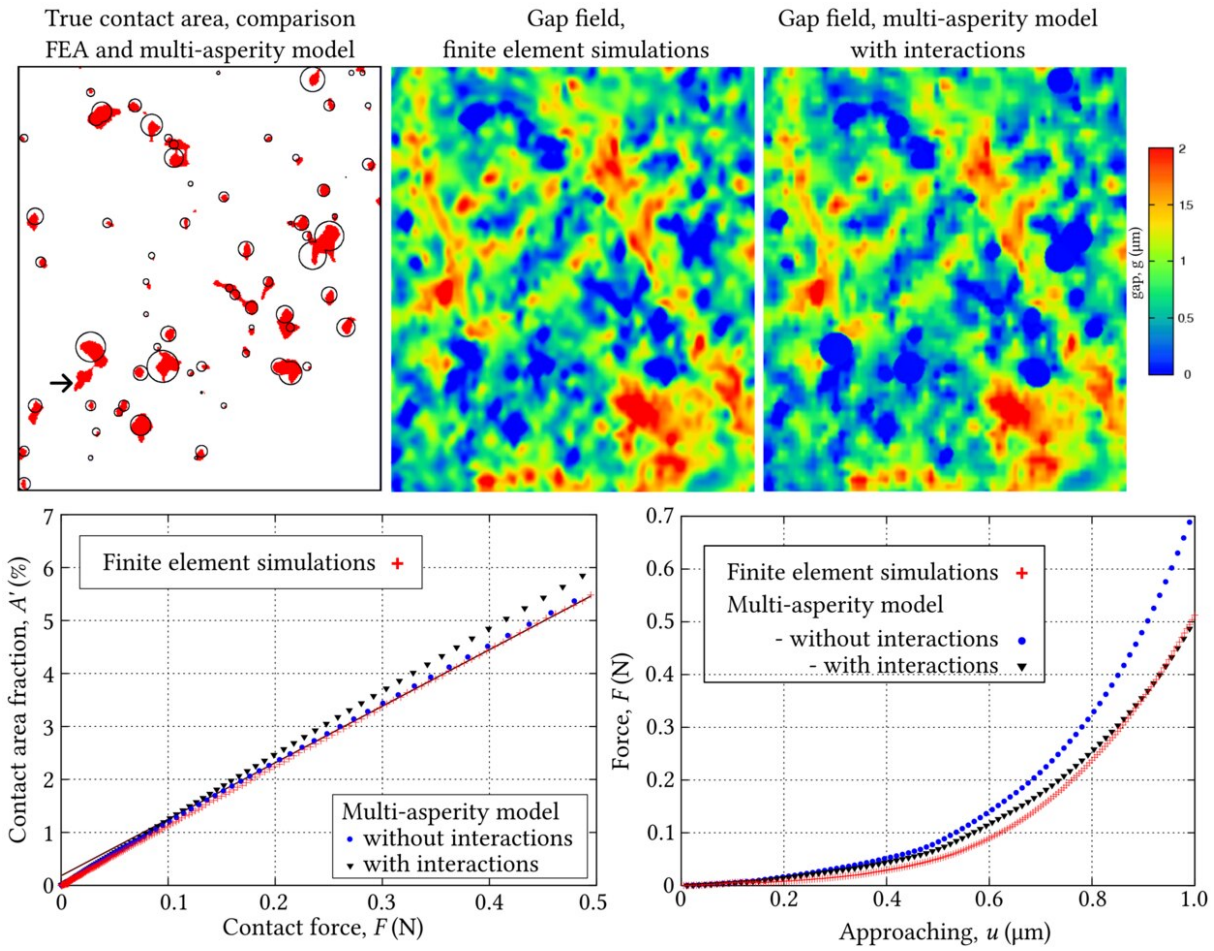

Figure 1.8: Comparison of a full-scale finite element simulation results and a simplified multi-asperity model with and without elastic interactions between asperities, at the maximal load we compare: upper left - contact area, upper right - gap field, lower panel: area-force and force-displacement curves, results from [6] (at further stage of J. Durand's thesis the detection algorithm for asperities was improved and the missing asperity identified by an arrow was incorporated in simulations).

Finally, in the early stage of my career I worked a little bit on the contact of rough surface of polycrystalline aggregates (Fig. 1.9), which rather validated the contact algorithms than permitted to obtain any physical insights into the topic. A simulation example is shown below: a finite element mesh with a polycristalline structure and the resulting cumulated plastic deformation after sever contact with a rigid flat.

References

- [6] V.A. Yastrebov, J. Durand, H. Proudhon, G. Cailletaud. "Rough surface contact analysis by means of the Finite Element Method and of a new reduced model". Comptes Rendus Mecanique, 339:473-490 (2011). [doi] [pdf]
- [26] A.G. Shvarts. "Coupling mechanical frictional contact with interfacial fluid flow at small and large scales" (2019). PhD thesis defended on March 20, 2019 at École des Mines de Paris in presence of the jury Res. Dir. D. Lasseux, Prof. M. Paggi, Prof. S. Stupkiewicz, Prof. J.A. Greenwood, Assist. Prof. V. Rey, Assist. Prof. N. Moulin, Prof. G. Cailletaud, Dr. J. Vignollet, Dr. V.A. Yastrebov. This PhD thesis was awarded by a CSMA award for one of two best theses in computational mechanics and by Hirn award for the best thesis in tribology. [HAL] [pdf]

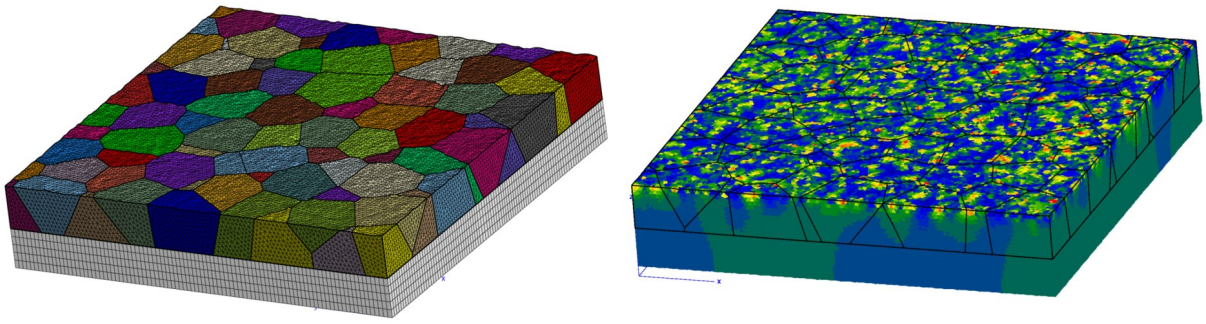

Figure 1.9: Study of rough contact between polycrystalline aggregate and a rigid flat.

1.2.6 Trapped fluid in contact interface

A classic study published in 1985 gives an impression that we fully understand how a sinusoidal surface of amplitude Δ and wavelength λ behaves in the presence of a compressible lubricant under the action of normal pressure [29]. Among other things, it follows from this study that if the fluid is trapped, it has no possibility to escape the trap whatever the value of the pressure applied. In our study [30] with Andrei Shvarts we were able to demonstrate numerically and analytically (using the solutions of Flamant and Cerutti on the asymptotic expansion of the forces of fluid on a sinusoidal surface) that the Kuznetsov's solution is not exact and that a fluid once trapped can escape by gradually opening the trap even in the context of small perturbations. The limit pressure for opening the trap within the limit of the infinitesimal slope $\Delta/\lambda \to 0$ converges to a very simple equation:

$$p_{\text{open}} = \frac{E}{2(1-2\nu)(1+\nu)}\left(1 - \frac{V_f(p_{\text{open}})}{V_0}\right),$$

where V_f is the volume of the fluid which, in the case of a compressible fluid, depends on the pressure, and where V_0 is the volume between two crests of the profile. For finite values of Δ/λ, the opening pressure is greater than this limit. Of course, for fluids with non-linear compressibility, up to two solutions can exist if the initial volume of the fluid is not less than the volume of the valley $V_{f0} \geq V_0$.

Even if the possibility for the fluid to escape the trap is interesting per se, this phenomenon is also important from practical point of view since it influences (1) the macroscopic friction, and (2) the behavior of engineering systems with trapped fluid under cyclic loading. The macroscopic coefficient of friction μ_{glob} can vary in a strongly nonlinear and non-monotonic way depending on the constitutive behavior of the solid as well as of the fluid. The equation for the evolution of the macroscopic of friction could be obtained in a trivial way:

$$\frac{\mu_{\text{glob}}}{\mu_{\text{loc}}} = 1 - \frac{p_f(p_0)}{p_0}\left[1 - \frac{A(p_0)}{A_0}\right],$$

on the other hand, the expressions for the evolution of the fluid pressure $p_f(p_0)$ and of the real contact area $A(p_0)$ with respect to applied pressure p_0 are difficult to guess/deduce in the general case. We therefore used numerical simulations to explore different possible scenarios. We have shown that the macroscopic coefficient of friction can either decrease in a monotonic way or evolve in a more complex way (cf. Fig. 1.10(a)). This discovery of the nonlinear relationship between the coefficient of friction and the pressure is a valuable result for tribology.

Another important consequence of the fluid entrapment is that in the presence of friction, high concentrations of shear stress can emerge under normal cyclic loading. This surprising result was revealed through numerical simulations, yet to explain it analytically we employed results from the linear elastic fracture mechanics (LEFM) for interface cracks at bi-material interfaces [31, 32] (cf. Fig. 1.10(b)). These high shear concentrations can cause an onset of fatigue cracks in vibration. Such cracks could be critical for vibrational resistance of some systems that must remain tightly sealed such as, for example, radioactive waste containers during transportation.

To construct our analogy between the LEFM and trap opening by the fluid, the following considerations were used. The fluid activation corresponds to the maximal extension of the contact zone (we shall denote the maximal contact half-length as a^*, and during the subsequent increase of the external pressure the width of the contact zone is monotonically decreasing. For sufficiently small slope of the wavy profile, the situation corresponding to contact half-length $a < a^*$ can be considered as a configuration of two bonded dissimilar solids with two aligned semi-infinite interfacial cracks in the interface, separated by $2a$, see Fig. 1.10(b). Using the superposition principle, the observed stress state, corresponding to the half-length of the contact patch a, can be represented as a superposition of the initial shear traction $\sigma_t^*(x)$, corresponding to the moment of activation of the fluid, and a stress induced by the same traction with the opposite sign, $\sigma_t^-(x) = -\sigma_t^*(x)$ applied only on the surfaces of the cracks in the intervals $x \in [-a^*, -a]$ and $[a, a^*]$, i.e. in the interval where the fluid penetrated. Such traction induces a singular shear stresses in the region between two cracks $x \in [-a, a]$, thus $\sigma_t^-(x)$ can be written as:

$$\sigma_t^-(x) = \begin{cases} -\sigma_t^*(x), & x \in [-a^*, -a] \cup [a, a^*] \\ \frac{1}{\sqrt{2\pi}} \mathrm{Im}\left\{ K(a, \sigma_t^*) \left(\frac{(x-a)^{i\epsilon}}{\sqrt{|x-a|}} - \frac{(x+a)^{i\epsilon}}{\sqrt{|x+a|}} \right) \right\}, & x \in [-a, a] \\ 0, & |x| > a^*, \end{cases} \tag{1.1}$$

where K is the complex stress intensity factor, see [31, 32], and two terms in brackets in Eq. (1.1) correspond to two semi-infinite cracks being considered, so that $\sigma_t^-(0) = \sigma_t^*(0) = 0$, Im is the imaginary part. Therefore, the resulting distribution of shear tractions is given by the superposition $\sigma_t(x) = \sigma_t^*(x) + \sigma_t^-(x)$. The complex stress intensity factor K is calculated using the existing analytical formula for considered configuration and shear traction distribution [31, 32]:

$$K(a, \sigma_t^*) = \left[k_1(a, \sigma_t^*) + i k_2(a, \sigma_t^*) \right] \sqrt{\pi} \cosh(\pi\epsilon), \tag{1.2}$$

where

$$\begin{aligned} k_1(a, \sigma_t^*) &= \frac{\sqrt{2}}{\pi} \int_a^{a^*} \frac{\sigma_t^*(x) \sin(\epsilon \ln(x-a))}{\sqrt{x-a}} dx, \\ k_2(a, \sigma_t^*) &= \frac{\sqrt{2}}{\pi} \int_a^{a^*} \frac{\sigma_t^*(x) \cos(\epsilon \ln(x-a))}{\sqrt{x-a}} dx, \end{aligned} \tag{1.3}$$

and the parameter ϵ accounts for the different properties of the two bonded solids, in case one of them being rigid, it equals to

$$\epsilon = -\frac{1}{2\pi} \ln(3 - 4\nu).$$

A sound similarity is found between numerical results and analytical formulae provided by the LEFM. Therefore, we have shown that during the process of trap opening due to increasing pressure in the fluid with friction taken into account, the tangential tractions near the contact edges are elevated up to the limit provided by the Coulomb friction law. Consequently, even if the majority of the interface remains in stick state, local slip zones emerge at the boundaries of contact zones. It is important to account for such an elevated shear stress near edges of contact zones, which surround trapped fluid, in the analysis of damage evolution and crack onset under monotonic and cycling loading, including fretting fatigue [33, 34].

Version française: Une étude classique publiée en 1985 donne l'impression que l'on comprend bien comment se comporte une surface sinusoïdale d'amplitude Δ et longueur d'onde λ en présence d'un lubrifiant compressible sous l'action d'une pression normale [29]. Entre autres, il suit de cette étude que si le fluide est piégé, il n'a pas de possibilité de s'échapper quelle que soit la valeur de la pression appliquée. Dans notre étude [30] avec Andrei Shvarts nous avons pu démontrer numériquement et analytiquement (en utilisant les solutions de Flamant et Cerutti sur l'expansion asymptotique des efforts de fluide sur une surface sinusoïdale) que la solution de Kuznetsov n'est pas exacte et qu'un fluide une fois piégé peut s'échapper en ouvrant graduellement le piége même dans le contexte de petites

perturbations. La pression limite d'ouverture du piège dans la limite de la pente infinitésimale $\Delta/\lambda \to 0$ converge vers une forme très simple :

$$p_{\text{open}} = \frac{E}{2(1-2\nu)(1+\nu)}\left(1 - \frac{V_f(p_{\text{open}})}{V_0}\right),$$

où V_f est le volume de fluide qui, dans le cas d'un fluide compressible, dépend de la pression, et où V_0 est le volume compris entre deux crêtes de la sinusoïde. Pour des valeurs finies de Δ/λ, la pression d'ouverture est supérieure à cette limite. Bien entendu, pour des fluides à compressibilité non-linéaire, jusqu'à deux solutions peuvent exister si le volume initial de fluide n'est pas inférieur au volume de la vallée $V_{f0} \geq V_0$.

La possibilité d'échappement du fluide est intéressante en soi, mais de plus ce phénomène influence (1) le frottement macroscopique, et (2) le comportement des systèmes comportant des fluides piégés sous un chargement cyclique. Le coefficient de frottement macroscopique μ_{macro} peut varier d'une manière très non linéaire en fonction du comportement du solide ainsi que du fluide. L'équation de ce changement est obtenue de façon triviale :

$$\mu_{\text{macro}} = \mu_{\text{micro}}\left(1 - \frac{p_f(p_0)}{p_0}\left[1 - \frac{A(p_0)}{A_0}\right]\right),$$

par contre, les expressions de la pression de fluide p_f et de l'aire de contact réelle A en fonction de la pression appliquée p_0 sont difficiles à déduire dans le cas général. Nous avons donc recouru à des simulations numériques pour explorer les différents scénarios possibles. Nous avons montré que le frottement macroscopique peut décroître d'une manière monotone ou bien évoluer d'une manière plus complexe (cf. Fig. 1.10(a)). Cette découverte de la relation non linéaire entre le coefficient de frottement et la pression est un résultat intéressant pour le monde de la tribologie.

Une autre conséquence importante du piégeage des fluides est qu'en présence de frottement, de fortes concentrations de contrainte de cisaillement peuvent émerger sous chargement normal cyclique. Cette conclusion insolite a été obtenue numériquement mais nous l'avons également expliquée analytiquement en faisant le recours à la mécanique linéaire de la rupture le long des interfaces bi-matériaux [31, 32] (cf. Fig. 1.10(b)). Ces fortes concentrations de cisaillement peuvent provoquer l'amorçage de fissures de fatigue en vibration, qui peuvent être critiques pour certains systèmes qui devrait rester fortement étanches comme, par exemple, des conteneurs de déchets radioactifs lors du transport.

References

- [30] A.G. Shvarts, V.A. Yastrebov. "Trapped fluid in contact interface". Journal of the Mechanics and Physics of Solids, 119:140-162 (2018). [doi] [arXiv] [pdf]

1.2.7 Creeping fluid flow in contact interface between rough surfaces

Representativity of rough surfaces in mechanical contact is of great importance, yet it is even more relevant for studies of permeability of contact interfaces especially for low and high pressures. This representativity becomes *crucial* to numerically studies near the percolation point associated with the existence of an infinite contact cluster. On the other hand, the finite element method is a CPU-time demanding tool for studies of rough surfaces with a sufficiently rich spectrum. Moreover, in many application problems, the strong coupling between the equations of the mechanics of solids and fluids is not necessary because the pressure in the fluid is lower by several orders of magnitude than those which develop in the contact. In this case, a framework much less greedy in terms of time and computing power can be used: this is the boundary element method. By adopting the one-sided coupling between the boundary element method responsible for the mechanical contact and the finite element method used to solve the Reynolds equation on the topography found by the first, we were able to tackle this interesting problem which is relevant for numerous applications, notably for systems where the tightness is ensured by the static contact (cf. Fig. 1.11).

By covering a wide range of roughness parameters, through thousands of simulations to capture the stochastic nature of the topography, we were able to establish a phenomenological law between the

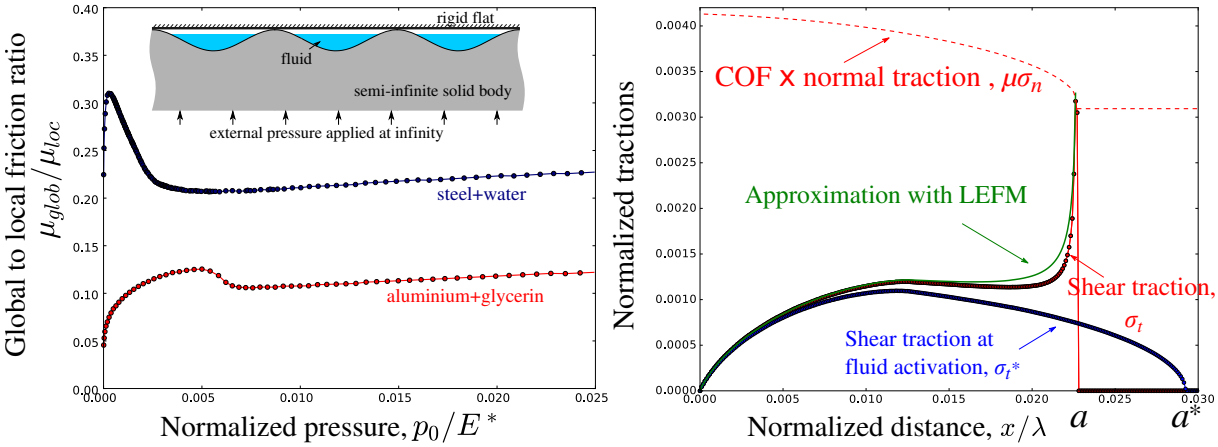

Figure 1.10: (a) Evolution of the friction coefficient for (i) steel/water and (ii) aluminum/glycerol combinations; (b) illustration of the high concentration of shear stress that arises near the contact edge upon increase in normal pressure accompanied by fluid expansion in the contact interface; comparison with the analytical solution inspired by the linear elastic fracture mechanics.

Version française: (a) Évolution du coefficient de frottement pour des combinaisons (i) acier/eau et (ii) aluminium/glycérol ; (b) illustration de la forte concentration de la contrainte de cisaillement qui surgit près du bord du contact lors de l'augmentation de la pression normale accompagnée par l'expansion du fluide dans l'interface de contact ; comparaison avec une solution analytique provenant de la mécanique linéaire de la rupture.

normalized interface permeability and the normal pressure p_0, which allows us to define the average flux Q as a function of the hydrostatic pressure drop ΔP_f over a distance L :

$$Q(p_0) \approx -\frac{41.70 m_0^{3/2} \Delta P_f}{\eta L} \cdot \exp\left(-42.57 \frac{p_0}{E^* \sqrt{m_2}}\right),$$

where η is the dynamic viscosity of the fluid, m_i is the i-th spectral moment and E^* is the effective modulus of the contact between two elastic solids. The two constants 41.70 and 42.57 are determined by numerical simulations and remain fairly invariant for all the surfaces studied. This phenomenological law is applicable within the exponential-decay regime for not too low pressures but well below the permeability pressure.

Besides this law, other important results have been obtained. For example, we showed that the self-consistent homogenization model applicable to the study of the permeability of contact interfaces, and which is based on the probability distribution of film thickness (equal to the aperture value), should include a correction to ignore the pockets of trapped fluid [35]. The normalized permeability K'_{eff}, it could be found from the corrected equation:

$$(1 - A'_{\text{eff}}) \int_0^\infty \frac{g^3 P(g)}{g^3 + K'_{\text{eff}} m_0^{3/2}} dg = \frac{1}{2},$$

where g is the gap, $P(g)$ its probability density and A'_{eff} is the non-conductive contact area including the contact area and trapped fluid. The probability density of the gap field was studied in [36], but we could obtain much more clean and statistically meaningful distributions and suggest their functional shape, which could help in analytical estimation of permeability [37].

In addition, we have analytically estimated [37] the asymptotic distribution of the film thickness in the vicinity of zero "gap" $g \to 0+$ for a parabolic indenter of radius of curvature R and for a contact patch of radius a:

$$P(g > 0) \xrightarrow[g \to 0+]{} \approx \frac{\pi^2 R}{2\sqrt{2}} \left(\frac{3.75 a^2}{\pi R g}\right)^{1/3} \approx 3.7015 \left(\frac{a^2 R^2}{g}\right)^{1/3}$$

The factor of this distribution will of course be modified for a contact area composed of several contact "spots". In the geometric intersection model (Winkler foundation), the linear size of the contact clusters scales as $P(a) \sim a^{-4+H}$, where H is the Hurst exponent [38], [14], this "scaling" remains approximately valid for accurate contact models including elastic interactions: at least for $H = 0.8$, it was found that $P(a) \sim a^{-2.9}$ [39]. By integrating over all contact points $int_{a_0}^{\infty} a^{2/3-4+H}\, da \sim a_0^{H-7/3}$ (the smallest linear cluster size a_0 was added) will provide a factor to the probability distribution of the "gap" $P(g \to 0+)$ but will not modify the power law $P(g) \to g^{-1/3}$ which has been recently demonstrated in another way in [40].

Finally, using a more elaborated – strongly coupled – fluid-solid computational framework, based on numerous simulations, we deduced a novel non-local permeability law [26], Sec. 9.3, pp. 155-158:

$$\ln K_{\text{eff}} = a_0 - \frac{\gamma}{E^*}\left(p_0 - \alpha p_f + l^* \nabla p_f\right),$$

where K_{eff} is the normalized permeability, p_0 is the external pressure, p_f is the average fluid pressure and ∇p_f is its gradient, E^* is the effective elastic modulus, γ and α are dimensionless parameters and l^* is the characteristic length scale. Naturally α should be very close to unity, whereas the characteristic length depends on the roughness parameters. This non-local permeability law implies that the fluid flux depends not only on the local difference in applied and fluid pressures $p_0 - \alpha p_f$ but also on the gradient of the latter.

Version française: La représentativité des surfaces rugueuses dans les études du contact mécanique est très importante, mais elle est encore plus pertinente pour des études de perméabilité des interfaces de contact surtout pour de faible et de forte pressions. Cette représentativité devient *cruciale* pour étudier numériquement des phénomènes près du point où se produit la percolation associée avec l'existence d'un cluster infini de contact. Par contre, la méthode des éléments finis est un outil très coûteux pour des études des surfaces rugueuses à spectre suffisamment riche. De plus, dans beaucoup de problèmes applicatifs, le couplage fort entre les équations de la mécanique des solides et des fluides n'est pas nécessaire car la pression dans le fluide est inférieure de plusieurs ordres de grandeur de celle qui se développe dans les zones de contact. Dans ce cas, un cadre beaucoup moins gourmand en termes de temps et de puissance calcul peut être utilisé : c'est la méthode des éléments de frontière. En adoptant, le couplage unilatéral entre la méthode des éléments de frontière responsable pour le contact mécanique et la méthode des éléments finis utilisée pour résoudre l'équation de Reynolds sur la topographie trouvée par la première, nous avons pu aborder ce problème intéressant et fort important pour des systèmes où l'étanchéité est assurée par le contact statique entre des surfaces (cf. Fig. 1.11).

En couvrant une large plage de paramètres de rugosité, grâce à des milliers de simulations afin de capturer la nature stochastique de la topographie, nous avons pu établir une loi phénoménologique entre la perméabilité normalisée de l'interface et la pression normale p_0, qui permet de définir le flux moyen Q en fonction de la chute de la pression hydrostatique ΔP_f sur une distance L :

$$Q(p_0) \approx -\frac{41.70 m_0^{3/2} \Delta P_f}{\eta L} \cdot \exp\left(-42.57 \frac{p_0}{E^* \sqrt{m_2}}\right),$$

où η est la viscosité dynamique du fluide, m_i est le i-ième moment spectral et E^* est le module effectif du contact entre deux solides élastiques. Les deux constantes 41.70 et 42.57 sont déterminées par des calculs numériques et restent assez invariables pour toutes les surfaces étudiées. Cette loi phénoménologique est applicable dans le régime de décroissance exponentielle pour des pressions pas trop faibles mais bien inférieures à la pression de perméabilité.

A part de cette loi, d'autres résultats importants ont été obtenus. Par exemple, nous avons démontré que le modèle auto-cohérent d'homogénéisation applicable à l'étude de la perméabilité des interfaces de contact, et qui se basent sur la distribution de probabilité d'épaisseur du film (égale à la valeur d'ouverture), devrait comporter une correction pour ignorer les poches de fluide piégé [35]. De plus, nous avons estimé [37] analytiquement la distribution asymptotique d'épaisseur du film au voisinage de zéro "gap" $g \to 0+$ pour un indenteur parabolique du rayon de courbure R et pour une tache de contact de rayon a:

$$P(g > 0) \xrightarrow[g \to 0+]{} \approx \frac{\pi^2 R}{2\sqrt{2}} \left(\frac{3.75 a^2}{\pi R g}\right)^{1/3} \approx 3.7015 \left(\frac{a^2 R^2}{g}\right)^{1/3}$$

Le facteur de cette distribution sera bien entendu modifié pour une aire de contact composée de plusieurs "spots" de contact. Dans le modèle d'intersection géométrique (fondation de Winkler), la taille linéaire des clusters de contact se dimensionne comme $P(a) \sim a^{-4+H}$, où H est l'exposant de Hurst [38, 14], ce "scaling" reste approximativement valable pour des modèles de contact précis incluant des interactions élastiques : au moins pour $H = 0.8$, il a été trouvé que $P(a) \sim a^{-2.9}$ [39]. En intégrant sur tous les points de contact $\int_{a_0}^{\infty} a^{2/3-4+H}\, da \sim a_0^{H-7/3}$ (la plus petite taille linéaire de cluster a_0 était ajouté) fournira un facteur à la distribution de probabilité du "gap" $P(g \to 0+)$ mais ne modifiera pas la loi de puissance $P(g) \to g^{-1/3}$ qui a été recemment démontré d'une autre façon dans [40].

Même si des surfaces à spectre *riche* sont pas accessibles à la méthode des éléments finis, nous avons fait une étude numérique de perméabilité des interfaces de contact entre surfaces rugueuses dans notre cadre monolithique développé pour ces problèmes fortement couplés. Nous avons établi une autre loi phénoménologique de perméabilité non locale. La non-localité dans ce cas se traduit par la dépendance de la perméabilité, pas seulement en fonction de la pression p_0 et de la pression de fluide p_f mais encore en fonction du gradient de pression de fluide ∇p_f. Cette loi $\boldsymbol{K}(p_0, p_f, \nabla p_f)$ a été identifiée pour la composante du tenseur de perméabilité colinéaire avec la direction de ∇p_f, sous la forme suivante :

$$K_x = \exp\left(c_0 - \frac{\gamma}{E^*}\left[p_0 - \alpha p_f + l^* \nabla_x p_f\right]\right),$$

où $\gamma, \alpha \approx 1$ sont des nombres adimensionnels (universels dans la plage étudiée des paramètres) qui ont été déduits des simulations numériques et l^* est la longueur caractéristique. Le travail sur cette loi n'est pas encore terminé, mais potentiellement il pourrait améliorer la précision des études de perméabilité des systèmes de fissures complexes saturées en compression qui font l'objet d'études en hydrogéologie.

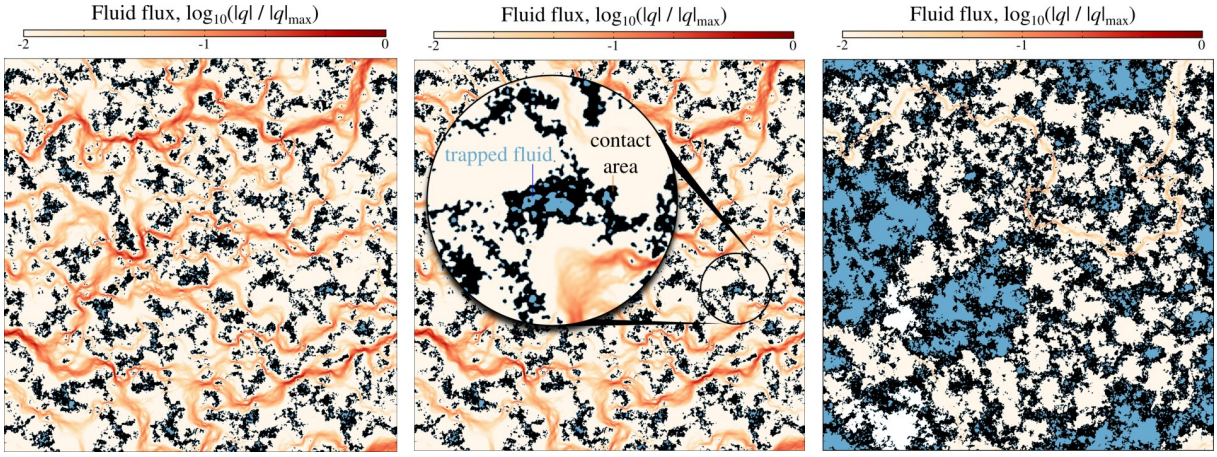

Figure 1.11: Viscous fluid flow through the contact interface shown in reddish color scale, contact area shown in black and trapped fluid shown in blue. Two configurations are shown for relatively small contact area and much larger contact area showing large portions of fluid trapped.

Version française: Flux d'écoulement dans l'interface de contact. Les taches de contact sont noires, le fluide piégé est en bleu. Deux instances sont présentées qui correspondent à des différentes valeurs de pression.

References

- [35] V.A. Yastrebov, G. Anciaux, J.F. Molinari. "Permeability of the contact interface between rough surfaces" (2021) in the final stage of writing, draft is provided [encrypted pdf]
- [37] V.A. Yastrebov, G. Anciaux, J.F. Molinari. "Gap distribution in contact interfaces between rough surfaces and transmissivity analysis" (2021) in the final stage of writing, draft is provided [encrypted pdf]

- [26] A.G. Shvarts. "Coupling mechanical frictional contact with interfacial fluid flow at small and large scales" (2019). PhD thesis defended on March 20, 2019 at École des Mines de Paris in presence of the jury Res. Dir. D. Lasseux, Prof. M. Paggi, Prof. S. Stupkiewicz, Prof. J.A. Greenwood, Assist. Prof. V. Rey, Assist. Prof. N. Moulin, Prof. G. Cailletaud, Dr. J. Vignollet, Dr. V.A. Yastrebov. This PhD thesis was awarded by a 🏆 CSMA award for one of two best theses in computational mechanics and by 🏆 Hirn award for the best thesis in tribology. [HAL] [pdf]

1.2.8 Coupled flow through a wavy channel

With some fairly strong assumptions, we were able to propose an analytical solution that describes the coupled flow of a viscous fluid along an elastic body with a sinusoidal surface brought into contact with a rigid plane [41]. This solution takes into account the deformation of the substrate by the contact forces and by the fluid pressure; the associated Reynolds equation is solved on the updated geometry. The solution predicts the average pressure in the fluid along the channel y of length L subject to the external pressure p_0, and the inlet and outlet fluid pressures p_i, p_o:

$$\frac{y}{L} = \frac{I(\rho) - I(\rho_i)}{I(\rho_o) - I(\rho_i)}, \quad \rho = \lambda \frac{p_0 - p_f(y)}{\pi E^* \Delta}$$

with Δ being the amplitude and λ being the wave-length, and the function I is given by

$$I(\rho) = \rho^2 + \frac{17}{9}\rho^3 - \frac{71}{128}\rho^4 + \frac{3}{2}\rho^2\left(1 - \frac{16}{9}\rho + \frac{13}{16}\rho^2\right)\ln(\rho) + \rho^3\left(1 - \frac{15}{16}\rho\right)\ln^2(\rho) + \frac{\rho^4}{4}\ln^3(\rho).$$

Using this solution, we can derive the flux at each point, which gives the equation

$$q_y(x,y) = \frac{g^3(x,y)}{12\eta}\left(\frac{L\lambda}{(I(\rho_o) - I(\rho_i))\ \pi E^* \Delta}\frac{dI(\rho)}{d\rho}\right)^{-1}$$

which in turn, after integrating provides us with the mean flow, which is in very good agreement with the results of the strongly coupled finite element calculation (see Fig. 1.12).

We believe that this solution for a three-dimensional coupled fluid/solid/contact problem represents a rare example of an approximate analytical solution for such complex problems. The associated numerical solution allows us to go well beyond the validity range of the analytical solution, and allowed us to predict the critical channel closure pressure, which depends only on the geometry Δ, λ, the elastic parameters E^* and, surprisingly, only on the inlet fluid pressure p_i and not on the outlet one. The resulting closing pressure is given by:

$$p_{\text{close}} = \frac{\pi E^* \Delta}{\lambda} + \frac{4}{5}p_i$$

🇫🇷 **Version française:** Avec quelques hypothèses assez fortes, nous avons pu proposer une solution analytique qui décrit l'écoulement d'un fluide visqueux le long d'un corps élastique à surface sinusoïdale mis en contact avec un plan rigide [41]. Cette solution prend en compte la déformation du substrat par les efforts de contact et par la pression dans le fluide ; l'équation de Reynolds associée est résolue sur la géométrie actualisée. La solution prédit la pression moyenne dans le fluide le long du canal y de longueur L soumis à la pression externe p_{ext}, et des pressions p_i, p_o du fluide d'entrée et de sortie :

$$\frac{y}{L} = \frac{I(\rho) - I(\rho_i)}{I(\rho_o) - I(\rho_i)}, \quad \rho = \lambda \frac{p_{\text{ext}} - p_f(y)}{\pi E^* \Delta}$$

Δ étant l'amplitude d'ondulation et λ étant la longeur d'onde, avec

$$I(\rho) = \rho - \frac{9}{4}\rho^2 + \frac{17}{9}\rho^3 - \frac{71}{128}\rho^4 + \frac{3}{2}\rho^2\left(1 - \frac{16}{9}\rho + \frac{13}{16}\rho^2\right)\ln(\rho) + \rho^3\left(1 - \frac{15}{16}\rho\right)\ln^2(\rho) + \frac{\rho^4}{4}\ln^3(\rho).$$

En utilisant cette solution, nous pourrons dériver le flux en chaque point, ce qui donne l'équation

$$q_y(x,y) = \frac{g^3(x,y)}{12\eta}\left(\frac{L\lambda}{(I(\rho_o) - I(\rho_i))\ \pi E^* \Delta}\frac{dI(\rho)}{d\rho}\right)^{-1}$$

qui après une intégration fournit le flux moyen, qui se compare très bien avec les résultats du calcul par élément finis fortement couplé (cf. Fig. 1.12).

Cette solution pour un problème couplé fluide/solide/contact à trois dimensions représente un rare exemple de solution analytique approchée pour des problèmes aussi complexes. La solution numérique associée permet d'aller bien au-delà du domaine de validité de la solution analytique, ce qui nous a permis de prévoir la pression critique de fermeture du canal, qui ne dépend que de la géométrie Δ, λ, des paramètres élastiques E^* et de la pression de fluide d'entrée p_i :

$$p_{\text{ferme}} = \frac{\pi E^* \Delta}{\lambda} + \frac{4}{5} p_i$$

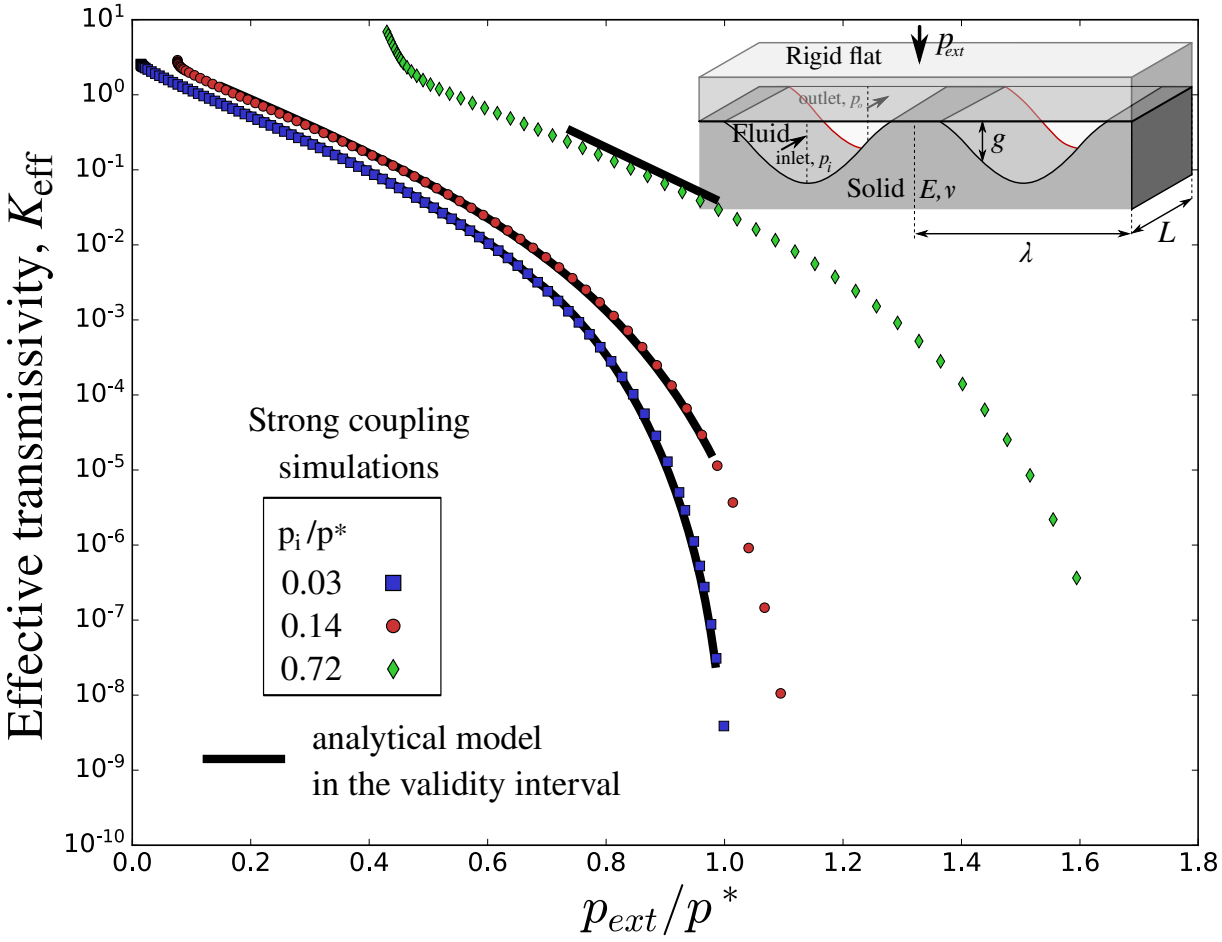

Figure 1.12: Effective transmissivity of a channel formed by a sinusoidal surface in contact with a rigid plane. Within its validity range, our analytical solution compares well with the results of the strongly coupled solid/fluid finite element calculation.

Version française: Transmissivité effective d'un canal formé par une surface sinusoïdale mise en contact avec un plan rigide. Dans son intervalle de validité, notre solution analytique se compare bien avec les résultats du calcul éléments finis solide/fluide fortement couplé.

References

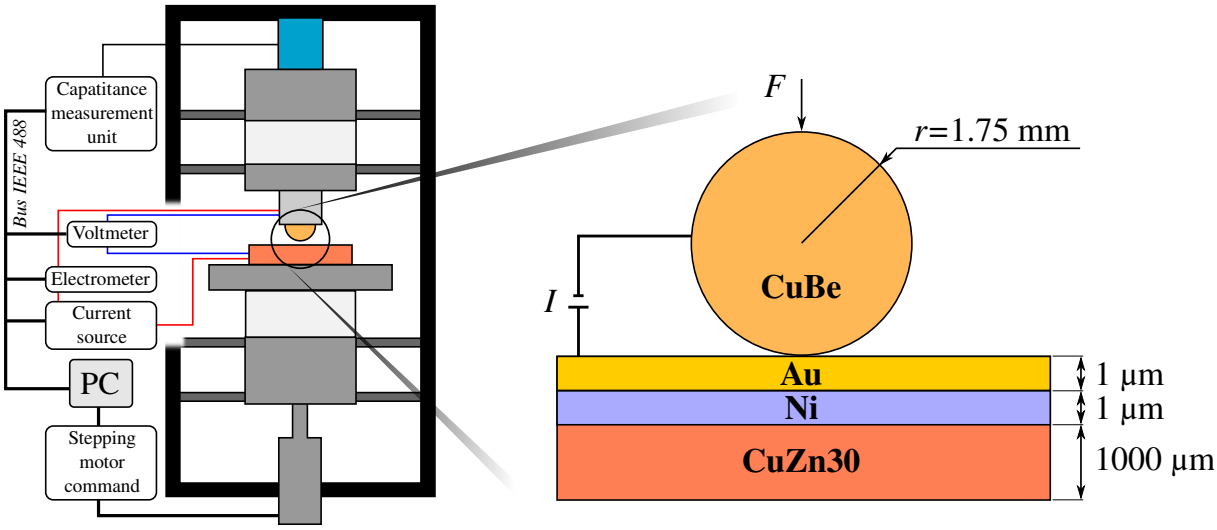

Figure 1.13: Experimental set-up for the study of roughness-induced contact electric resistance.

- [41] A.G. Shvarts, V.A. Yastrebov. "Fluid flow across a wavy channel brought in contact". Tribology International, 126:116-126 (2018). [doi] [arXiv] [pdf]

1.2.9 Electric contact between rough surfaces

In the framework of postdoc of Frederick Sorel Mballa Mballa co-supervised by Georges Cailletaud, Henry Proudhon, Frédéric Houzé and Sophie Noël funded by Labex LaSIPS we worked on the electric contact in ball/substrate configuration taking into account surface roughness as well as accurate material models. Nonlinear material models for brass substrate as well as for nickel and gold micron-thickness electroplated coatings were properly calibrated, beryllium bronze of the ball indenter was assumed to be elastic. $J2$ plasticity was used for all substrate materials with a single kinematic hardening for nickel and gold whereas for the brass it was supplemented with two other kinematic hardening rules as well as with the isotropic hardening. However, even such an elaborated model of the brass was not enough to capture the experimentally measured resistance/force hysteresis loops [42], we demonstrated that the thickness of Ni and Au layers was not crucial for this analysis. Nevertheless, in this project we successfully combined three different models to estimate the electric resistance of contact interfaces Fig. 1.14:

1. macroscopic (smooth surfaces) finite element simulation of indentation with advanced material modelling which provided us with the macroscopic force/displacement/area curves;
2. experimental roughness analysis which was taken into account at the microscopic scale to model the distribution of conductive spots, we used an iterative elasto-plastic model of interacting contact spots which in mean-field sense has to verify the the macroscopic pressure and contact area obtained in model 1.;
3. to estimate the evolution of the electric contact resistance R_c of the resulting contact interface, we used Greenwood's model [43]:

$$R_c = \frac{\rho^*}{2\sum a_i}\left(1 + \frac{2}{\pi}\frac{\sum\sum_{i\neq j} a_i a_j / d_{ij}}{\sum a_i}\right),$$

where ρ^* is the effective resistivity, a_i is the size of i-th contact spot and d_{ij} is the distance between i-th and j-th spots.

In addition, a full scale 3D finite element model incorporating surface roughness and all material models was constructed and solved for relevant loading conditions, however, the final thermal analysis was not conducted Fig. 1.14, therefore these results remain unpublished. Hopefully, this work could be finalized in the framework of PhD thesis of Paul Beguin on the thermal contact.

Regardless all our efforts to match the experimental resistance via modelling, our results were located on the minimal level of resistance identified in experiments and only upon using the hardest version for the brass' yield stress (σ_y = 550 MPa). The most convincing hypothesis of this discrepancy is the presence of non-conductive oxidized zones on the side of beryllium bronze ball, which has to considerably increase the electric resistance. In perspective, it would be interesting to restart this project keeping the same materials of the substrate but ensuring a coating of the bronze balls with a gold layer to ensure conductivity of all contact spots.

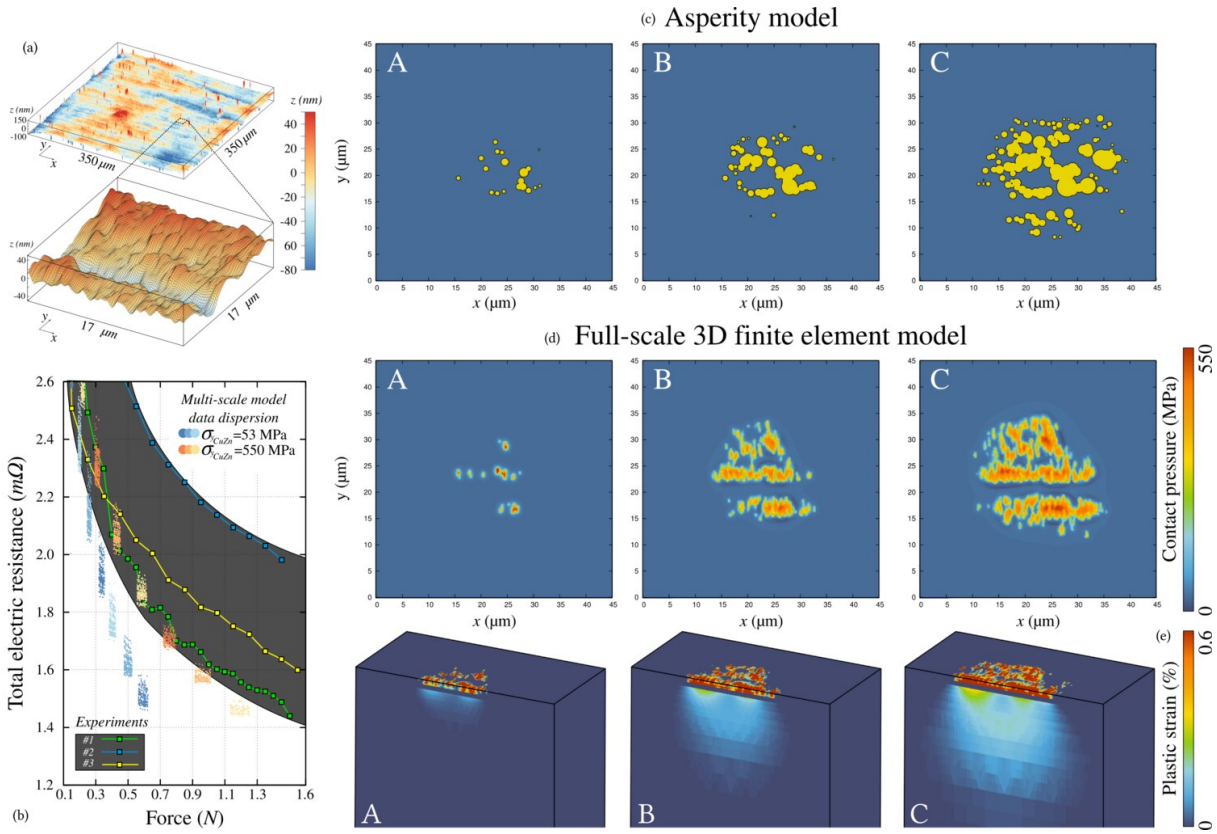

Figure 1.14: (a) a characteristic surface roughness of rolled brass after being electroplated with nickel and gold (AFM) which was used in (c) multi-scale model employing multi-asperity elasto-plastic contact model and (d-e) direct finite element analysis of mechanical contact, in (e) a cut through the substrate is shown to highlight plastic deformations of the brass; (b) contact resistance results of the three-level (multi-scale) model (clouds of points obtained in numerous simulations of rough surface locations) compared to experimental results (dashed area and three particular curves). Note that figures (c) and (d) cannot be compared directly because they do not correspond to exactly the same location on the rough surface. As seen in (e) nickel layer (thin line separating two plastically deformed media: gold coating and brass substrate) remains in elastic regime.

References

- [42] V.A. Yastrebov, G. Cailletaud, H. Proudhon, F.S. Mballa Mballa, S. Noël, Ph. Testé, F. Houzé. "Three-level multi-scale modeling of electrical contacts: sensitivity study and experimental validation". In Proceedings of the Holm 2015 61st IEEE Holm Conference on Electrical Contacts, pp. 414-422 (2015). [doi] [pdf]

- Presentation "Three-level multi-scale modeling of electrical contacts" constructed together with Georges Cailletaud and given by him at the 61st IEEE Holm Conference on Electrical Contacts, San Francisco, USA. 14 October, 2015 [pdf]

1.2.10 Greenwood's elliptic model

In a *simplified elliptic model* of rough contact recently suggested by James A. Greenwood [24] the asymptotic solutions obtained by the author are valid only for small values on Nayak's parameter $\alpha < 10$, which is not representative for real rough surfaces. We derived a better asymptotic solution valid for higher values of this parameter.

According to Greenwood's simplified elliptic model of rough surface contact, the true contact area fraction $A' = A/A_0$ and the mean pressure p_0 are given by the following equations, respectively

$$A' = \frac{\sqrt{\alpha}}{6} \int_{\hat{g}=0}^{\infty} \int_{\xi=s}^{\infty} P(\xi, \hat{g}) \frac{(\xi - \hat{s})}{\hat{g}} \, d\xi \, d\hat{g},$$

$$p_0 = \Omega \frac{2\alpha^{3/4}}{9\sqrt{\pi}} \int_{\hat{g}=0}^{\infty} \int_{\xi=s}^{\infty} P(\xi, \hat{g}) \frac{(\xi - \hat{s})^{3/2}}{\sqrt{\hat{g}}} \, d\xi \, d\hat{g},$$

where $\Omega = E^* \sqrt{m_2/\pi}$, $\hat{s} = s/\sqrt{m_0}$ is the normalized separation between the effective rough surface and a rigid flat, $\hat{g} = g/\sqrt{m_4}$ is the normalized geometric mean curvature, m_0 is the variance of roughness, m_2 is the variance of the roughness gradient, E^* is the effective elastic modulus, and $\alpha = m_0 m_4 / m_2^2$ is the Nayak's parameter with m_4 being the fourth spectral moment of the isotropic normal roughness. The joint probability of asperities with the summit at normalized elevation $\xi = z/\sqrt{m_0}$ and the normalized mean geometric curvature $\hat{g}$ was obtained by Greenwood as

$$P(\xi, \hat{g}) = \frac{9}{2\sqrt{2\pi}} \sqrt{\frac{\alpha}{\alpha - 1}} \, \hat{g}^3 \, \exp\left[-\frac{\alpha}{2(\alpha - 1)} \xi^2 + \frac{3\hat{g}^2}{2} \right] \operatorname{erfc}\left(3 \sqrt{\frac{(\alpha - 1)}{2(2\alpha - 3)}} \left\{ \hat{g} + \frac{\sqrt{\alpha}}{3(\alpha - 1)} \xi \right\} \right)$$

So it was shown by Greenwood that for large separations $\hat{s}$, the asymptotic solutions for pressure and area are given by

$$\hat{A} \sim \operatorname{erfc}(\hat{s}/\sqrt{2}), \quad \hat{p}_0 \sim \operatorname{erfc}(\hat{s}/\sqrt{2}), \tag{1.4}$$

After some algebra, we showed that the true asymptotics for high values of Nayak parameter α are given by the following expressions:

$$\boxed{A' \sim \sqrt{\alpha} \hat{s}^{3/2} \operatorname{erfc}(\hat{s}/\sqrt{2}), \qquad p_0 \sim \alpha^{3/4} \frac{\operatorname{erfc}(\hat{s}/\sqrt{2})}{\hat{s}}} \tag{1.5}$$

References

- Yastrebov, V.A. "Some observations on Greenwood's simplified elliptic model of rough contact", this short note is in a draft stage.

1.2.11 Size and material effects in indentation

The power law decay of the roughness power spectral density (PSD) is approximately preserved down to the sub-micron scale [44], where various *size effects* (Fig. 1.17) in material deformation become pronounced.

Therefore with Samuel Forest, and now in interaction with Vikram Phalke we studied size effects in normal deformation of small asperities. It is known that, contrary to sharp indenters which demonstrate

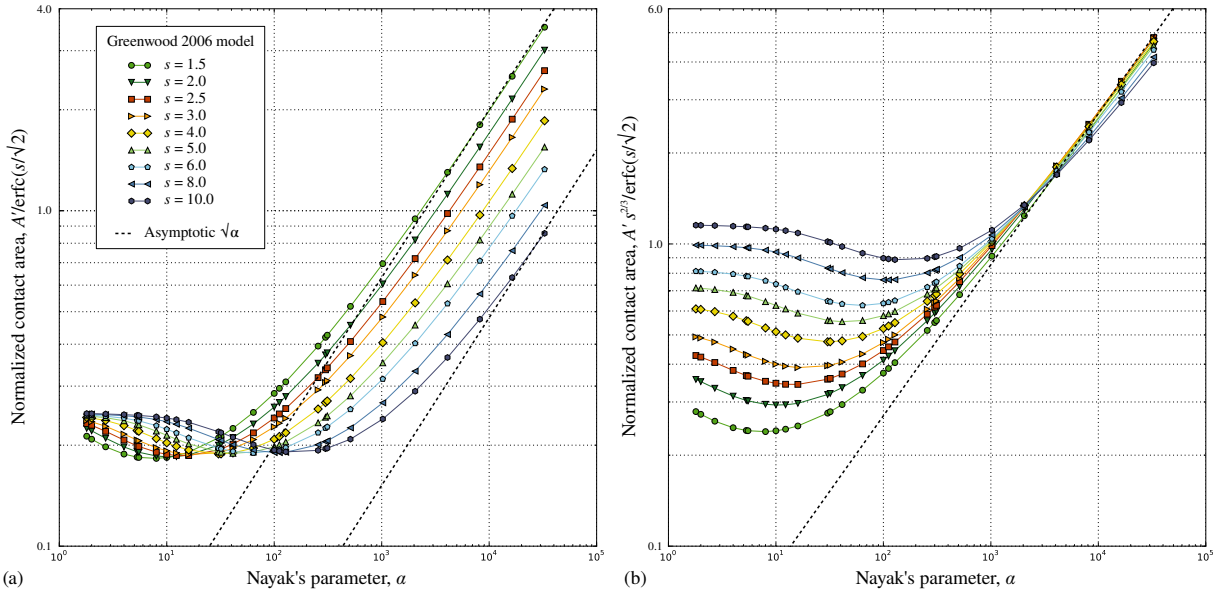

Figure 1.15: True contact area evolution with Nayak's parameter α as predicted by simplified elliptic model [24]: (a) classical normalization Eq. (1.4) [10, 24] valid only for small α and huge separations s, (b) new normalization Eq. (1.5) valid for big $\alpha > 1000$ and arbitrary separation s.

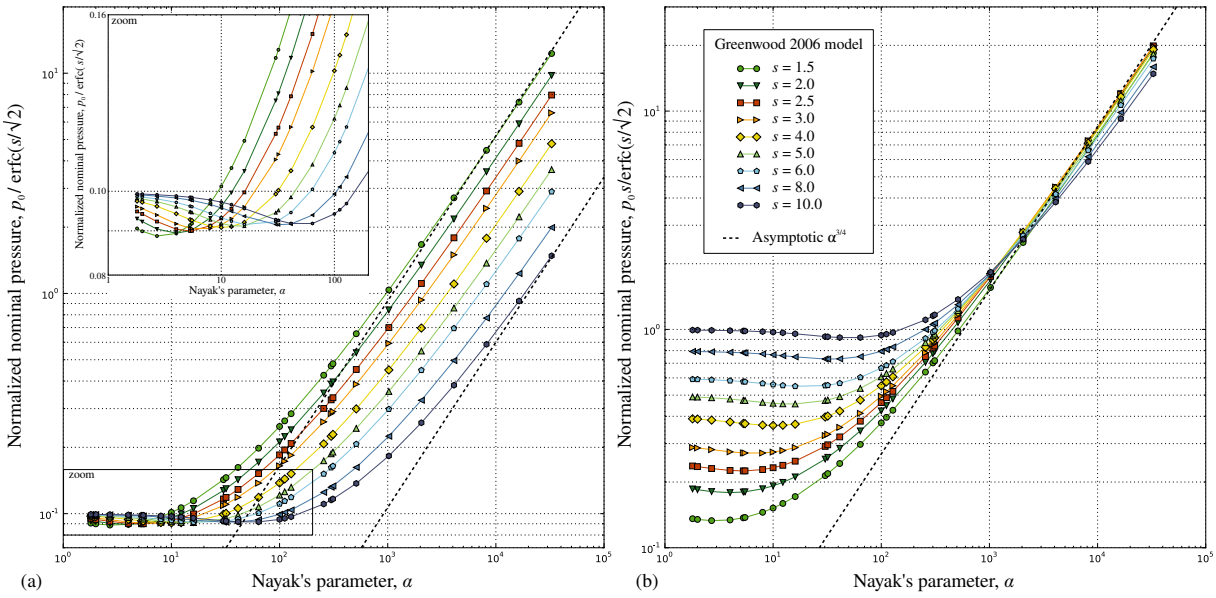

Figure 1.16: Nominal pressure evolution with Nayak's parameter α as predicted by simplified elliptic model [24]: (a) classical normalization Eq. (1.4) [10, 24] valid only for small α and huge separations s, in the inset zoom on the region of moderate α where the minimum value of the nominal pressure is reached; (b) new normalization Eq. (1.3.6) valid for big $\alpha > 500$ and reasonable separations $s < 6$.

different hardness for different penetration depths [45, 46], smooth indenters demonstrate the size effect with the radius of their curvature [47]:

$$\frac{H}{H_0} = \sqrt{1 + \frac{R_0}{R}},$$

where H is the material hardness for the indenter of radius R, H_0 is the macroscopic hardness and

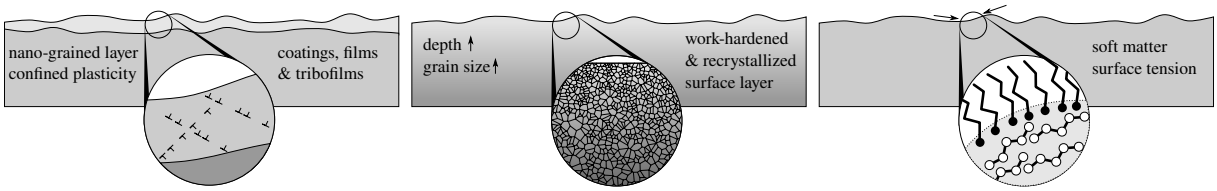

Figure 1.17: Various size effects justifying the difference between near surface small-scale contact and macroscopic or structural-scale contact: thin coatings, oxide layer, grain size due to work-hardening, surface energy.

R_0 is the characteristic curvature radius (material parameter). This size effect if not easy to capture in computational models, and our first attempt undertaken, in which we used Cosserat continuum in axisymmetric configuration, was unsuccessful. Rather expectedly, while varying elastic l_e and plastic l_p characteristic lengths [48] we could capture a saturated *small-scale* response, *large-scale* response and a smooth transition between them, but we could not show an increasing hardness for decreasing size of the indenter: the hardness $H = F/\pi a^2$ remained almost constant for all l_e and l_p. More specifically, both the nominal pressure F/R^2 and the relative contact radius a/R were shown to increase for a given indentation d/R under decreasing indenter radius R, however, their ratio F/a remains unchanged, see Fig. 1.18.

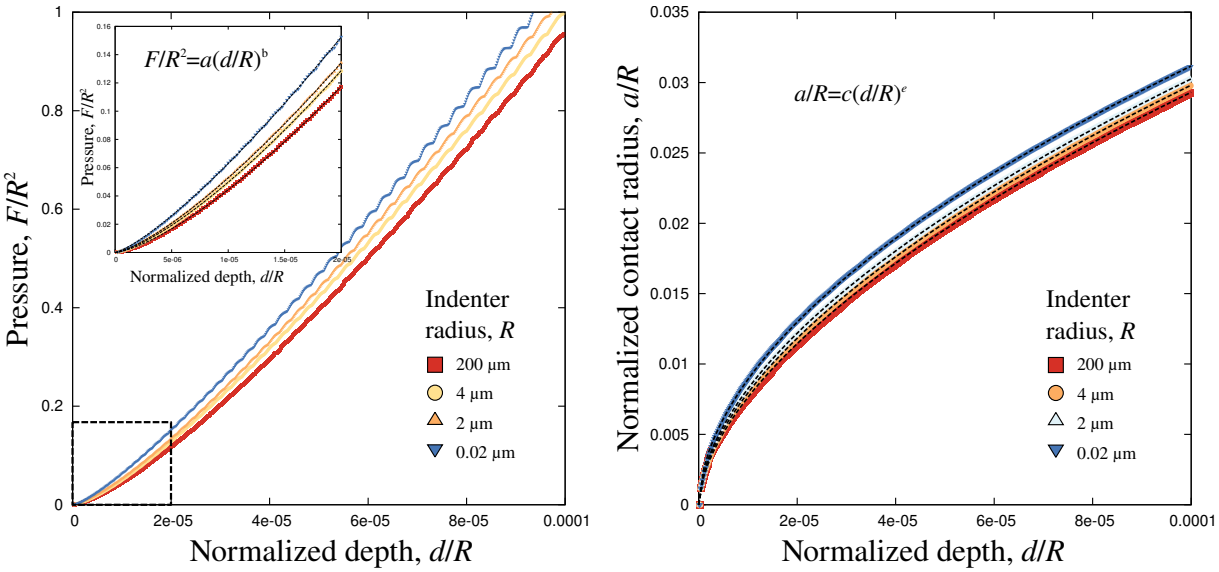

Figure 1.18: Normalized force-penetration and radius-penetration for a spherical indenter using Cosserat continuum.

Nevertheless, we could demonstrate a characteristic change in accumulation of plastic deformation: for smaller curvature radii the plastic deformation accumulates near the surface whereas for larger radii, the plastic accumulation follows a classical under-surface onset and plastic core growth. Currently we are working with more advanced gradient plasticity models with the objective to capture size effects in isotropic and homogeneous ($J2$) and in crystal plasticity. Another study on the indentation of a single crystal where experimental results were compared with finite element simulations could be mentioned here [49], however, my participation in this study was very marginal: I simply assisted Prajwal Sabnis in contact simulations of this indentation.

A simple empirical size-dependent model was created at the asperity scale and thanks to my multi-asperity framework with elastic interactions, I could solve indentation of rough surfaces by a spherical indenter (see Fig. 1.19). However, the lack of macroscopic plastic deformation in this study render it slightly artificial, so these results were not published.

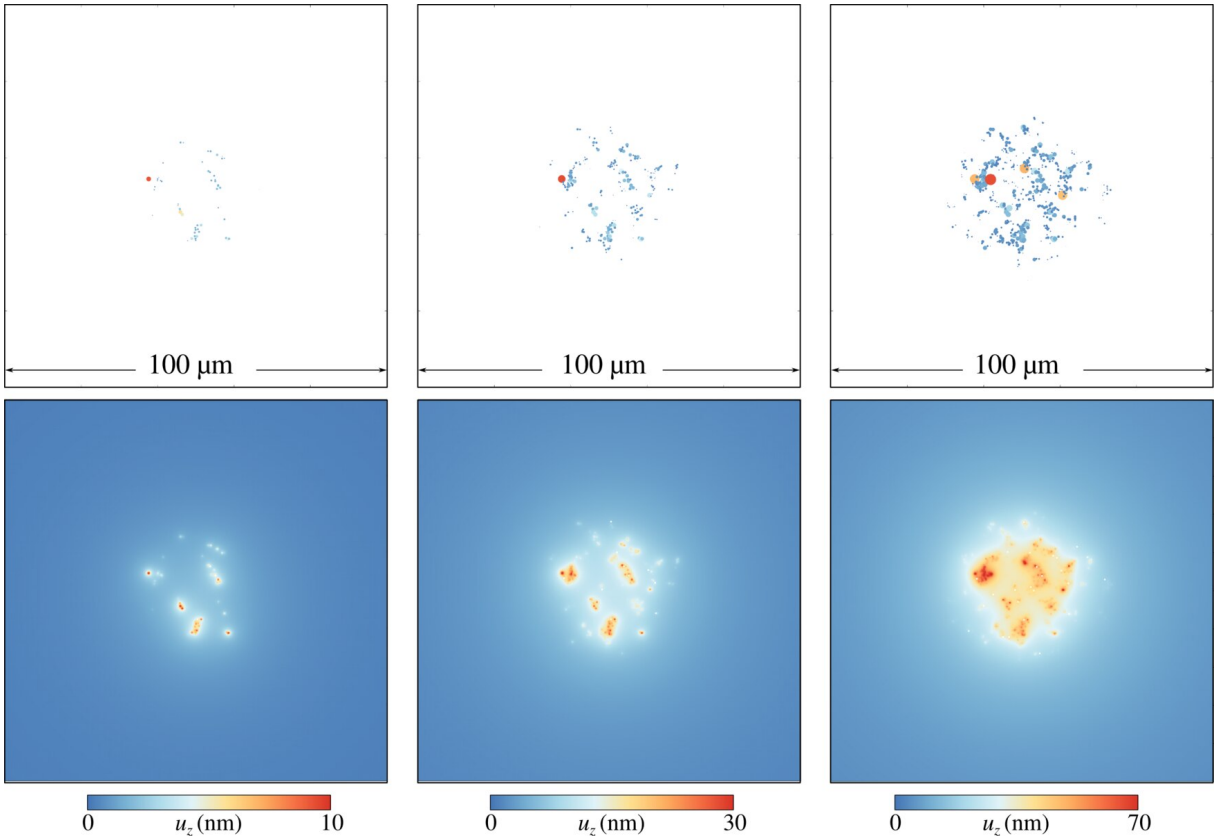

Figure 1.19: Deformation of a rough surface under spherical indentation taking into account size-dependent elasto-plastic deformation of elastically-interacting asperities: upper panel - view of contacting asperities, lower panel - total deformation of the substrate.

References

- [49] P. A. Sabnis, S. Forest, N. K. Arakere, V.A. Yastrebov. "Crystal plasticity analysis of cylindrical indentation on a Ni-base single crystal superalloy". International Journal of Plasticity, 51:200-217 (2013). Note: my participation to this study was very marginal. [doi] [pdf]
- V.A. Yastrebov, S. Forest "Mechanical contact between rough elastic-plastic solids: scale effect in deformation of asperities" In book of abstracts 52th SES technical meeting Texas A&M, College Station, USA, 25-29 October (2015). [pdf]

1.2.12 Model for electric-arc-induced damage in contactors

In the thesis of Aurélien Fouque we studied degradation of $AgSnO_2$ contactors under repetitive action of electric arcs. An intense experimental campaign carried out by Aurélien and Schneider Electric allowed us to measure to which extend the demixing is related to the arc power and duration, what is the shape of the crater, what is the maximal depth of melting pull, which is characterized by different recrystallized microstructure [50], what is the chemical composition of the near surface layer after the impact, etc. Long multi-arc experiments (up to 50 000 arcs) enabled us to follow the evolution of the demixed layer, which goes far beyond the maximal melting depth. Therefore, we deduced that the growth of the demixed silver layer must be accompanied with the silver transfer from one electrode to another. All these data was incorporated in a model which can handle:

- elasto-plastic contact with and without elastic interactions on realistic geometries,
- demixing of $AgSnO_2$,

- hardness dependence on the SnO_2 content,
- increased porosity of solidified $AgSnO_2$ and increased material loss due to projection of droplet of demixed Ag,
- topographical changes due to crater formation at a random point within the contact area of the previous contact,
- silver transfer from one contactor to another by debonding,
- final welding corresponding to a large enough contact area (the energy of the opener is below the one needed to break the weld).

The resulting model calibrated on experimental data could reproduce many aspects related to the deterioration of contactors leading to the ultimate welding. In this study, I followed the experimental campaign from a distance, but I took the lead in the development of the multiphysical model. In Fig. 1.20 one could see how the contact area, surface topography, as well as demixing on both electrodes, every 50th cycle is shown. In Fig. 1.21, one could see the cut through the multi-arc model showing the amount of demixed silver compared with SEM images after the same number of cycles, the maximal depth measured in simulations and experiments is also shown. Results of a parametric study are presented in Fig. 1.22.

References

- A. Fouque. Contribution à l'étude du couplage thermique-mécanique-électrique dans les contacts électriques : application à l'élaboration d'un modèle de durée de vie d'un contacteur. PhD thesis, Paris-Saclay University (2020). PhD advisors: G. Cailletaud, V. Esin (MINES ParisTech) & F. Houzé, , Ph. Testé, R. Landfried (GeePS, CentraleSupélec) in collaboration with Schneider Electric represented by A. Bonhomme, M. Lisnyak, J.L. Ponthenier [pdf]

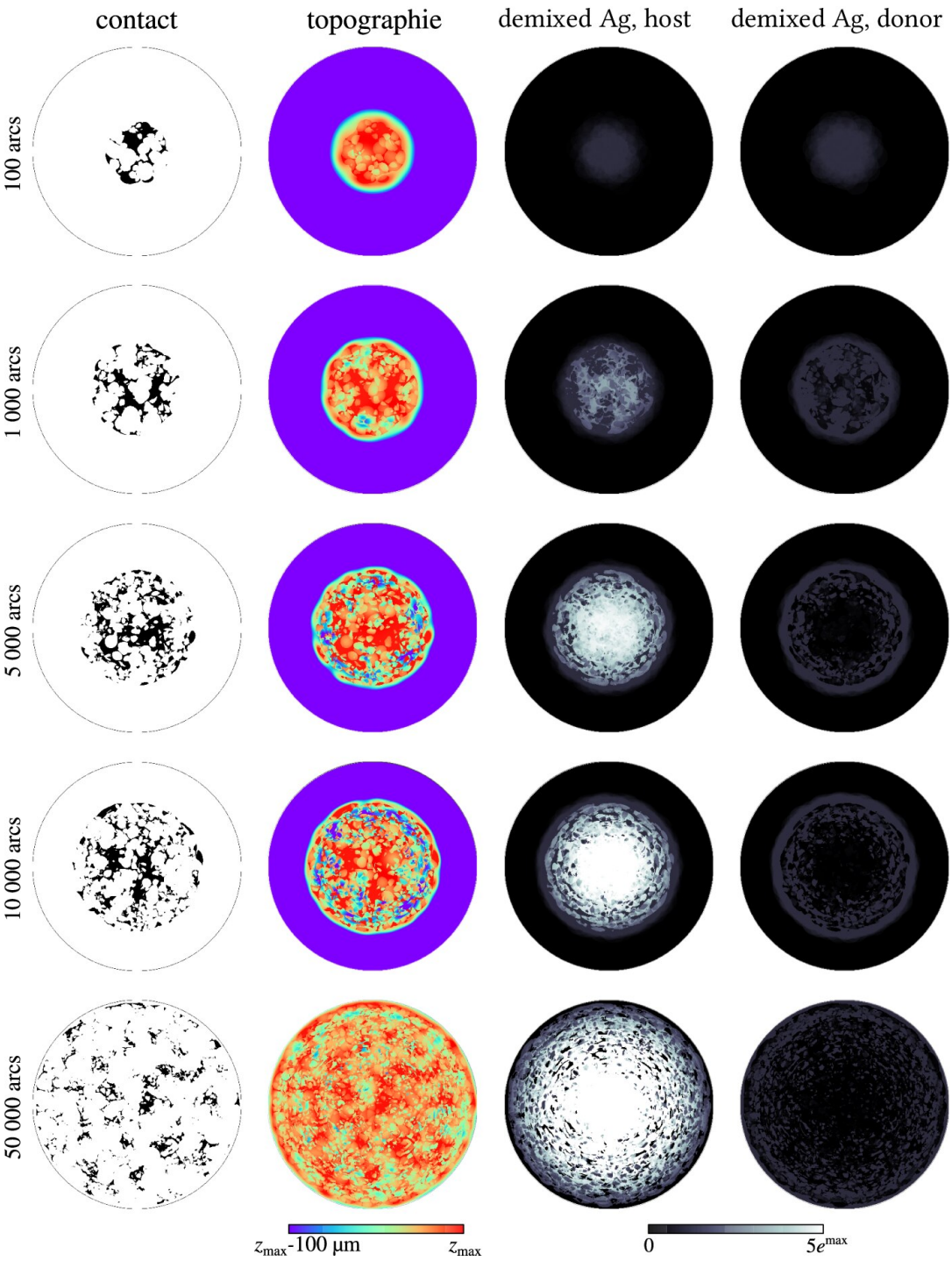

Figure 1.20: Results of the multi-arc demixing model, from left to right: contact area, effective surface topography, demixed silver on the host-electrode and on the donor-electrode.

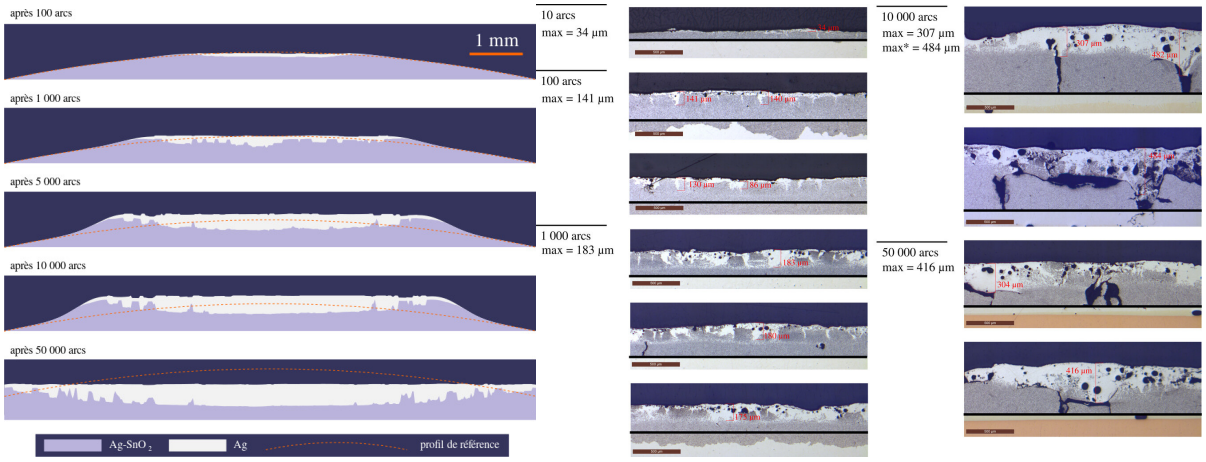

Figure 1.21: *On the left* – cut through a model showing the topography and the amount of demixed silver after different number of arc's impacts, *on the right* – experimental images (SEM) showing the demixing of the silver in one of electrodes after different number of arc's impacts.

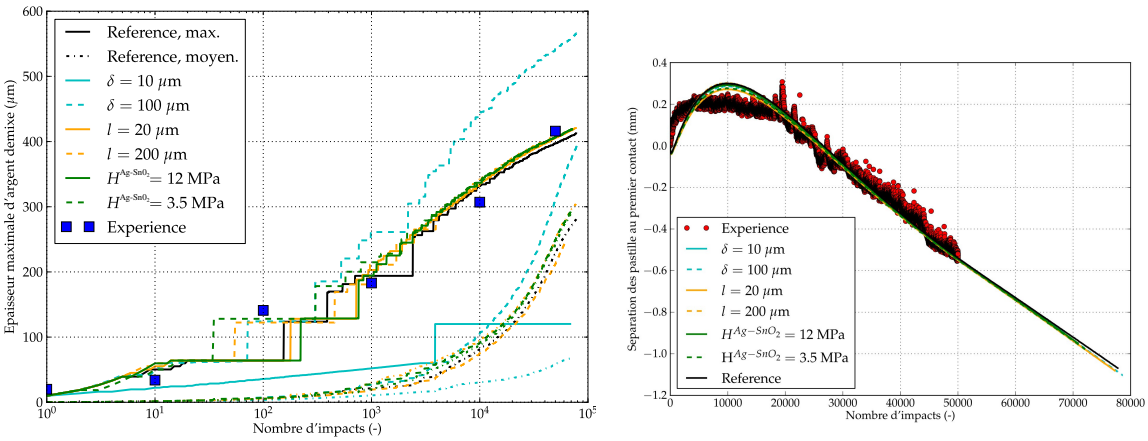

Figure 1.22: A parametric study demonstrating how the maximal silver penetration depth evolves with the number of arcs: (left) – experimental data and model prediction for different parameters are shown, (right) – evolution of the distance between two closed electrodes under the same squeezing force demonstrates the initial material swelling (due to induced porosity) and further material loss (due to the decrease of viscosity in the pure silver liquid phase).

1.3 Friction & wear

1.3.1 Sliding in frictional interfaces: stability and regularization

Being inspired by experiments [51] of Jay Fineberg's group, in our early study [52] with David S. Kammer using velocity weakening friction law, we reproduced some experimental results, identified directionality effect and looked for an energetic criterion for slip propagation. At the same time, we questioned the validity of supersonic slip propagation which we observed in our numerical simulations, for more discussion on this topic, the reader is referred to Section on supersonic slip pulses.

Finally, we discovered that the validity of the obtained results could demonstrate a strong dependence on the mesh density [53, 54, 55]. Therefore, we carried out a more fundamental study [56] on a deformable-rigid configuration using Prakash-Clifton regularization [57] for Coulomb's friction law:

$$\dot{\tau} = -\frac{|v| + v_0}{L}(\tau - \mu p),$$

where τ is the limit frictional traction, v is the slip velocity, v_0 is a reference velocity, L is the characteristic regularization length, μ is the coefficient of friction and p is the contact pressure assumed positive in contact. We studied the effect of the mesh density h and regularization length L on the convergence of slip events triggered by elliptic spatio-temporal pressure drop inspired from [55]. All triggered slip pulses eventually died.

The main result of this study are the following. We first confirmed that mesh-converged solutions are achievable in the stable regime (for friction coefficients smaller than one, see [58]) of the considered problem without any numerical damping in the bulk. We delimited a mesh-convergence map with respect to the characteristic length L of the Prakash-Clifton friction law (see Fig. 1.24). This map confirmed that mesh-converged solutions for smaller lengths L need finer mesh discretizations. In addition to the mesh convergence, we discovered a convergence of the solution with respect to the characteristic length L itself. Considering a given slip event, a critical characteristic length L_c exists, such that $\forall L : L < L_c$, the slip behavior of the interface remains the same. To confirm and explain this observation, we analyzed the regularization's effect on a range of temporal frequencies of the frictional strength. The damping of low frequencies, which are the essential part of the slip event, becomes vanishingly small for small characteristic lengths and no longer influences the propagation of the interface rupture. This insight enables the definition of a theoretical domain $L > L_c$ of influence of the Prakash-Clifton friction law with respect to the characteristic length of the regularization and the frequency content of the slip event. Outside of this domain $L < L_c$, the damping of the slip event's frequencies becomes negligible and the interface rupture propagates as if it was governed by Coulomb's friction law despite the presence of the regularization. In conclusion, the presented results suggest that the experimental determination of the physical length scale L_{ph} of the Prakash-Clifton friction law requires the temporal power spectrum density of the analyzed slip event to contain enough energy in the high-frequency domain. We therefore proposed a verification procedure for the slip event's frequency content, which is crucial to a successful determination of L_{ph}, because if the propagation of slip is fully determined by frequencies below a critical value, the real physical length scale L_{ph} of the Prakash-Clifton friction cannot be measured. The observed length scale instead would correspond to the critical length L_c, which could be significantly higher than the physical length scale L_{ph}.

References

- [52] D.S. Kammer, V.A. Yastrebov, P. Spijker, J.F. Molinari. "On the propagation of slip fronts at frictional interfaces". Tribology Letters, 48(1):27-32 (2012). [doi] [arXiv] [pdf]
- [56] D.S. Kammer, V.A. Yastrebov, G. Anciaux, J.F. Molinari. "The existence of a critical length scale in regularised friction". Journal of the Mechanics and Physics of Solids, 63:40-50 (2014). [doi] [arXiv] [pdf]

1.3.2 Slip stability under non-uniform pressure distribution

A slip-weakening friction law can be seen as a simplified form of a generalized "rate and state" law. The former simplified form allows to make a direct link with the linear elastic fracture mechanics [59, 60, 61].

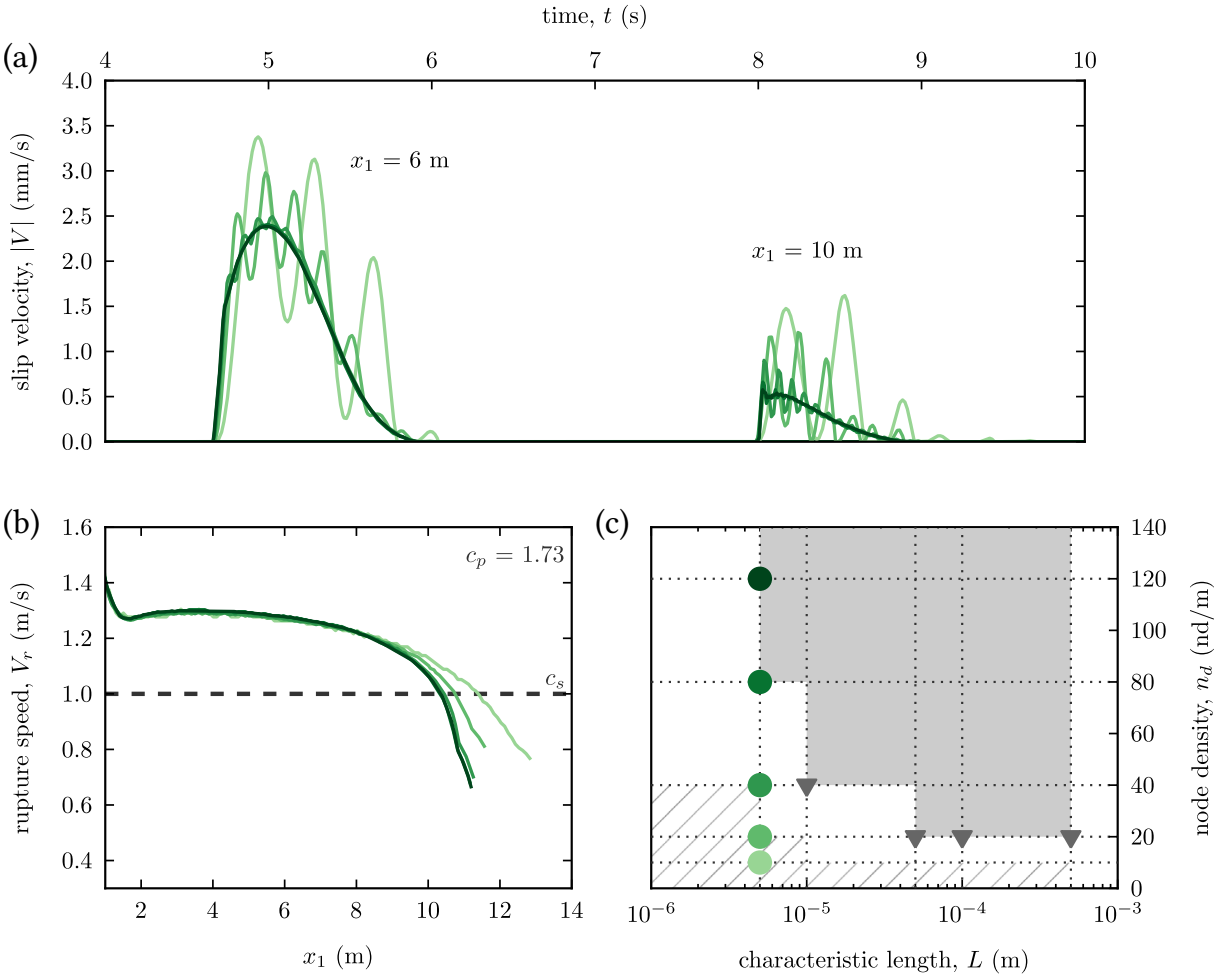

Figure 1.23: Illustration of mesh convergence for a frictional interface rupture with simplified Prakash-Clifton regularization $L = 5$ μm and $v_0 = 100$ μm/s. (a) The evolution of the slip velocity over time is shown at two positions. (b) The rupture speed change along the propagation distance x_1. (c) The convergence map in the $L - n_d$ plane (n_d is the mesh density) indicates the zone of mesh-converged (gray area) whereas within the hatched area the results are considered to be non-converged. The circles designate the simulations presented in (a) and (b). The triangles mark mesh-converged simulations for different L.

This analogy makes it possible to study the stability/instability of the sliding front propagation via the well-known fracture mechanics methods, i.e. by comparing the energy release rate G with its critical value G_c. The energy release rate $G(x)$ of the frictional front depends on the external loading as well as on the residual stresses in the slip zone. As for G_c, it is proportional to the local contact pressure $G_c(x) \sim p(x)$. Until recently the studies focused on the uniform pressure, i.e. on the constant critical energy release rate, like in classical fracture mechanics, with some notable exceptions [62, 63]. In my recent study, under the "small scale yielding" (SSY) assumption [64], I managed to derive [65], under moderate and controllable assumptions, some fairly accurate results for two model pressure distributions (a) parabolic pressure profile:

$$\sigma(x) = \sigma_0 + \kappa x^2/2$$

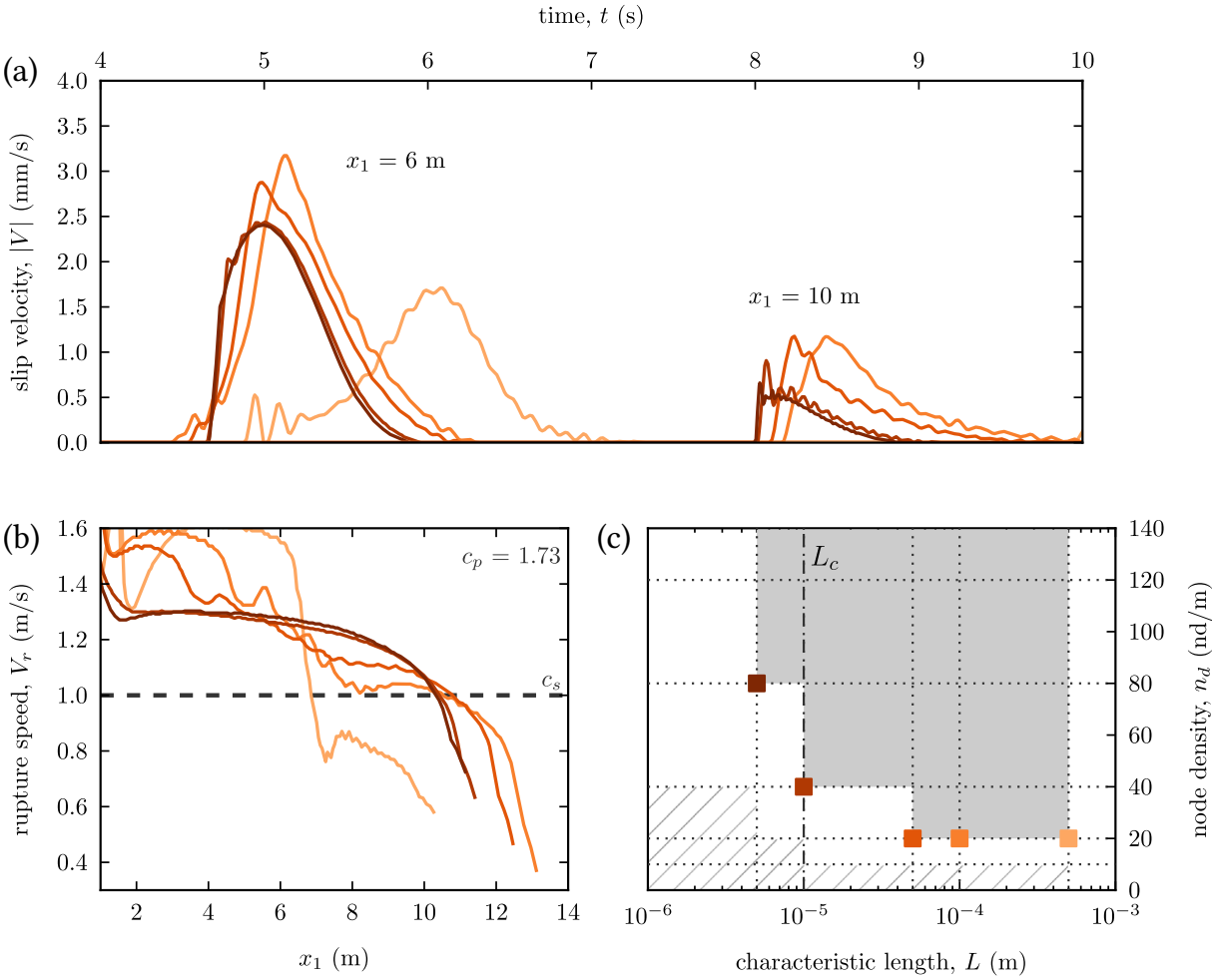

Figure 1.24: The slip velocity in (a) and the rupture speed in (b) of *mesh-converged simulations* are shown for different characteristic lengths L. As one can see, both the morphology of the slip profile and the velocity of the slip front vary with the length L however the further mesh refinement does not change these results. (c) The squares indicate the mesh density n_d and characteristic length L of the simulations presented in (a) and (b). All shown results are in the mesh-converged area of the $L - n_d$ plane. L_c marks the critical characteristic length of the simplified Prakash-Clifton friction law for the presented interface rupture, below which all converged simulations have the same global and local behavior.

and (b) localized pressure valley:

$$\sigma(x) = \sigma_0 + \begin{cases} 8\Delta\sigma\left(\dfrac{x}{\lambda}\right)^2 & , \text{ if } |x| \le \lambda/4 \\ \Delta\sigma\left(\dfrac{8|x|}{\lambda} - \dfrac{8x^2}{\lambda^2} - 1\right) & , \text{ if } \lambda/4 < |x| \le \lambda/2 \\ \Delta\sigma & , \text{ if } |x| > \lambda/2. \end{cases}$$

I have studied many slip scenarios in the case of an isolated valley (stable-instable, stable-instable-stable, etc.) for parameters relevant for geological faults (see Fig. 1.25). Among other analytical results, I derived the minimum value of the pressure σ_0 needed to trigger the unstable slip for a given curvature:

$$\frac{\sigma_0}{\mu} > \left[\frac{3(f_s - f_k)^2}{8\pi^2 f_k} \cdot \frac{\kappa d_c^2}{(1-\nu)^2\mu} \cdot \frac{(2f_k + f_0)^2}{(f_0 - f_k)^5}\right]^{1/3},$$

where μ is the shear modulus, ν is the Poisson's ratio, f_s, f_k are static and kinetic coefficients of friction, d_c is the characteristic slip-weakening distance. The arrest length for a parabolic valley was found to be:

$$a_s \approx 4\sqrt{\frac{\sigma_0(f_0 - f_k)}{5\kappa f_k}} - \frac{(f_s - f_k)d_c}{\pi(1-\nu)(f_0 - f_k)^2} \cdot \frac{\mu}{\sigma_0},$$

I have also obtained an interesting result making a link between the macroscopic shear load rate $\dot{\tau}_0 = \sigma_0 \dot{f}_0$ and the crack-arrest rate $\dot{a}_s$:

$$\frac{\dot{a}_s}{\dot{\tau}_0} \approx \sqrt{\frac{4}{5\sigma_0\kappa f_k(f_0^0 + \dot{f}_0 t)}} + \frac{2(f_s - f_k)d_c}{\pi(1-\nu)(f_0^0 + \dot{f}_0 t)^3} \cdot \frac{\mu}{\sigma_0^2}$$

This equation allows to estimate the stable slip front advancement at geological scales as well as at the lab scales. For example, for the frictional experiments of Fineberg's group [51], the *stable* crack advancement rate compared to the rigid loading rate is given by

$$\frac{\dot{a}_s}{\dot{u}} \approx 10^7 \frac{1}{\sqrt{\kappa}} \left[\frac{\mathrm{Pa}^{1/2}}{\mathrm{m}^{1/2}}\right]$$

Suggesting that for small systems, even for a very slow loading $\dot{u} \ll c_s$, where c_s is the transverse load speed, the local stable slip can be hardly distinguishable from a dynamic one and can be even supersonic. This result clearly explains the puzzling "slow slip events" obtained by the experimentators and also observed at geological scales [66, 51].

Version française: Une loi de frottement qui s'adoucit avec la distance de glissement peut être vue comme une forme simplifiée d'une loi de "rate and state" généralisée. L'avantage de la première est qu'un lien avec la mécanique linéaire de la rupture s'établit directement [59, 60, 61]. Cela permet donc d'étudier la stabilité/instabilité de la propagation du front de glissement via des méthodes établies de la mécanique de la rupture en comparant le taux de la restitution d'énergie G avec sa valeur critique G_c. Le taux de restitution d'énergie $G(x)$ dépend du chargement externe ainsi que des contraintes résiduelles dans la zone de glissement. Quant à G_c, il est proportionnel à la pression de contact locale $G_c(x) \sim p(x)$. Jusqu'à récemment les seuls cas étudiés sont à pression uniforme, avec quelques exceptions notables [62, 63]. Dans mon étude récente, sous l'hypothèse de SSY [64] ("small scale yielding") j'ai réussi à dériver quelques résultats assez précis pour (1) la longueur de déstabilisation et (2) la distance d'arrêt de glissement, pour une distribution de pression (a) parabolique et (b) du type vallée isolée de pression (cf. Fig. 1.25). En outre, j'ai étudié de nombreux scénarios de glissement dans le cas d'une vallée isolée (stable-instable, stable-instable-stable, etc) et j'ai déduit la valeur minimale de pression σ_0 nécessaire pour déclencher le glissement instable :

$$\frac{\sigma_0}{\mu} > \left[\frac{3(f_s - f_k)^2}{8\pi^2 f_k} \cdot \frac{\kappa d_c^2}{(1-\nu)^2\mu} \cdot \frac{(2f_k + f_0)^2}{(f_0 - f_k)^5}\right]^{1/3}.$$

Tous ces résultats font le lien entre plusieurs paramètres de frottement (coefficients statique f_s et dynamique f_k, longueur caractéristique d'adoucissement d_c), la distribution de pression (valeur minimale σ_0, largeur de la vallée λ, courbure κ), et l'élasticité des corps (module de cisaillement μ). Ces résultats sont intéressants pour la physique des séismes car ils permettent d'analyser des scénarios de glissement dans des failles avec une hypothèse de distribution de pression plus élaborée que celle qui était considérée jusqu'à présent. En outre, mes résultats suggèrent une nouvelle interprétation des "slow slip" découverts par l'équipe de Fineberg [67, 51]. La finalisation de l'article cité ci-dessous nécessite encore quelques calculs analytiques qui n'ont pas encore été achevés.

References

- [65] Yastrebov, VA. "Slip propagation along slip-weakening interfaces with a non-uniform contact pressure distribution" (2021). Draft is available [encrypted pdf]
- Presentation "Slip propagation at interfaces with a non-uniform contact pressure distribution", CECAM Workshop "Modeling tribology: friction and fracture across scales". Lausanne, Switzerland. January 29, 2019 [pdf]

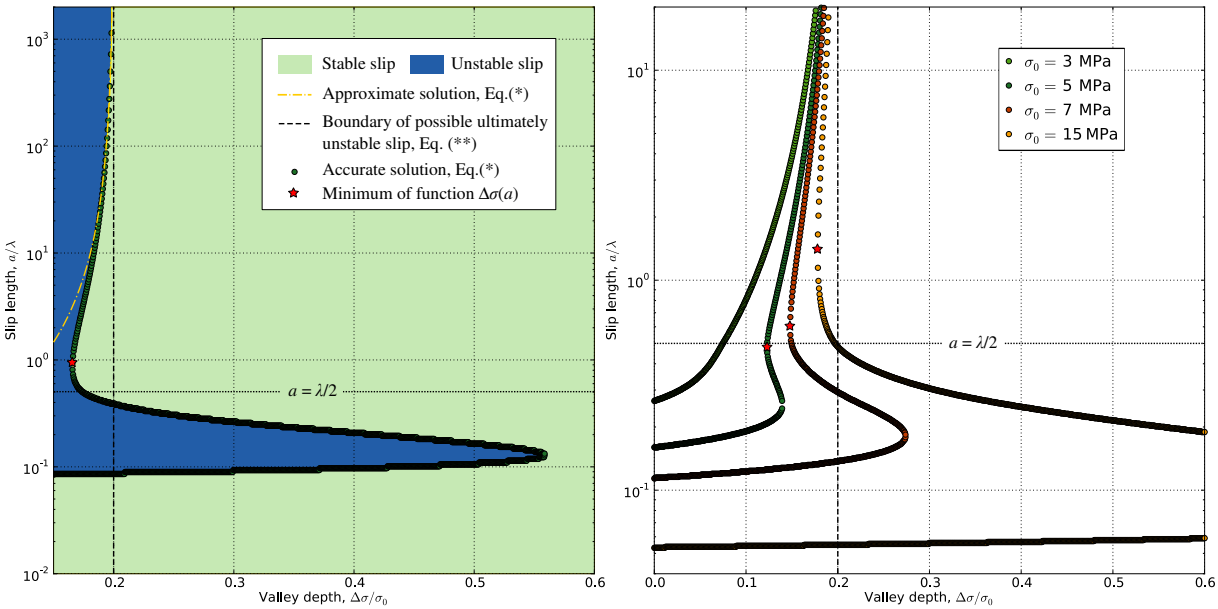

Figure 1.25: Slip stability map in the contact interface with a pressure valley located in the λ interval of depth $\Delta\sigma$ for different valley pressures σ_0. The blue and green zones determine possible slip lengths in unstable and stable regimes, respectively.

Version française: Carte de stabilité du glissement dans l'interface de contact avec une vallée de pression localisée dans l'intervalle λ de profondeur $\Delta\sigma$ et de pression minimale σ_0. Les zones bleue et verte déterminent des longueurs de glissement possible dans des régimes instables et stables respectivement.

1.3.3 Opening waves: sliding without slipping

In a theoretical study that combines analytical calculations and dynamic finite element simulations with implicit integration, I explored the complex phenomenon of sliding of an elastic layer (E, ν, rho) of height H on a rigid substrate with an interface governed by a Coulomb's friction law with a friction coefficient f. In finite systems, the elasto-dynamic slip under the action of frictional forces is strongly coupled to the propagation of elastic waves in the system which serves as a wave-guide and ensures their dispersive propagation [68]. By reducing the infinite system to a periodic system with period L, and introducing the notation $r = H/L$ the uniform sliding stability can be determined by solving the transcendental equation:

$$\begin{aligned} & f\left[\sin(2\pi\kappa_d Kr) + \kappa_s\kappa_d \sin(2\pi\kappa_s Kr)\right]\left(-2\kappa_d\kappa_s \sin(2\pi\kappa_d Kr) + (\xi^2 + \gamma^2\kappa_d^2)\sin(2\pi\kappa_s Kr)\right) - \\ & - f\kappa_s\kappa_d\left[\cos(2\pi\kappa_d Kr) - \cos(2\pi\kappa_s Kr)\right]\left(2\cos(2\pi\kappa_d Kr) + (\xi^2 + \gamma^2\kappa_d^2)\cos(2\pi\kappa_s Kr)\right) + \\ & + i\kappa_d\left[2 + \xi^2(\kappa_s^2 - 1)\right](\cos(2\pi\kappa_d Kr)\sin(2\pi\kappa_s Kr) + \kappa_s\kappa_d\cos(2\pi\kappa_s Kr)\sin(2\pi\kappa_d Kr)) = 0 \end{aligned} \tag{1.6}$$

with

$$\kappa_d = \sqrt{k_d^2/k^2 - 1}, \quad \kappa_s = \sqrt{k_s^2/k^2 - 1}, \quad k = 2\pi K/L, \quad \xi = \frac{2\nu}{(1-2\nu)}, \quad \gamma = \sqrt{\frac{2(1-\nu)}{1-2\nu}},$$

The numerical solution of this equation shows that uniform sliding in a finite size system is always unstable, but it also predicts the velocity of stick-slip fronts that form due to this instability, which compares well with the numerical results. Numerically, we have also shown that the macroscopic friction depends on the imposed slip velocity, even if locally the Coulomb friction law does not depend on the velocity! This interesting result confirms the analytical calculation of G.G. Adams [69] by transposing it to finite size systems. This theoretical part has not been published yet, but I hope to restart this work very soon.

When the friction coefficient is very high (above 1), the sliding regime differs greatly from the local stick-slip regime. It is distinguished by the emergence of opening waves that allow macroscopic sliding almost without friction [70], a theoretical phenomenon that attracted a particular attention of the fracture mechanics community at some point [71, 72, 73] but, as it seems to me, was forgot for a while. On the other hand, these opening waves are different from Schallamach waves and they propagate at intersonic speeds in the interface. In this scenario the released elastic energy transforms almost entirely into elastic waves and allows the body to "jump" into a deformed configuration that is antisymmetric with respect to the sliding onset configuration to adhere again. This "jump" reverses the direction of the frictional force which thus becomes macroscopically *"negative"* (!) (cf. Fig. 1.26). These unusual results, which echo other theoretical results [74, 75], await their experimental verification. The confirmation of this process will allow the optimization of friction-based systems and better understanding of slip dynamics.

Version française: Dans une étude théorique qui combine des calculs analytiques et des simulations par éléments finis dynamique avec l'intégration implicite, j'explore le phénomène complexe de glissement d'une couche élastique (E, ν, rho) de hauteur H sur un substrat rigide avec une interface gouvernée par une loi de Coulomb avec un coefficient de frottement f. Dans des systèmes de taille finie, le glissement élasto-dynamique sous l'action des efforts de frottement est fortement couplé à la propagation des ondes élastiques dans le système qui sert de guide d'ondes et assure la propagation dispersive [68]. En réduisant le système infini à un système périodique avec une période L, et en introduisant la notation $r = H/L$ la stabilité de glissement uniforme peut être déterminée en résolvant l'équation transcendante :

$$\begin{aligned} & f\left[\sin(2\pi\kappa_d Kr) + \kappa_s\kappa_d \sin(2\pi\kappa_s Kr)\right]\left(-2\kappa_d\kappa_s \sin(2\pi\kappa_d Kr) + (\xi^2 + \gamma^2\kappa_d^2)\sin(2\pi\kappa_s Kr)\right) - \\ & - f\kappa_s\kappa_d\left[\cos(2\pi\kappa_d Kr) - \cos(2\pi\kappa_s Kr)\right]\left(2\cos(2\pi\kappa_d Kr) + (\xi^2 + \gamma^2\kappa_d^2)\cos(2\pi\kappa_s Kr)\right) + \\ & + i\kappa_d\left[2 + \xi^2(\kappa_s^2 - 1)\right](\cos(2\pi\kappa_d Kr)\sin(2\pi\kappa_s Kr) + \kappa_s\kappa_d\cos(2\pi\kappa_s Kr)\sin(2\pi\kappa_d Kr)) = 0 \end{aligned} \tag{1.7}$$

avec

$$\kappa_d = \sqrt{k_d^2/k^2 - 1}, \quad \kappa_s = \sqrt{k_s^2/k^2 - 1}, \quad k = 2\pi K/L, \quad \xi = \frac{2\nu}{(1-2\nu)}, \quad \gamma = \sqrt{\frac{2(1-\nu)}{1-2\nu}},$$

La résolution numérique de cette équation montre que le glissement uniforme dans un système de taille finie est toujours instable, mais elle prédit également la vitesse des fronts de "stick-slip" qui se forment à cause de cette instabilité, qui se compare bien avec les résultats numériques. Numériquement, nous avons également montré que le frottement macroscopique dépend de la vitesse de glissement imposée, même si localement la loi de frottement de Coulomb ne dépend pas de la vitesse ! Ce résultat intéressant confirme le calcul analytique de G.G. Adams [69] en le transposant aux systèmes de taille finie. Cette partie théorique n'a pas encore été publiée, mais j'espère poursuivre ce travail très bientôt.

Quand le coefficient de frottement est très élevé, le régime de glissement diffère beaucoup du régime de stick-slip habituel. Il se distingue par l'émergence d'ondes d'ouverture qui permettent de glisser macroscopiquement presque sans frotter [70]. Par contre, ces ondes d'ouverture sont différentes des ondes de Schallamach et elles se propagent à des vitesses intersoniques dans l'interface. Dans ce scénario l'énergie élastique libérée se reporte presque entièrement dans les ondes élastiques et permet au corps de "sauter" dans une configuration déformée antisymétrique par rapport à la configuration du début de glissement pour y adhérer de nouveau. Ce "saut" inverse la direction de la force de frottement qui devient donc macroscopiquement "négative" (cf. Fig. 1.26). Ces résultats insolites, qui font écho avec d'autres résultats théoriques [74, 75], attendent leur vérification expérimentale. La confirmation de ce processus permettra d'optimiser des systèmes basés sur le frottement, par exemple des freins.

References

- [70] V.A. Yastrebov. "Sliding without slipping under Coulomb friction: opening waves and inversion of frictional force". Tribology Letters, 62(1):1-8 (2016) [doi] [arXiv] [pdf]
- V.A. Yastrebov "Elastodynamic Friction" presentation from the course "Contact Mechanics and Elements of Tribology" (seminar lecture) [pdf]

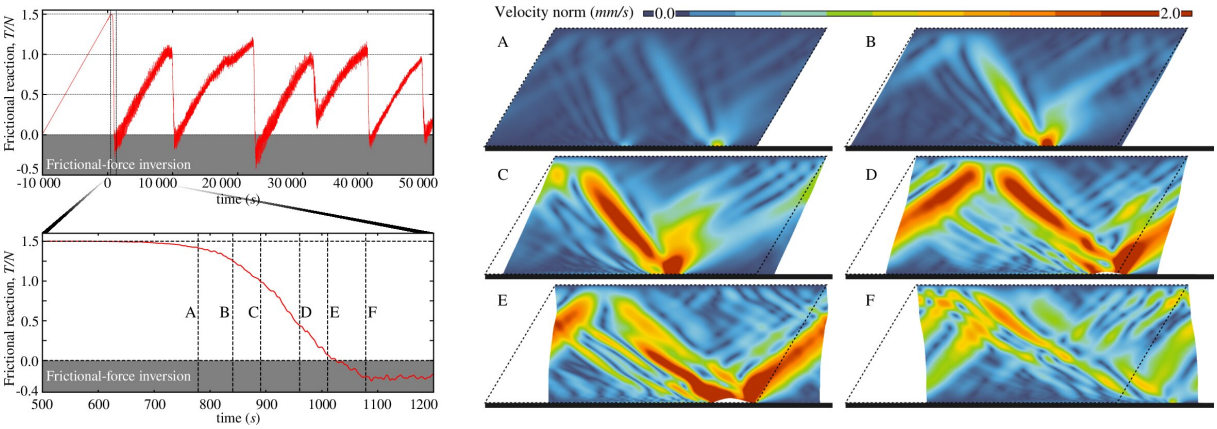

Figure 1.26: Inversion of the frictional force with time and emergence of opening waves in the interface (displacements are magnified by a factor of 150).

Version française: Changement de signe de la force de frottement au cours du temps et émergence des ondes d'ouverture dans l'interface (les déplacements sont multipliés par un facteur 150).

1.3.4 Supersonic slip pulses in Coulomb's driven frictional interfaces

In his brilliant paper G.G. Adams [69] studied the possibility of radiation of bulk waves by an isolated slip pulse propagating under classical Coulomb's friction law at the interface between an elastic half-plane and a rigid plane. Naturally, the trace speed of these bulk waves in the interface are supersonic, i.e. the slip front propagates as supersonic velocity $c > c_p$. This result causes questions on the causality of such theorized events. This interesting result inspired our interest and with David S. Kammer, and since recently with his group at ETHZ, we started to study numerically the possibility to initiate self-sustained supersonic slip pulses in such frictional interfaces. In reality, the slip velocity of such pulses is only marginally higher than the longitutidal wave speed c_p and strongly depends on the Poisson's ratio ν, the directionality of the triggering event, and the whole system dynamics is strongly affected by the proximity of the stress state in the interface to the frictional limit $0 \leq |\tau|/(\mu p) < 1$. Currently, apart from the theoretical study of related slip pulses, we could demonstrate that in some scenarios the slip propagation is unstable regardless the fact of being in theoretically stable regime for a uniform slip ($\mu < 1$, see [58]), the Prakash-Clifton regularization slows down the frictional pulses thus preventing from obtaining a mesh converged and supersonic pulses at the same time. Nevertheless, some numerical results (Fig. 1.27) for particular configurations make us hope that supersonic slip pulses in semi-infinite systems can exist in absence of wave-guide modes and without the influence of reflected waves hitting the interface. The work continues.

1.3.5 Multiscale simulation of hardmetal interaction with rocks

In the framework of NEXT-DRILL project, with Georges Cailletaud, Charlie C. Li and Alexandre Kane we supervised PhD project of Dmitry Tkalich. The origin of the wear of hardmetal inserts in rotary-percussive hard-rock drilling is a puzzling phenomenon. We suspect that this wear cannot be explained by abrasive interaction with rock debris, but rather by a friction-induced tensile stress state on the leading edge of hardmetal insert during the oblique impacts of the rock [76]. We carried out multi-scale finite element simulation including (see Fig. 1.28):

- accurate full-field microstructural representation of the hardmetal (WC/binder) for different volume fraction of the binder,
- calibration of the mean-field β-model [77] on various monotonic loadings of full-field microstructures with Drucker-Prager model for WC grains and $J2$ plasticity for the binder,
- full-scale simulation of a frictional oblique impact of a hardmetal insert using mean-field β-model at every Gauss point of the insert and an elastic rock Behavior,

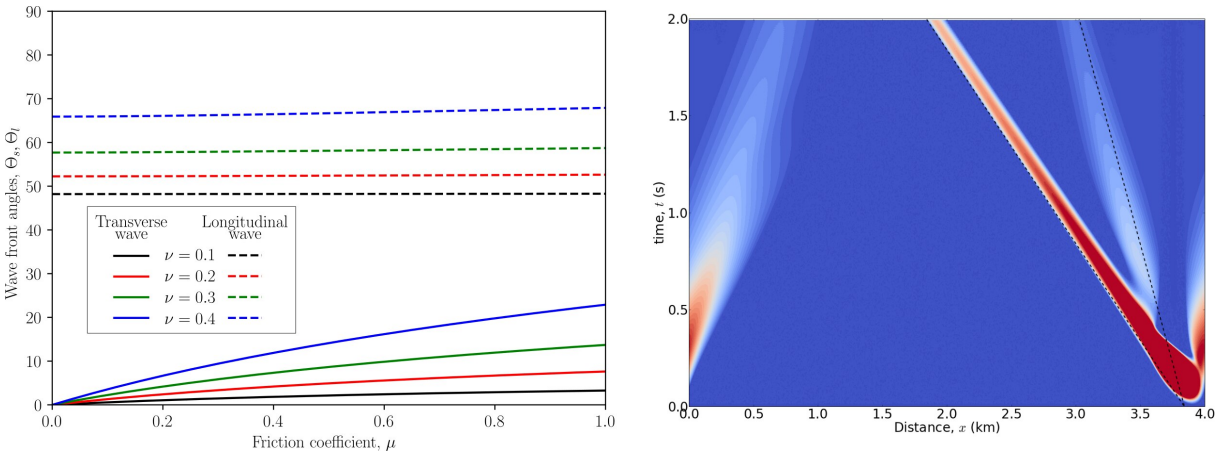

Figure 1.27: *(left)* – Adams' solution for the inclination angle of radiated bulk waves demonstrating that their trace speed increases with the coefficient of friction and with the Poisson's ratio, *(right)* – simulation results (for periodic BC) for supersonic triggering event demonstrating an emerging self-sustained slip pulse propagating at the longitudinal wave speed in the direction opposite to the shear direction ($\mu = 0.2$, $\nu = 0.4$), still it is not a supersonic pulse.

- loading trajectory recovered in full-scale simulations are applied on the microstructural scale to reveal the underlying deformation and "damage" mechanisms.

This study demonstrated strong "plastic deformation" of WC grains near the leading of drilling inserts impacting the rock, which in the real life context would imply cracking and subsequent elimination of WC grains, which being ejected in the contact interface can cause more damage in intimate rock-tool contacts.

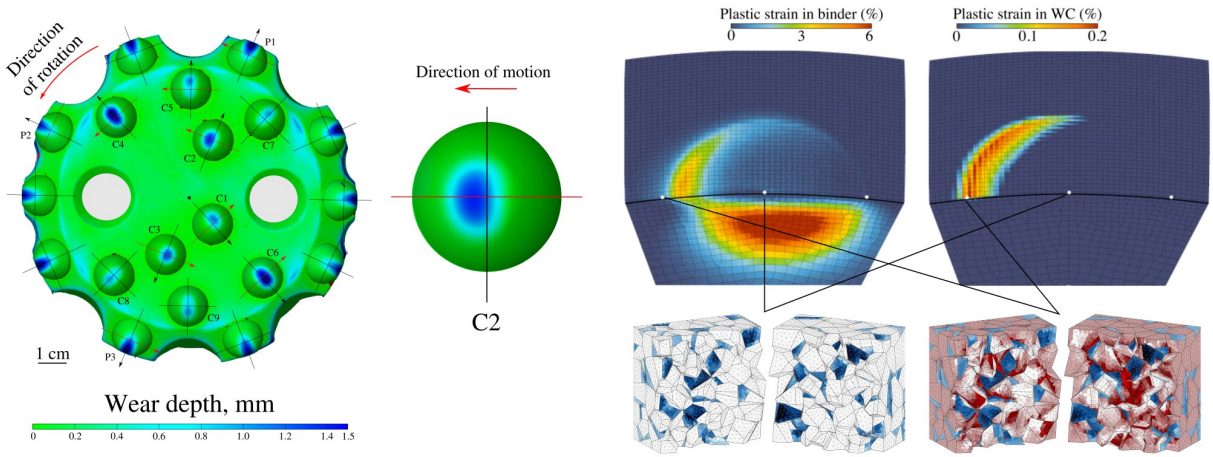

Figure 1.28: Wear pattern on percussive-rotary drill crown and hardmetal (WC/Co) inserts after drilling 80 m in hard rock formations. The asymmetry of the wear pattern is highlighted. On the right – accumulated plastic slip in WC and the binder, obtained in structural impact simulations using the calibrated mean-field model, below we show the results of accumulated plastic deformation on the microstructural level for the leading edge and central locations obtained using the full-field FE model after simulating the full loading cycle $\sigma(t)$ coming from the macro-scale simulation: blue - plasticity in the binder, red - plasticity in WC grains.

Wear pattern on percussive-rotary drill crown and hardmetal (WC/Co) inserts after drilling 80 m in hard rock formations. The asymmetry of the wear pattern is highlighted. On the right – accumulated

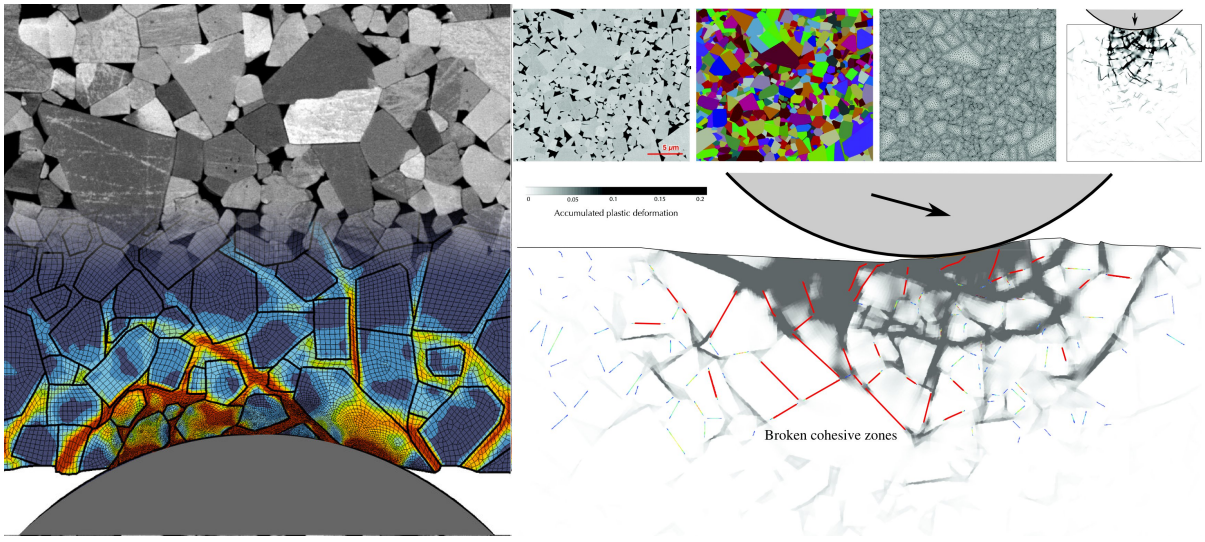

Figure 1.29: *Left* – Simulation of an impact of a hardmetal microstructure by a rigid indenter representing a smooth hard fraction of the rock, plastic deformations in the binder and WC grains is shown, in the background the true SEM image of the microstructure is shown. *Right* – construction procedure of plane WC/Co microstructure directly from SEM image and associated simulations of the normal and oblique impacts, red lines show fully debonded WC/Co and WC/WC interfaces.

plastic slip in WC and the binder, obtained in structural impact simulations using the calibrated mean-field model, below we show the results of accumulated plastic deformation on the microstructural level for the leading edge and central locations obtained using the full-field FE model after simulating the full loading cycle $\sigma(t)$ coming from the macro-scale simulation: blue - plasticity in the binder, red - plasticity in WC grains.

In addition, within the same study we studied small scale damage and plasticity of hardmetal composites in interaction of hard fractions of hard-rocks, both plastic deformation and interface debonding were included in the full model (see Fig. 1.29).

References

- [78] D. Tkalich, A. Kane, A. Saai, V.A. Yastrebov, M. Hokka, V.T. Kuokkala, M. Bengtsson, A. From, C. Oelgardt, Ch. C. Li. "Wear of cemented tungsten carbide percussive drill-bit inserts: laboratory and field study". Wear, 386:106-117 (2017). [doi] [pdf]
- [76] D. Tkalich, V.A. Yastrebov, G. Cailletaud, A. Kane. "Multiscale Modeling of Cemented Tungsten Carbide in Hard Rock Drilling". International Journal of Solids and Structures, 128:282-295 (2017). [doi] [pdf]
- Presentation "Multiscale wear modelling of cemented tungsten carbide tools in hard rock drilling" given at the conference "Computational Modeling of Complex Materials Across the Scales", Nov 8, 2017. Paris, France [pdf]

1.3.6 Pressure-dependent friction

According to the adhesive theory of friction, the maximum tangential force that the friction interface can undergo without sliding results simply from the product of the tangential resistance τ_c by the contact area A; as the contact area evolves in a first approximation linearly with the pressure p_0 applied to the apparent area A_0, the maximum friction force can be described as $T = \tau_c A \sim \tau_c p_0 A_0 \sim \tau_c N$, N being the normal force. This provides the explanation of the Coulomb friction model. But if one improves the model describing the evolution of the contact area with the pressure, one can find a finer law [18] which takes into account the dependency on the pressure. Thanks to these results, it is straightforward

to obtain the following pressure-dependent expression for the coefficient of friction:

$$\mu(p_0) = \mu_0 \left(1 - \frac{g(\alpha)}{\sqrt{2m_2}} \cdot \frac{p_0}{E^*}\right) \quad \text{with} \quad \mu_0 = \frac{f(\alpha)\tau_c}{E^* \sqrt{2m_2}} \tag{1.8}$$

where the $f(\alpha), g(\alpha)$ are universal functions of the Nayak parameter which have been determined numerically in [18], and E^* is the effective elastic modulus of the interface. Of course, this dependence remains phenomenological, but it nevertheless makes the link between the evolution of the pressure and the characteristics of the surface such as m_2 and α, as well as with the elastic constants of the materials in contact ν_i, E_i which are contained in E^*. This law remains valid for linearly elastic materials and up to approximately 15 % of the contact area.

In another study of contact in presence of a strongly non-compressible fluid trapped in the contact zone [30], we were able to demonstrate via simulations that the static frictional limit $\max(F_t)$ can behave like a non-monotonic function reaching its maximum and decreasing for very high pressures p, i.e. the friction can decrease while the pressure increases:

$$\frac{\partial \max(F_t)}{\partial |p|} < 0.$$

The friction can vanish completely for a critical pressure! The curve of the evolution of static friction with pressure Fig. 1.30 looks like the Drucker-Prager (or Mohr-Coulomb) law with a cap, which describes, among other materials, the behavior of rocks containing a multitude of pressurized cracks in the presence of fluid. This similarity to some extent confirms the validity of this rather exotic result of the decreasing friction.

Version française: Selon la théorie adhésive du frottement, la force maximale tangentielle que l'interface frottant peut subir sans glissement résulte simplement du produit de la résistance tangentielle τ_c par l'aire de contact A ; comme l'aire de contact évolue en première approximation linéairement avec la pression p_0 appliquée sur l'aire apparente A_0, la force de frottement maximale peut être décrite comme $T = \tau_c A \sim \tau_c p_0 A_0 \sim \tau_c N$, N étant la force normale. Ceci fournit l'explication du modèle de frottement de Coulomb. Mais si l'on améliore le modèle décrivant l'évolution de l'aire de contact avec la pression, on peut trouver une loi plus fine[18] qui prend en compte la dépendance à la pression. Grâce aux résultats obtenus en[18], il est très facile d'obtenir le coefficient de frottement suivant :

$$\mu(p_0) = \mu_0 \left(1 - \frac{g(\alpha)}{\sqrt{2m_2}} \cdot \frac{p_0}{E^*}\right) \quad \text{avec} \quad \mu_0 = \frac{f(\alpha)\tau_c}{E^* \sqrt{2m_2}}$$

où les $f(\alpha), g(\alpha)$ sont des fonctions universelles du paramètre de Nayak qui ont été déterminées numériquement dans [18], et E^* est le module élastique effectif de l'interface. Bien entendu, cette dépendance reste phénoménologique, mais elle fait néanmoins le lien entre l'évolution de la pression et les caractéristiques de la surface telles que m_2 et α, ainsi qu'avec les constantes élastiques des matériaux en contact ν_i, E_i qui sont contenues dans E^*. Cette loi reste valide jusqu'à approximativement 15 % de l'aire de contact.

Dans une autre étude du contact en présence d'un fluide fortement non-compressible piégé dans les zones de contact [30], nous avons pu démontré par des simulations que la limite de frottement statique $\max(F_t)$ peut se comporter comme une fonction non-monotone et pour des pressions très élevée p, diminue avec la pression croissante:

$$\frac{\partial \max(F_t)}{\partial |p|} < 0,$$

qui pour une pression critique peut rendre le frottement statique nulle ! La courbe de l'évolution du frottement statique avec la pression Fig. 1.30 fait penser à la loi de Drucker-Prager (or Mohr-Coulomb) avec "un cap" décrivant, entre autres, le comportement des roches comportant une multitude de fissures en contact et en présence de fluide. Cette similitude est une confirmation même si partielle et implicite de la validité de ce résultat exotique sur le frottement decroissant avec la pression.

References

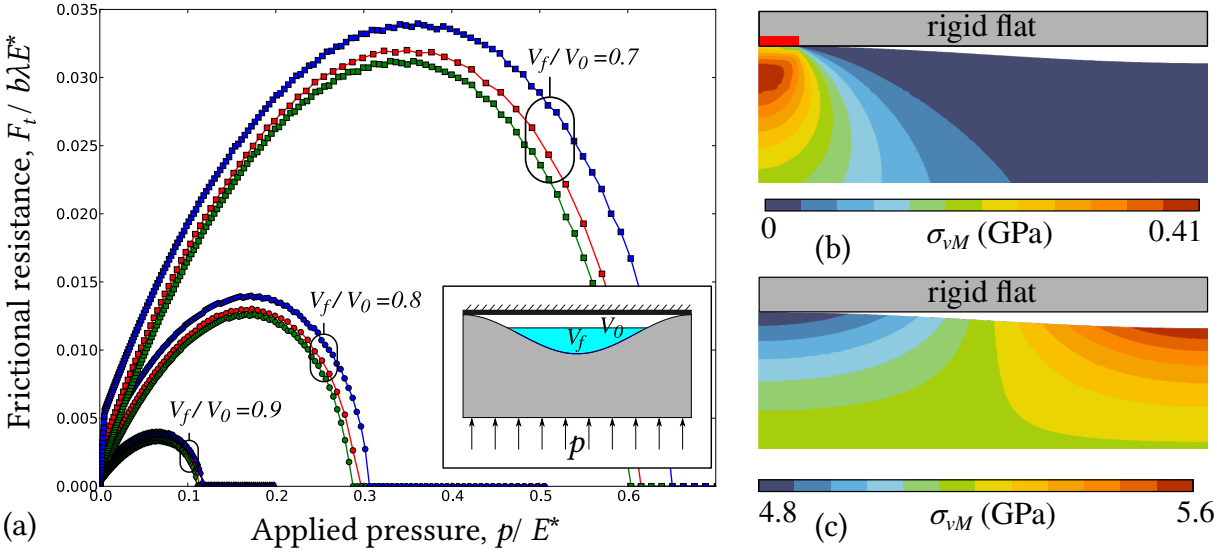

Figure 1.30: (a) The evolution of the static friction as a function of the applied pressure p/E^*, the curve is non-monotonic and looks like a Drucker-Prager model with a "cap", the von Mises stress state in the wavy profile (only a half is shown) brought in contact with a rigid flat in presence of the non-saturated incompressible fluid in the interface (b) at low pressure and (c) at the moment when the fluid opens the trap and occupies the entire contact interface (the red area shows the size of the contact).

Version française: (a) L'évolution du frottement statique en fonction de la pression appluquée, la courbe est non-monotone et ressemble au comportement du modèle de Drucker-Prager avec un "cap", l'état de contrainte de von Mises (b) peu après la mise en contact et (c) à l'ouverture du contact par le fluide qui s'échape du piége (la zone rouge démontre la taille du contact, juste une demi onde du profil sinusoïdale est montrée).

- [18] V.A. Yastrebov, G. Anciaux, J.F. Molinari. "The role of the roughness spectral breadth in elastic contact of rough surfaces". Journal of the Mechanics and Physics of Solids, 107:469-493 (2017) [doi] [arXiv] [pdf]
- [30] A.G. Shvarts, V.A. Yastrebov. "Trapped fluid in contact interface". Journal of the Mechanics and Physics of Solids, 119:140-162 (2018). [doi] [arXiv] [pdf]

1.4 Materials

1.4.1 Microstructure model and mechanical behavior of cemented tungsten carbides

It is not difficult to reconstruct plane microstructure of cemented tungsten carbide using high quality SEM images Fig. 1.31, even though we did not succeed to fully automatize such a procedure.

Reconstruct a three dimensional microstructure even using X-ray (diffraction) tomography presents a really challenging task because of the sub-micron size of binder pools and WC grains. Therefore, for our study of hardmetal mechanical behavior we developed an algorithm based on multiple truncation of Voronoi-grains by a randomly oriented planes. This algorithm enabling to construct microstructural CAD models for gmsh was implemented in voro++ library (I hope in near future render this implementation publically available in addition to generating hardmetal microstructures, this implementation allows to simply construct CAD models from voro++ tesselations), a trivial voxel-based implementation is also available.

The obtained 2D and 3D microstructures were used to study mechanical behavior and statistics of stress-strain state in characteristic loading paths in drilling with and without taking into account residual

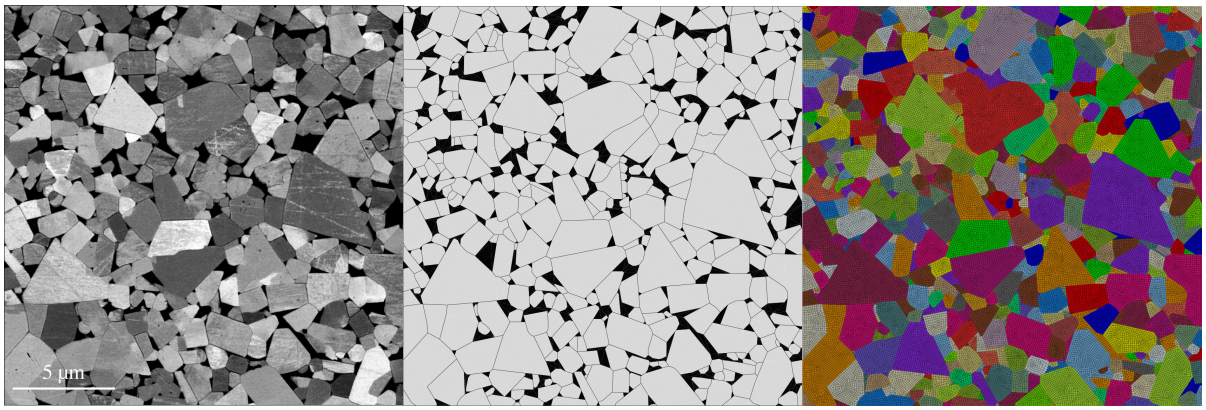

Figure 1.31: SEM image of WC/Co → outlined microstructure → finite element mesh [79]

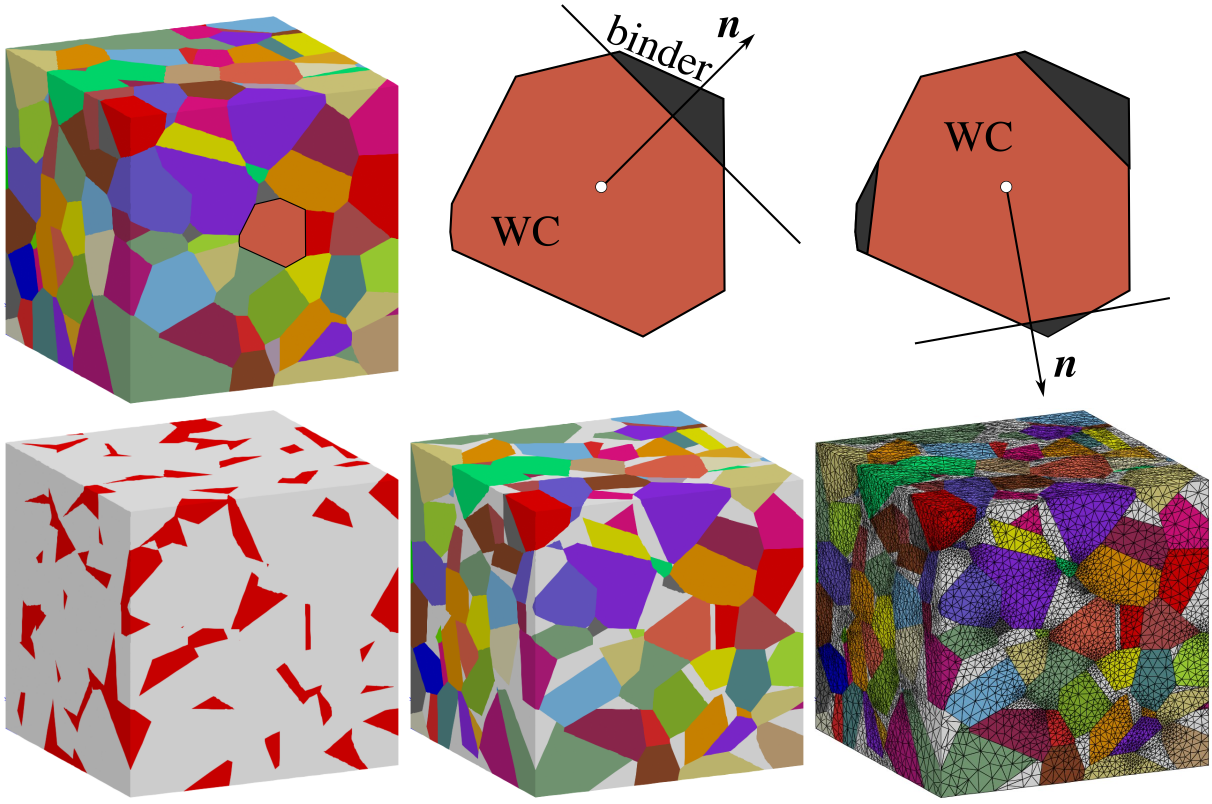

Figure 1.32: Demonstration of the truncated-Voronoi algorithm for reconstruction of cemented tungsten carbide microstructure: initial voronoi tesselation → truncation of every grain (number of truncation and volume fraction are the used defined parameters) → binder shown in red, WC grains in multicolor → resulting finite element mesh.

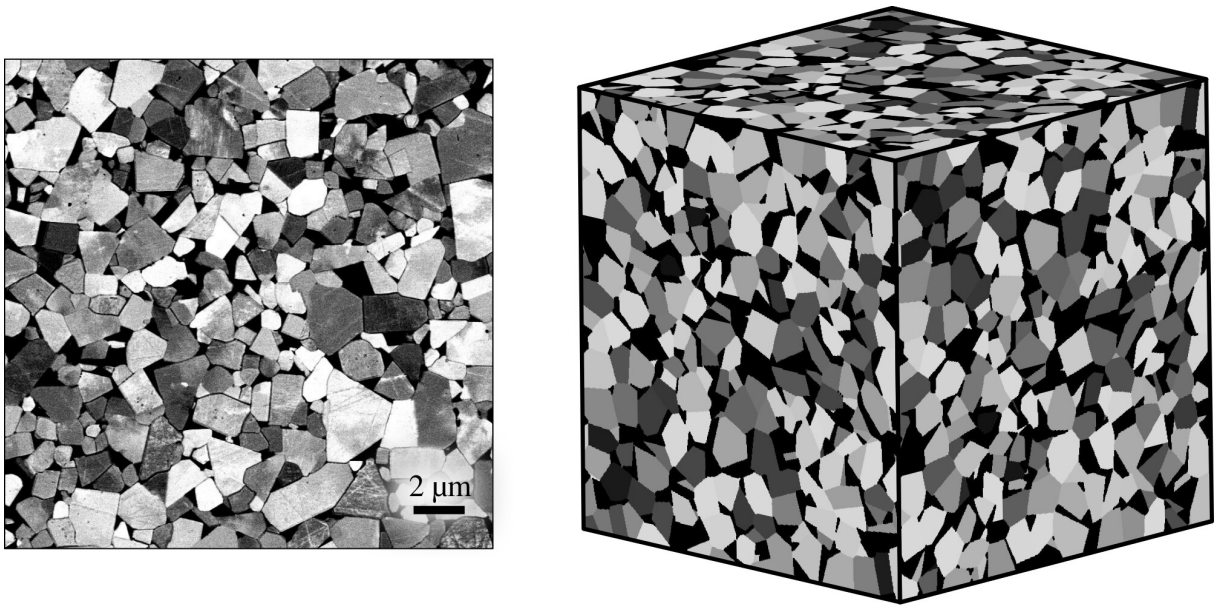

Figure 1.33: Comparison of SEM image of WC/Co microstructure and a generated microstructure for the same binder volume fraction.

cooling-induced stresses. The **first interesting result** is that the cooling-induced stress state under simple loading conditions (shear, tension, compression) results in two-maxima pressure distributions as shown in Fig. 1.34. Therefore, a mean-field model used with residual thermal stresses would report a meaningless results for the mean pressure located in between two maxima, thus missing completely the true contact state in the microstructure.

The **second interesting result** coming from this micromechanical study is that the β mean-field model is incapable to deal correctly with strongly hydrostatic stress states. In Fig. 1.35 we compare initial yield surfaces obtained for mean-field and full-field models, demonstrating a pronounced cap for the latter and its absence for the former. In contact and impact, high hydrostatic pressures represent a very common stress state near the contact surface, so the mean-field models should be adjusted in order to capture correctly such regimes. Therefore, Georges Cailletaud suggested to convert the original β-model into a hierarchical model or two-scale β-model to capture properly the plastic onset under strongly hydrostatic deformation regimes. With Dmitry Tkalich we started to work on the implementation of this model, yet unfortunately this promising project was not finished.

References

- [79] D. Tkalich, G. Cailletaud, V.A. Yastrebov, A. Kane. "A micromechanical constitutive modeling of WC hardmetals using finite-element and uniform field models". Mechanics of Materials, 105:166-187 (2017). [doi] [pdf]

- [76] D. Tkalich, V.A. Yastrebov, G. Cailletaud, A. Kane. "Multiscale Modeling of Cemented Tungsten Carbide in Hard Rock Drilling". International Journal of Solids and Structures, 128:282-295 (2017). [doi] [pdf]

- Presentation "Multiscale wear modelling of cemented tungsten carbide tools in hard rock drilling" given at the conference "Computational Modeling of Complex Materials Across the Scales", Nov 8, 2017. Paris, France [pdf]

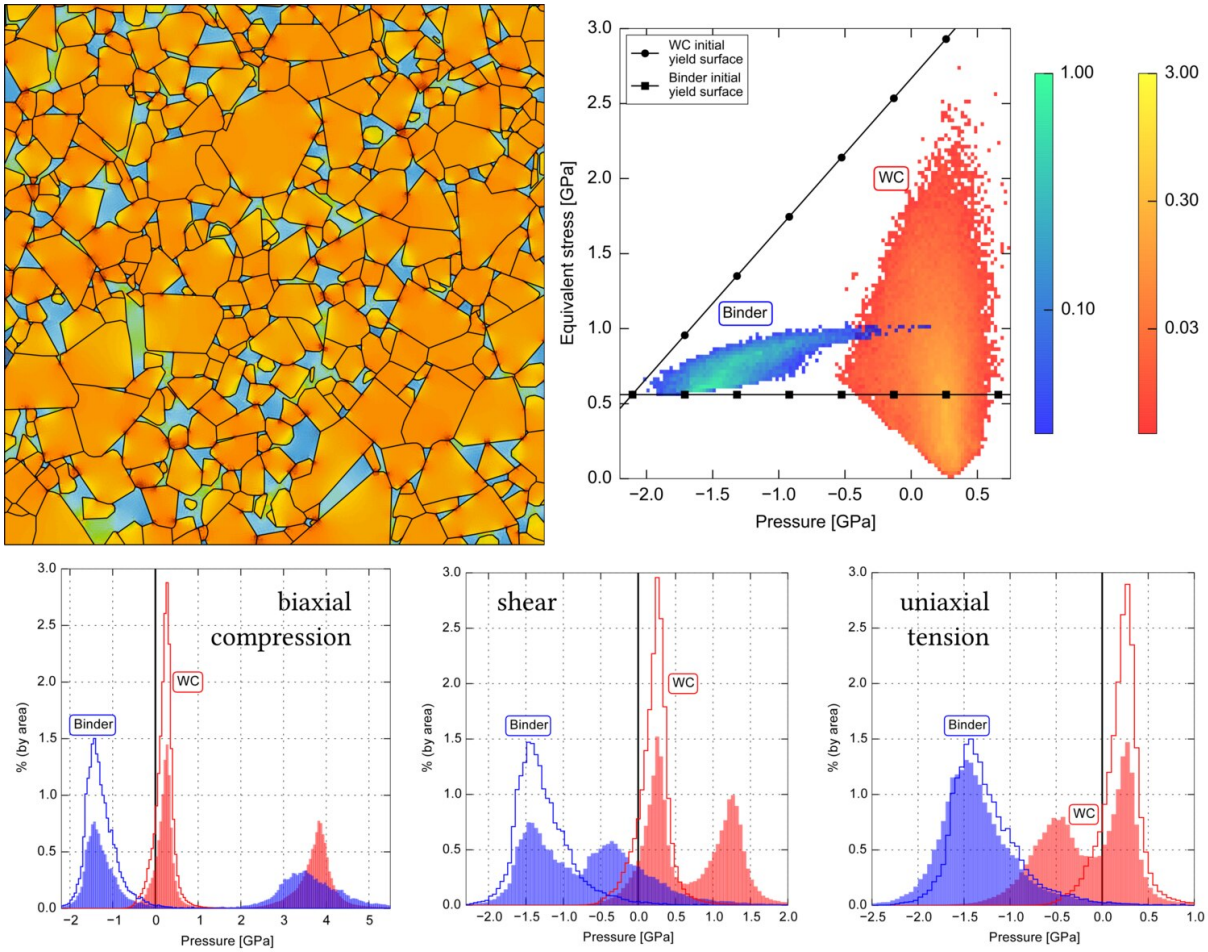

Figure 1.34: Contour plot of pressure distribution in WC/Co microstructure after thermal contraction from 800 °C to 20 °C emerging due to the different in thermal expansion coefficients of cobalt and WC, pressure-$J2$ map after thermal contraction; lower panel – histograms of pressure distributions in binder and WC after biaxial compression, shear and uniaxial tension (initial histogram right after thermal contraction is shown by a solid line) demonstrating double-peak distribution for which the mean value is meaningless.

1.5 Dynamics of architected materials

Since 2015, I have been working on architected materials with internal contact and friction interaction which endow, at the macroscopic scale, these materials with novel properties such as controlled anisotropic asymmetry, dependence of the loading history within the elastic domain, volumetric non-destructive dissipation, and strong coupling between deformation and thermal and/or electric fields. Among the most successful results I could mention the project on the annihilation of elastic waves in elastically asymmetric media resulting from internal contact interactions.

Version française: Depuis 2015 je travaille sur des matériaux architecturés avec l'interaction de contact et de frottement qui donnent au matériau à l'échelle macroscopique des propriétés nouveaux et forts intéressants: comme l'asymétrie anisotrope contrôlée, dépendance de l'historique du chargement dans le domaine élastique, dissipation volumique, et un couplage fort entre la déformation et des champs thermiques et/ou électriques. Parmi les résultats les plus abouti je peux citer le projet sur l'annihilation des ondes élastique dans des milieux qui se comporte d'une manière asymétrique à cause des contacts internes.

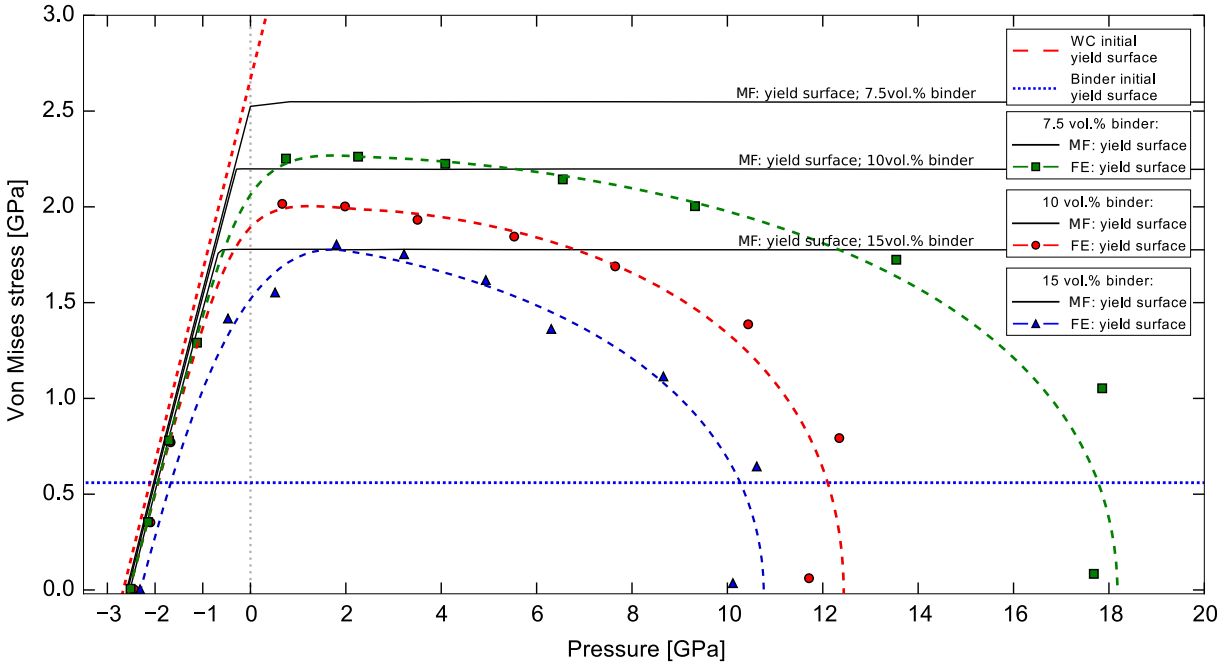

Figure 1.35: Yield surface of WC/Co hardmetal for different binder contents (7.5%, 10%, 15%). Markers and colored master curves show the results of full-field finite element simulations (FE), black solid lines represent the results obtained by the mean-field (MF) β-model. [76].

1.5.1 Wave propagation in asymmetric materials

A new concept for architected materials was developed in [80], in which elastic asymmetry can be finely tuned by combining internal contacts and components of different stiffness. By studying the propagation of one-dimensional elastic waves in the resulting elastically asymmetric media, we found that the overlap of tensile and compressive wave components propagating at different velocities results in the emergence of energy cascades leading to partial or, in special cases, almost complete wave annihilation. This annihilation represents a new and powerful mechanism of signal damping. The main advantage of the proposed architected materials consists in the possibility to increase considerably the contrast of the elastic asymmetry, which would allow to keep the damping device relatively small even with respect to the incident wavelength.

In realistic cases of incident waves containing many modes, only partial annihilation can occur, however, the signal after passing through a relatively long bimodular segment appears "polarized" in positive or negative deformation. This observation was made in the study of self-affine incident wave packets (Gaussian envelope) passing through a bimodular section. This analysis allowed to obtain a fairly universal form Fig. 1.36 of the ratio of the transmitted energy W_{out} to the injected energy W_{in} (the so-called transmission factor $\mathcal{T}$) with respect to the length L of the bimodular segment for different elastic contrasts (the ratios of Young's moduli in tension and compression $E^-/E^+ = \gamma$):

$$\mathcal{T}'(L') = \frac{W_{out} + W_{refl}}{W_{in}} = \mathcal{T}'_{min} + (\mathcal{T}'_{max} - \mathcal{T}'_{min}) \exp\left(-(L'/L'_*)^{3/2}\right) + \frac{W_{refl}}{W_{in}}, \tag{1.9}$$

where the last term, which takes into account the reflection of the waves for $\gamma < 1$, can be estimated as:

$$\frac{W_{refl}}{W_{in}} \approx \left(\frac{\sqrt{\gamma} - 1}{\sqrt{\gamma} + 1}\right)^2$$

and the renormalized length of the bi-modular segment is given by:

$$L' = \begin{cases} \dfrac{L}{l}\dfrac{2}{1-\sqrt{\gamma}}, & \text{if } \gamma > 1, \\ \dfrac{L}{l}\dfrac{2}{\sqrt{1/\gamma}-1}, & \text{if } \gamma \leq 1, \end{cases}$$

where l is the characteristic size of the underlying architecture.

The demonstrated effective damping and sign polarization mechanisms can be used in shock absorbing and wave filtering systems, and, hypothetically, in seismic protection against surface waves. We are currently working on the study of the behavior of these asymmetric materials in 2D/3D, where the elastic compression/tension asymmetry must be reinforced by the shear asymmetry and also equipped with an elastic anisotropy.

The computational code for the simulation of one-dimensional wave propagation in asymmetric media with absorbing boundaries is made available on Zenodo.

Version française: Un nouveau concept pour les matériaux architecturés a été développé dans [80], dans lequel l'asymétrie élastique peut être finement ajustée en combinant des contacts internes et des composants de rigidité différente. En étudiant la propagation des ondes élastiques unidimensionnelles dans les milieux élastiquement asymétriques résultants, nous avons constaté que le chevauchement des composantes d'onde de traction et de compression se propageant à des vitesses différentes se traduit par l'émergence de cascades d'énergie conduisant à une annihilation partiel ou, dans des cas particuliers, presque complète des ondes. Cette annihilation représente un nouveau et puissant mécanisme d'amortissement du signal. Le principal avantage des matériaux architecturés proposés consiste en possibilité d'augmenter considérablement le contrast de l'asymétrie élastique, ce qui permettrait de maintenir la dispositif d'amortissement relativement petit même par rapport à la longueur d'onde incidente.

Dans une situation plus réaliste d'une onde incidente contenant de nombreux modes, seule une annihilation partielle peut se produire, cependant, le signal après avoir traversé un segment bimodulaire relativement long apparaît "polarisé"" en déformation positive ou négative. Cette observation a été faite dans l'étude de paquets d'ondes incidentes auto-affines (enveloppe gaussienne) traversant une section bimodulaire. Cette analyse a permis d'obtenir une forme assez universelle Fig. 1.36 du rapport de l'énergie transmise W_{out} à l'énergie injectée W_{in} (facteur de transmission $\mathcal{T}$) par rapport à la longueur L du segment bimodulaire pour des contraste des modules de Young de traction et compression $E^-/E^+ = \gamma$:

$$\mathcal{T}'(L') = \frac{W_{\text{out}} + W_{\text{refl}}}{W_{\text{in}}} = \mathcal{T}'_{\text{min}} + (\mathcal{T}'_{\text{max}} - \mathcal{T}'_{\text{min}}) \exp\left(-(L'/L'_*)^{3/2}\right) + \frac{W_{\text{refl}}}{W_{\text{in}}},$$

où le dernier term prenant en compte la reflexion des ondes pour $\gamma < 1$ peut être estimé comme :

$$\frac{W_{\text{refl}}}{W_{\text{in}}} \approx \left(\frac{\sqrt{\gamma}-1}{\sqrt{\gamma}+1}\right)^2$$

et la longueur renormalisée est donnée par l'expression suivante :

$$L' = \begin{cases} \dfrac{L}{l}\dfrac{2}{1-\sqrt{\gamma}}, & \text{if } \gamma > 1, \\ \dfrac{L}{l}\dfrac{2}{\sqrt{1/\gamma}-1}, & \text{if } \gamma \leq 1, \end{cases}$$

où l est la taille characteristique de l'architecture sous-jacente.

Les mécanismes d'amortissement et de polarisation de signe efficaces démontrés peuvent être utilisés en cas de choc systèmes d'absorption et de filtrage des ondes, et, hypothétiquement, dans la protection sismique contre les ondes surfaciques. Nous travaillons actuellement sur l'étude du comportement de ces matériaux asymétriques en 2D/3D, où l'asymétrie élastique de compression / traction doit être renforcée par l'asymétrie de cisaillement et aussi complétée par une anisotropie élastique.

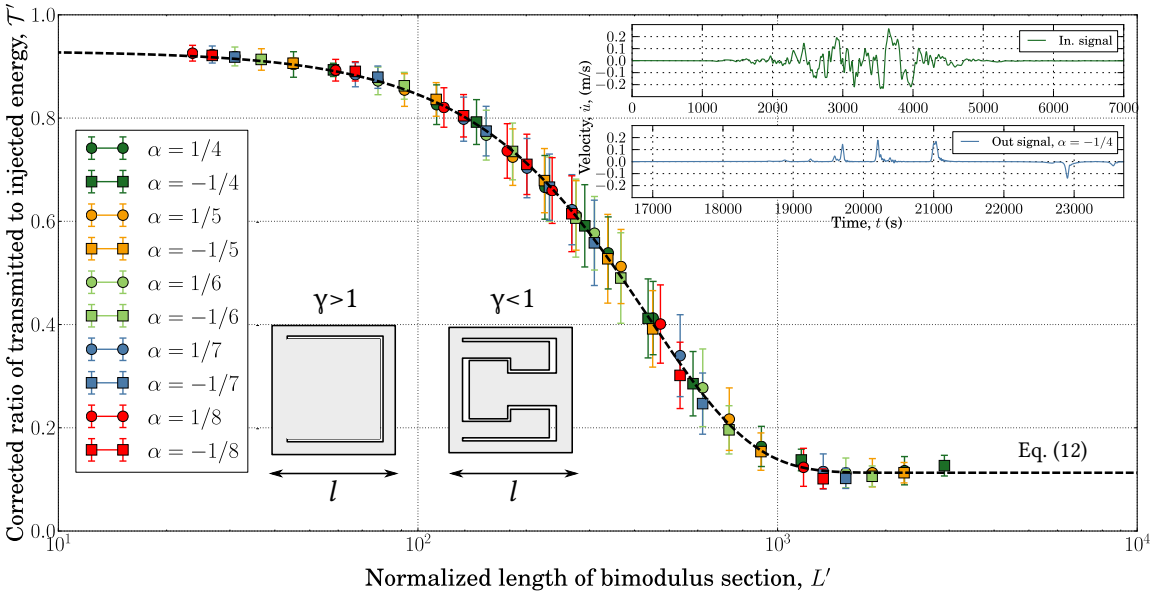

Figure 1.36: The ratio of transmitted to injected energy $\mathcal{T}'$ for the length of the bi-modular segment found by direct simulations and the equation describing this transmission factor Eq. (1.9) using relevant re-normalization. The shape of the input and output signal are presented for $\alpha = (1-\gamma)/(1+\gamma) > 1$; typical architectures giving the asymmetric properties is also shown.

Version française: Le rapport de l'énergie transmis par rapport à l'énergie injectée pour la longueur du segment bimodule trouvé par la simulation explicite et l'équation analytique Eq. (1.9) avec la renormalisation pertinente. La forme du signal d'entrée et de sorti sont présentés pour $\alpha = (1-\gamma)/(1+\gamma) > 1$ ainsi que les architectures types donnant les propriétés asymétriques.

Le code de calcul pour la simulation de la propagation d'ondes unidimensionnelles dans des milieux asymétriques avec des frontières absorbantes a été mise à disposition de tous sur Zenodo

References

- [80] V.A. Yastrebov. "Wave propagation through an elastically-asymmetric architected material" (2021). Minor revision in Compte Rendu Mécanique (Diamond Open Access). Preprint is available [arXiv]
- Presentation "Wave propagation through contact-based elastically asymmetric materials" European Solid Mechanics Conference, July 2, 2018. Bologna, Italy [pdf]

1.5.2 Vibration of asymmetric materials

The very first time I met "chaos" was when I started to explore using simple simulations vibrational behavior of asymmetric materials with internal contacts. My personal story is very similar to the story of the first discovery of chaos and butterfly effect: since I was not aware of this story, I discovered the chaos on my own. I studied a very simple 2-DOFs system of springs and masses:

$$\ddot{X} + 2\alpha C\dot{X} + kK(X)X = F,$$

where $F = [\sin(\omega t), 0]^\intercal$ is the external forcing vector (note that the amplitude is set to 1 because the studied non-linearity is amplitude independent), X is the displacement vector, α is the normalized by mass damping parameter and C is the associated damping matrix, k is the stiffness parameter normalized by mass, and $K(x)$ is the discontinuous stiffness matrix depending on the sign of the deformation:

$$K = \begin{bmatrix} \beta_1(x_1 - x_2) & -\beta_1(x_1 - x_2) \\ -\beta_1(x_1 - x_2) & \beta_1(x_1 - x_2) + \beta_2(x_2) \end{bmatrix},$$

where

$$\beta_1(x) = \begin{cases} \gamma, & \text{if } x < 0 \text{ compression;} \\ 1, & \text{if } x \geq 0 \text{ tension;} \end{cases} \qquad \beta_2(x) = \begin{cases} 1, & \text{if } x < 0 \text{ compression;} \\ \gamma, & \text{if } x \geq 0 \text{ tension.} \end{cases}$$

and the parameter γ is the elastic contrast in tension and compression. So the stiffness matrix can take four different forms (lower index xy indicates the deformation state of the first x and the second y spring respectively, and can take values t for tension, and c for compression):

$$K_{tt} = \begin{bmatrix} 1 & -1 \\ -1 & 1+\gamma \end{bmatrix}, \quad K_{tc} = \begin{bmatrix} 1 & -1 \\ -1 & 2 \end{bmatrix}, \quad K_{cc} = \begin{bmatrix} \gamma & -\gamma \\ -\gamma & 1+\gamma \end{bmatrix}, \quad K_{ct} = \begin{bmatrix} \gamma & -\gamma \\ -\gamma & 2\gamma \end{bmatrix},$$

At $\omega \to 0$ the system behaves symmetrically in tension and compression with the effective stiffness:

$$k_{\text{eff}} = \frac{2\gamma}{\gamma + 1} k.$$

However, at non-zero frequency the system behaves in a non-conventional manner. First, contrary to two resonances, it posses many more so-called sub-harmonic resonances depending on the damping parameter α. Second, at some frequencies the system can demonstrate multi-period, quasi-periodic and truly chaotic regimes. However, the difficulty of the study is that in true temporal simulations with arbitrary initial conditions and under small damping, the stabilization of the cycle can take thousands of cycles and in order to be sure that the detected regime is truly chaotic, sometimes millions of cycles must be simulated. A more sophisticated strategy consisting in the search of n-period solutions cannot always ensure the solution because of Hopf bifurcations making Poincaré-points "turn in round". Nevertheless, I could carry out a relatively broad parametric study $\{\omega \in [0.1, 7] \times \gamma \in [1, 5] \times \alpha \in [0.01, 0.2]\}$ with $\{10\,000 \times 800 \times 10\}$ discretization points and with thousands of cycles simulated for some of them (see Fig. 1.39). However, these maps shown below could be incomplete since basins of attraction were not fully explored.

This study did not create new fundamental knowledge, it simply helped me to explore yet rather superficially and mainly "experimentally" the field of nonlinear dynamics. The fact that search for different dynamic regimes could be rather CPU-time consuming, we started to explore this non-linear dynamics using machine learning algorithms in the framework of 3 months internship of Yirun Zou. We started with simply trying to forecast the trajectory of one of the DOFs without the knowledge of the second DOF dynamics using a simple Multi-Layer Perceptron (MLP) neural network. Even though this attempt was quite successful, the true objective: predict the dynamic regime knowing the behavior over few first cycle appeared too ambitious and was not explored. An interesting result was that some trained MLPs could predict complex multiple-period cycles even though within their training data such cycles were absent.

References

- Presentation "Nonlinear Oscillator: an attempt to predict butterfly effect by machine learning" with Yirun Zou [pdf]

1.6 Glacial earthquakes: bedrock/glacier/iceberg/ocean interaction

1.6.1 Capsizing iceberg model

During the PhD project of Amandine Sergeant-Boy, we developed a simplified but still local fluid-solid interaction (FSI) model which apart from the hydrostatic pressure $\boldsymbol{p}_f(z) = \rho g \langle z_0 - z \rangle \boldsymbol{n}$, could approximately evaluate and apply the hydrodynamic pressure $\boldsymbol{p}_d(\boldsymbol{v}_s, \boldsymbol{v}_f, \boldsymbol{n})$ within the finite strain finite element framework. The model of hydrodynamic pressure could take into account a background fluid velocity field $\boldsymbol{v}_f$ and resulted in an acceptable approximating of the drag force Fig. 1.40. Thanks to this simplified model we could make a link between seismic signals and the source force induced by the iceberg-glacier interaction [81], see Fig. 1.41 and ultimately, Amandine Sergeant Boy on her own could carry out a global study on ice loss in Greenland using inverse analysis [82].

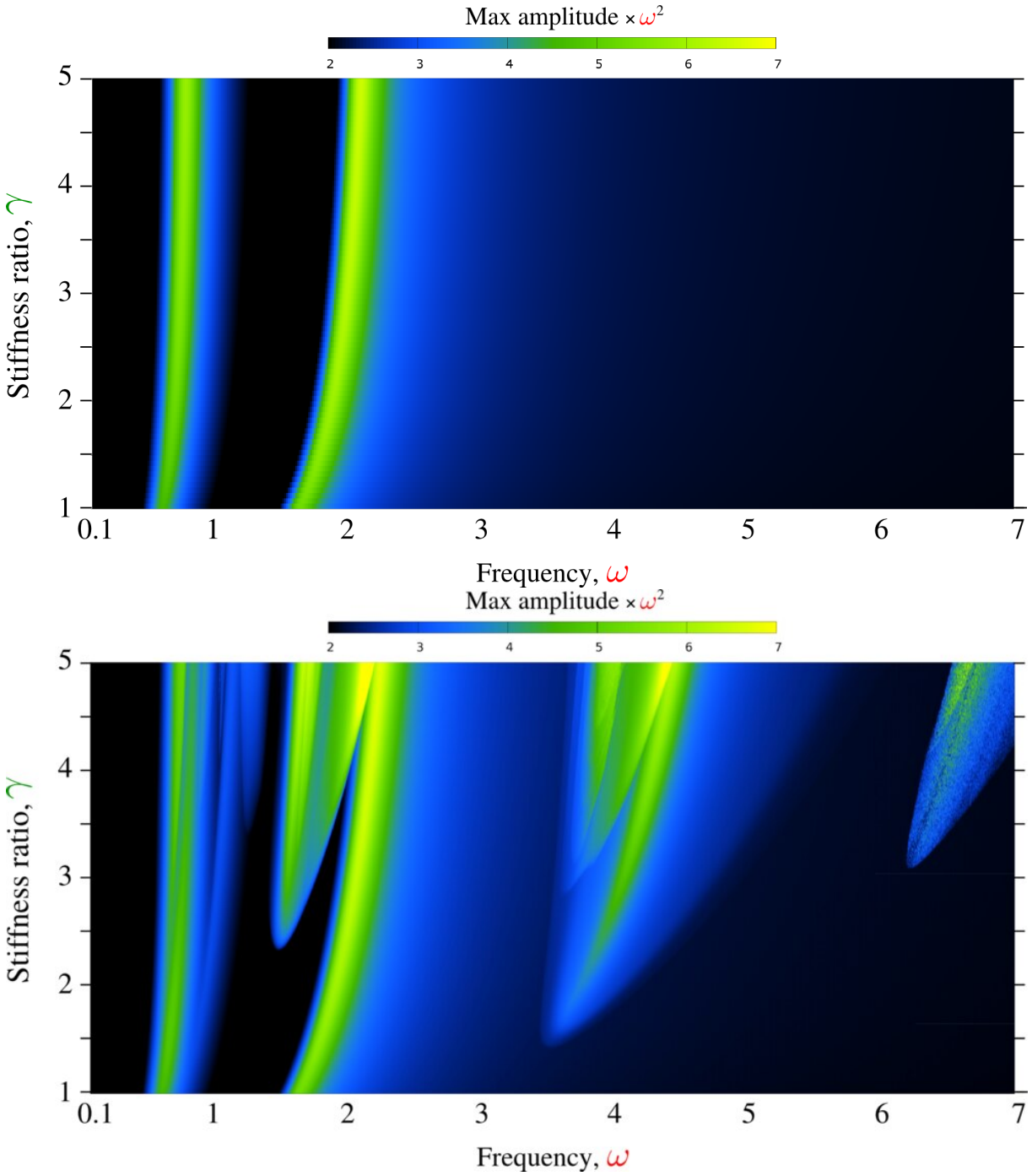

Figure 1.37: *First panel:* frequency ω – elastic contrast γ – normalized maximal amplitude $a\omega^2$ map for a symmetric 2-DOF material with the effective stiffness.
Second panel: frequency ω – elastic contrast γ – normalized maximal amplitude $a\omega^2$ map for an *asymmetric* 2-DOF material.

Nevertheless, using a multi-DOF FE model for iceberg capsizes was an excessive solution, so we re-implemented the model for simple rigid solid dynamics with a leap-frog (Störmer-Verlet) integration in time and with the contact handled by the penalty method applied both to the penetration and to

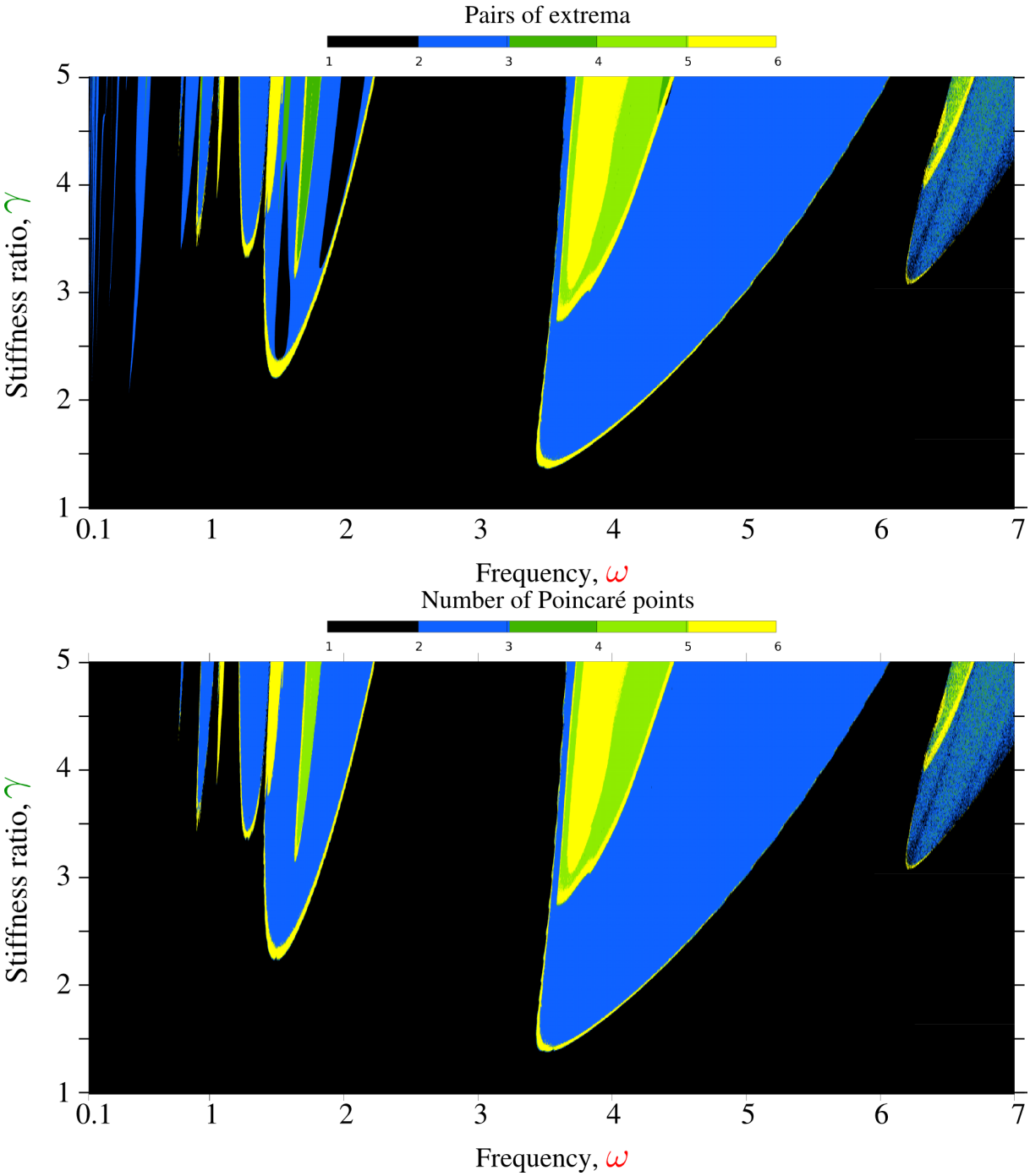

Figure 1.38: *First panel:* frequency ω – elastic contrast γ – number of extrema in the amplitude for an *asymmetric* 2-DOF material.
Second panel: Frequency ω – elastic contrast γ – number of Poincaré points per convergent cycle, equivalent to the number of periods, for an *asymmetric* 2-DOF material.

its rate to avoid spurious high frequency oscillations. In addition, this new model was complemented with a phenomenological added-masses and the moment of inertia using theoretical results of [83]. The resulting model was successfully compared with full scale 2D CFD simulations made by Patrick Queutey and Alban Leroyer using their powerful in-house ISIS-CFD software. However, this comparison was

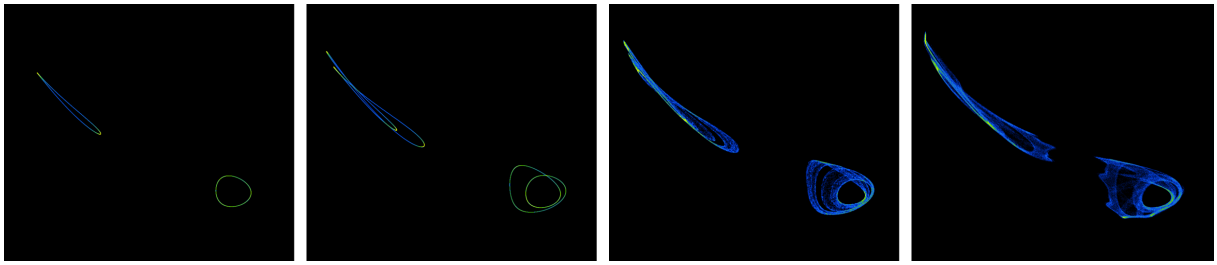

Figure 1.39: 2D projection of 4D density of Poincaré points $p(x_0, \dot{x}_0, x_1, \dot{x}_1)$ for $\alpha = 0.05$, $\gamma = 5$, from left to right $\omega = \{1.212, 1.214, 1.215, 1.2155\}$ – from Hopf-type trajectory (pseudo-periodic solution) to two-branch chaotic attractor (in terms of Poincaré points).

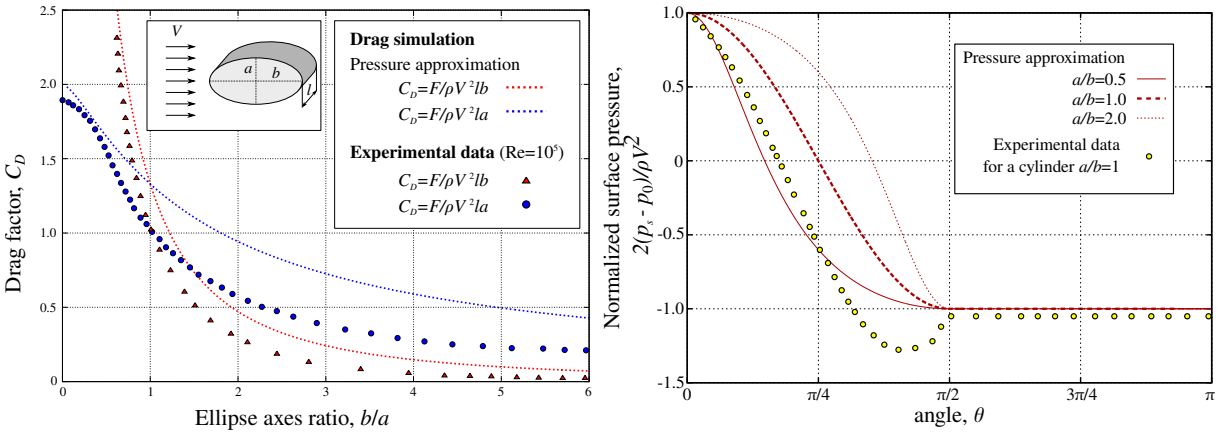

Figure 1.40: *(Left)* – drag factor (normalized drag force) for a solid of elliptic section found by our simplified geometrical drag model and compared with experimental results; *(right)* – pressure distribution obtained on an elliptic section using our simplified drag model and approximate experimental data for a circular section.

only possible in absence of contact, which cannot be handled by ISIS-CFD, i.e. we studied a rather artificial for the nature situation of an iceberg capsize in open ocean [84]. Nevertheless, this comparison allowed us to understand better the capsize dynamics, the effect of the scale and involved hydrodynamic forces and processes. The original drag model was slightly improved by adjusting better the added-mass and drag factors for rectangular icebergs of different aspect ratios. All results are compared with lab experiments in Fig. 1.42. Remarkably, our simple model can reproduce quite well kinematics of the iceberg capsize as well as the associated forces and moments.

References

- [81] A. Sergeant, V.A. Yastrebov, A. Mangeney, O. Castelnau, J.P. Montagner, E. Stutzmann. "Numerical modeling of iceberg capsize responsible for glacial earthquakes". Journal of Geophysical Research: Earth Surface, 123:3013-3033 (2018). [doi] [pdf]
- [82] A. Sergeant, A. Mangeney, V.A. Yastrebov, F. Walter, J.-P. Montagner, O. Castelnau, E. Stutzmann, P. Bonnet, V.J.L. Ralaiarisoa, S. Bevan, A. Luckman. "Monitoring Greenland ice-sheet buoyancy-driven calving discharge using glacial earthquakes". Annals of Glaciology, 60(79):75-95 (2019). Open access. [doi] [pdf]
- [84] P. Bonnet, V.A. Yastrebov, P. Queutey, A. Leroyer, A. Mangeney, O. Castelnau, A. Sergeant, E. Stutzmann, J.-P. Montagner. "Modelling capsizing icebergs in the open ocean". Geophysical Journal International, 223(2):1265-1287 (2020). [doi] [arXiv]

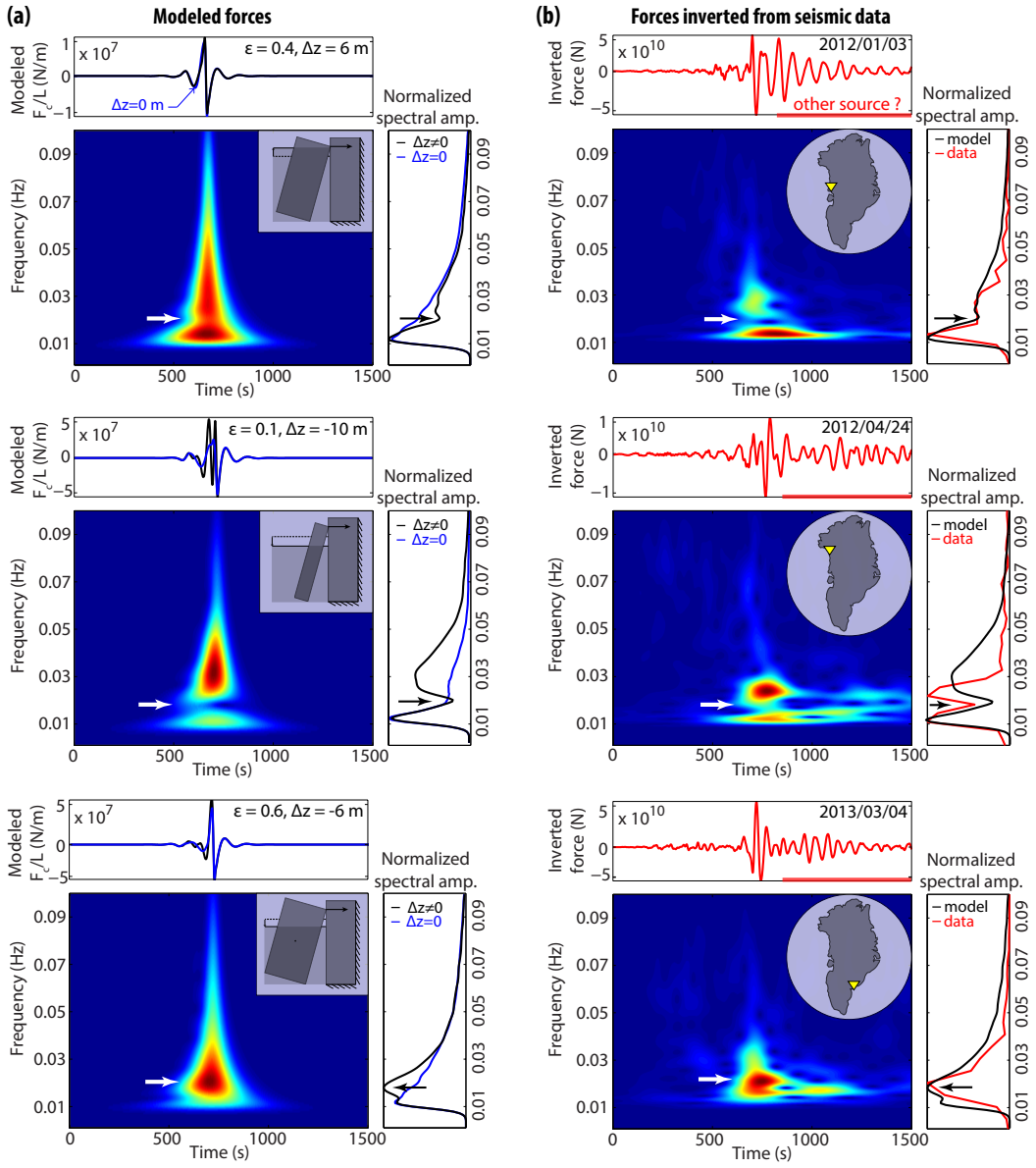

Figure 1.41: Comparison of the forces (a) simulated with our simple iceberg-capsize model and (b) inverted from seismic data, both forces are filtered between 0.01 and 0.1 Hz, as well as the associated normalized spectrograms and power spectra. These simulated and inverted forces are for systems of non-equilibrium buoyancy (i.e., $\Delta z \neq 0$). For the field data in Greenland (column (b)), locations of the calving events and GLISN stations used in the waveform inversion are indicated on inset maps by red stars and yellow triangles, respectively. The power spectra panels show the forces inverted from seismic data (red curves), modeled with either submarine or subaerial icebergs (black curves), and modeled with initially neutrally buoyant icebergs (blue curves). The comparison between models and data show that seismic data spectral peaks or gaps indicated by arrows can be explained by the initial buoyant state of the capsizing icebergs, especially when they are out of their flotation level when they calve and start to capsize [81].

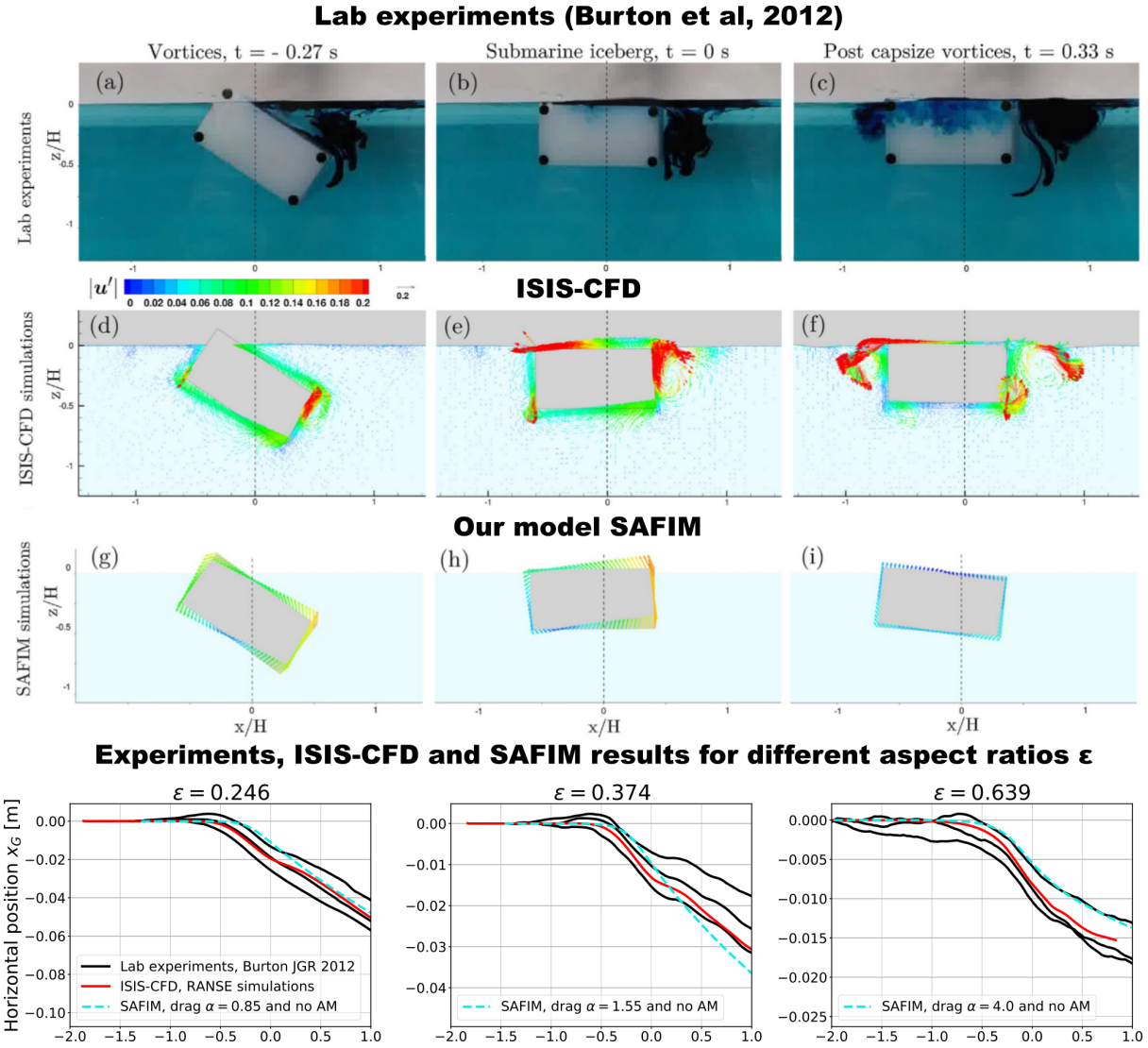

Figure 1.42: Lab experiments from [85] compared with RANSE CFD simulations carried out by Patrick Queutey and Alban Leroyer using their powerful in-house ISIS-CFD software and compared with results of our Semi-Analytical Floating Iceberg Model (SAFIM). The lower model compares horizontal dynamics of the iceberg obtained numerically using our two models with experimental results.

1.6.2 Deformation of the glacier in response to iceberg capsize

Glacier flow combined with the sliding on the bedrock is slowed by frictional forces arising from volume dissipation in the visco-elasto-plastic ice as well as from melting and re-solidification of the ice in the rock/ice interface. The resulting friction law is viscous and is often referred to as Weertman law [86]. In our studies of glacial earthquakes in Greenland caused by capsize of unstable icebergs in contact with glaciers, we studied the visco-elasto-plastic deformation of the latter accompanied such events. At short time scales, the behavior of ice can be seen as elastic, and assuming that the glacier can be approximated by a bar interacting with the bedrock by Weertman's law, we obtain, after some simplifications, a parabolic equation for the perturbation of displacement $u'(x,t)$ as a function of the axial force exerted by

the iceberg $F(t)$. This equation is equivalent to the heat diffusion problem and takes the following form:

$$\begin{cases} \dfrac{\partial^2 u'}{\partial x^2} = \dfrac{\tau_*}{EH}\dfrac{\partial u'}{\partial t}, \\ \left.\dfrac{\partial u'}{\partial x}\right|_{x=L} = -\dfrac{F(t)}{EH}, \\ u'|_{x=0} = 0 \\ u'|_{t=0} = 0 \end{cases}$$

where the parameter EH/τ_* (with τ_* being the parameter of Weertman's law, E Young's modulus and H the height of the glacier) is similar to the heat diffusivity. The solution of this equation can be found quite easily via Green's functions to obtain the following form of the total displacement:

$$u = a + \frac{\rho_i g H \sin\alpha}{\tau_*}t - \frac{2}{\tau_* L}\sum_{n=0}^{\infty}(-1)^n \sin\left(\frac{(2n+1)\pi x}{2L}\right)\int_0^t F(t')\exp\left(-\frac{(2n+1)^2\pi^2 EH}{4L^2\tau_*}(t-t')\right)dt', \qquad (1.10)$$

where ρ_i is the density of the ice, g is the acceleration of gravity and α is the angle of the bedrock's inclination. The numerical evolution of the integral in the Fourier series is quite heavy for an arbitrary form of the force $F(t)$. Therefore, we suggested an analytical form of this force which is in good agreement with CFD calculations of the iceberg/glacier front interaction. This form allows to simplify the evaluation of the mentioned integral. This simplification permits to rapidly evaluate the glacier's dynamics in response to capsizing icebergs and thus permits to carry out a relatively broad parametric study for outlet glaciers in Greenland. In Fig. 1.44, the displacement of the typical glacier near the terminus caused by the capsize of a typical iceberg obtained by the integration of equation Eq. (1.10) is shown. In addition, this study allowed us to make interesting connections between the behavior of ice as an elastic solid in the short term and its non-Newtonian flow in the longer term. The article is in preparation [87]. In parallel, a broad parametric finite element study with a 2D model was carried out both on model geometry with a constant slope and on a realistic geometry of Helheim glacier and its bedrock located in South-East Greenland. These simulations were carried out for different iceberg-capsize scenarios: top-out and bottom-out capsize which trigger different deformation regimes in the glacier, which could not been modeled with a simple 1D model described above. The work on related papers is in progress.

In order to model short-time-scale events, we need to know the initial state of the visco-elasto-plastic glacier which implies that we need to model its history taking into account its interaction with the ocean and the bedrock. Therefore, mainly in the framework of Pauline Bonnet PhD project, we studied a lot different models of marine sheets and carried out numerous numerical simulations, which we compared both with analytical solutions and numerical models of others.

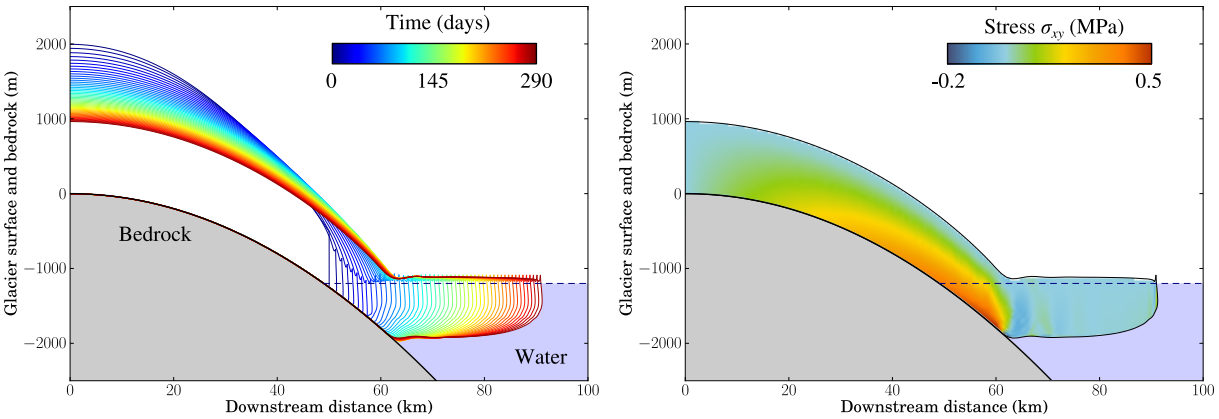

Figure 1.43: FE simulation of accelerated glacier flow into the ocean under Weertman friction law.

Version française: Le glissement des glaciers sur le lit rocheux est freiné par les efforts de frottement spécifique provenant de la dissipation volumique dans la glace visco-élasto-plastique ainsi que de la fusion et resolidification de la glace dans l'interface roche/glace. La loi de frottement résultante est de type visceux et elle est souvent referencée comme une loi de Weertman [86]. Dans nos études des séismes glaciaires au Groenland provoqués par le retournement des icebergs instables en contact avec les glaciers, on a étudié également la déformation visco-élasto-plastique de ces derniers. Aux échelles de temps courts, le comportement de la glace peut être vu comme élastique, et dans l'hypothèse où le glacier peur être approximé par une bar intéragissant avec le lit rocheux par la loi de Weertman, on obtient, après quelques simplifications, une équation parabolique pour la perturbation du déplacement $u'(x,t)$ en fonction de la force exercée par l'iceberg $F(t)$. Cette équation est équivalente à celui du problème de diffusion de la chaleur et prend la forme suivante :

$$\begin{cases} \dfrac{\partial^2 u'}{\partial x^2} = \dfrac{\tau_*}{EH}\dfrac{\partial u'}{\partial t}, \\ \left.\dfrac{\partial u'}{\partial x}\right|_{x=L} = -\dfrac{F(t)}{EH}, \\ u'|_{x=0} = 0 \\ u'|_{t=0} = 0 \end{cases}$$

où le paramètre EH/τ_* -avec τ_* le paramètre de la loi de Weertman, E module de Young et H la hauteur du glacier) est similaire à la diffusivité de la chaleur. La solution de cette équation peut être assez facilement trouvée via des fonctions de Green pour obtenir la forme suivante du déplacement totale:

$$u = a + \frac{\rho_i g H \sin\alpha}{\tau_*} t - \frac{2}{\tau_* L}\sum_{n=0}^{\infty}(-1)^n \sin\left(\frac{(2n+1)\pi x}{2L}\right)\int_0^t F(t')\exp\left(-\frac{(2n+1)^2\pi^2 EH}{4L^2\tau_*}(t-t')\right)dt',$$

où ρ_i est la densité de la glace, g est l'accélération de la pesanteur et α est l'angle de l'inclinaison du lit rocheu. L'évolution numérique de l'integral dans le série de Fourier est assez lourde pour une quelconque forme de la force $F(t)$. Pour cela, nous avons trouvé une forme analytique de cette force qui est en accord avec des calculs CFD de l'interaction iceberg/front glacier et qui permet de simplifier l'évaluation de l'integrale mentionné. Cette simplification nous a permis de mieux comprendre la déformation du glacier en réponse au retournement de l'iceberg et faire l'analyse paramétrique pour des glaciers emissaire au Groenland. Sur Fig. 1.44, le déplacement du glacier type près du terminus provoqué par le vêlage d'un iceberg-type obtenu par l'integration de l'équation Eq. (1.10) est repésenté. En outre cetté étude nous a permis a faire des liens intéressant entre le comportement de la glace en tant qu'un solide élastique à court terme et son écoulement non-Newtonien au temps plus longue. L'article est en phase de préparation [87].

References

- [87] Yastrebov, V.A., Bonnet, P., Mangeney, A. and Castelnau, O. "Effect of iceberg's capsize on the deformation of marine-terminating glaciers", en préparation (2021). Draft of the article is available [encrypted pdf]

1.7 Computational mechanics

1.7.1 Correction of discretization error in spectral BEM

The numerical study of the growth of the real contact area between rough surfaces under the action of the applied pressure requires a very fine discretization. First of all, a fairly wide spectrum of a surface should be represented. Additionally, the discretization must be sufficient to correctly solve the mechanical problem in classical terms of the mesh convergence. If the spectrum of the surface is well represented by the discretization, the error on the measurement of the contact area is concentrated exclusively at the

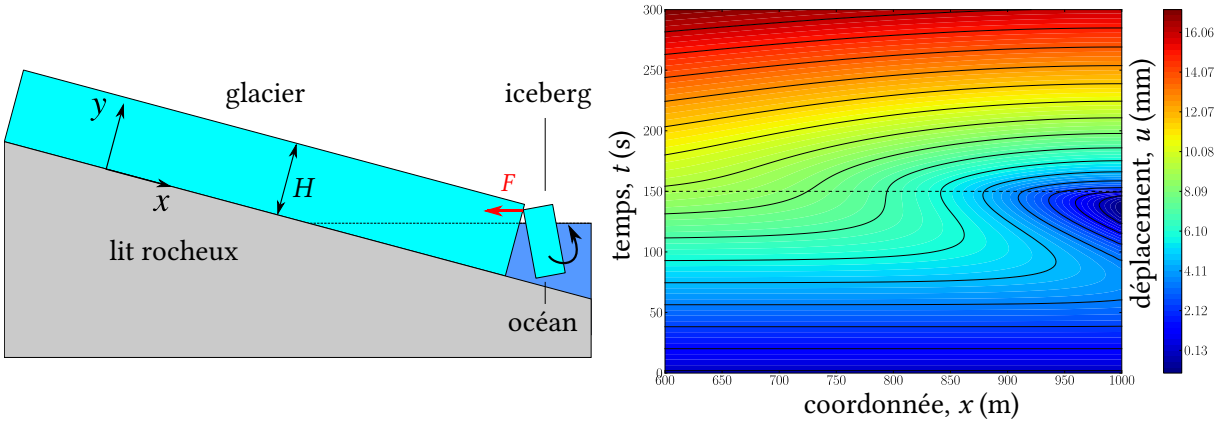

Figure 1.44: Displacements in the glacier induced by its sliding on the constant slope superimposed with the displacement caused by the force excerted by capsize of an unstable iceberg.

Version française: Déplacements dans le glacier induits par son glissement sur la pente constante superposé avec le déplacement provoqué par le retournement d'une iceberg instable.

edge of the contact zones ("spots" of contact) whose number can be very high depending on the size and the representativity of the surface, i.e. on the cutoff frequencies in the surface spectrum. The more representative the surface, the greater the number of contact zones, and therefore the greater the ratio between the perimeter P and the area A. For a grid of spacing h, the relative error E_r on the contact area is proportional to the ratio $E_r = |A* - A|/A = \beta Ph/A$ where $A*$ is the exact solution obtained for $h \to 0$ [9]. Basically, this form of error suggests that the real solution lies between the value obtained in simulations A and the same area without the area of its peripheral contact/non-contact transition zone of one-element thickness, i.e. $A - Ph < A* < A$. On the other hand, the value of β is not easy to estimate. But we found a trick ...

Take a square and cut it in two part by a randomly oriented straight line; what will be in average the ratio between the area of the smallest part A_{sm} to the area of the square A_{square}? The answer is

$$\left\langle \frac{A_{\text{sm}}}{A_{\text{carré}}} \right\rangle = \frac{\pi - 1 + \ln 2}{6\pi} \approx 0.150387618994810151606955$$

If we use this number so that the contact area estimated by the numerical calculation is deprived of this fraction of its peripheral crown, and the latter is corrected by the transformation of the metric from $p = 1$ (Manhattan metrics because we work on the square grid) to $p = 2$ (Euclidean metrics) via a factor $\pi/4$ for shapes isotropic in average, we obtain a simple expression to estimate the contact area by minimizing the discretization error:

$$A_{\text{corr}} = A - \frac{\pi - 1 + \ln 2}{24} P_1 h, \tag{1.11}$$

where P_1 is the total perimeter of the contact zones calculated on the square grid. This simple equation makes it possible to obtain the contact area very precisely even for very modest discretizations [88] (Fig. 1.45). As demonstrated in Section 1.2.3, this error compensation technique allowed us to go beyond the state of the art in the study of "rough contacts" and obtain new insights in the study of rough contact.

Version française: L'étude numérique de l'évolution de l'aire de contact réelle entre des surfaces rugueuses sous l'action de la pression appliquée nécessite une discrétisation très fine. Il s'agit tout d'abord de représenter proprement un spectre assez large d'une surface mais par ailleurs la discrétisation doit être suffisante pour résoudre correctement le problème mécanique. Si le spectre de la surface est bien représenté par la discrétisation, l'erreur sur la mesure de l'aire de contact se localise sur le bord des zones et des "taches" de contact dont le nombre peut être très élevé en fonction de la coupure aux basses fréquences. Plus la surface est représentative, plus grand est le nombre de zones de contact, et donc plus grand est le ratio entre le périmètre P et l'aire A. Pour une grille d'espacement h, l'erreur relative E_r sur l'aire de contact est proportionnelle au ratio $E_r = |A* - A|/A = \beta Ph/A$ où $A*$ est la solution

exacte pour $h \to 0$ [9]. En gros, cette forme d'erreur suggère que la vraie solution se trouve entre la valeur obtenue par des simulations A et la même aire privée de sa couronne périphérique d'épaisseur h, i.e. $A - Ph < A* < A$. Par contre la valeur de β n'est pas facile à estimer. Nous avons donc trouvé une astuce...

Prenons un carré et coupons le en deux par une droite arbitraire ; quel sera le rapport entre l'aire du plus petit morceau A_{sm} et l'aire du carré $A_{\text{carré}}$ en moyenne ? La réponse est

$$\left\langle \frac{A_{\text{sm}}}{A_{\text{carré}}} \right\rangle = \frac{\pi - 1 + \ln 2}{6\pi} \approx 0.150387618994810151606955$$

Si on utilise ce nombre de façon à ce que l'aire de contact estimée par le calcul numérique soit privée de cette fraction de sa couronne périphérique, et qu'à son tour celle-ci soit corrigée par la transformation de la métrique $p = 1$ (celle de Manhattan comme on travaille sur la grille carrée) à $p = 2$ via un facteur $\pi/4$, nous obtenons une simple expression pour estimer l'aire de contact en minimisant l'erreur de discrétisation :

$$A_{\text{corr}} = A - \frac{\pi - 1 + \ln 2}{24} P_1 h,$$

où P_1 est le périmètre total des zones de contact calculé sur la grille carrée. Cette équation simple permet d'obtenir l'aire de contact très précisément même pour de très modestes discrétisations [88] (Fig. 1.45). Comme cela va être démontré dans le résultat suivant, c'est cette technique de compensation d'erreur qui nous a permis d'aller au-delà de l'état de l'art dans l'étude des "contacts rugueux".

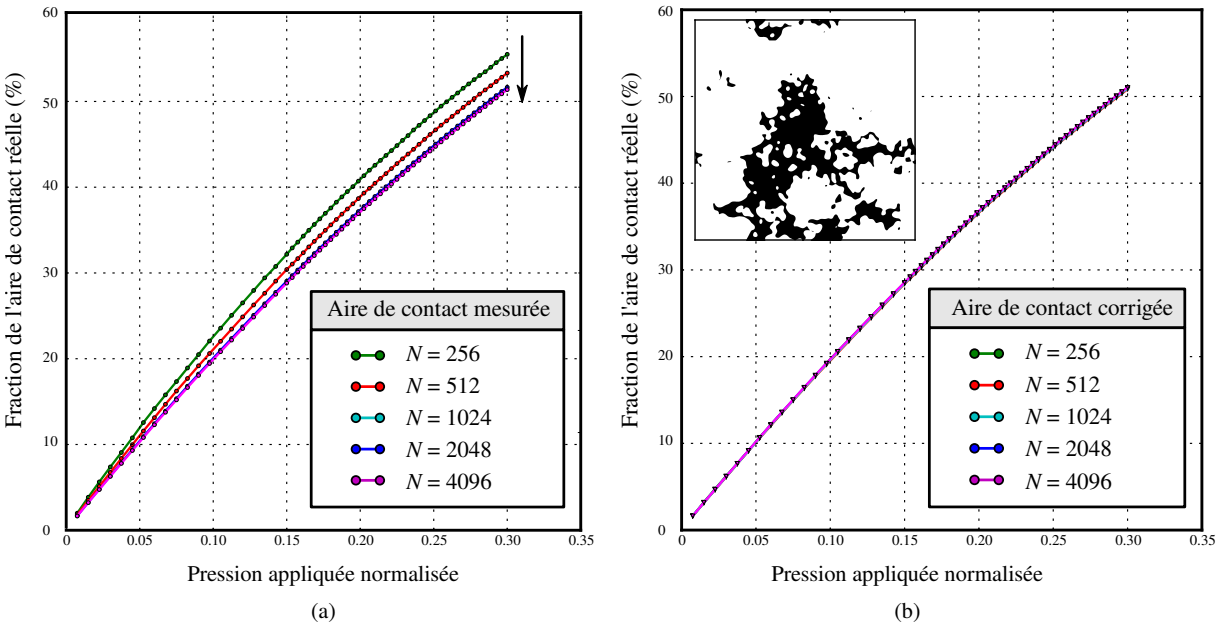

Figure 1.45: Convergence of the simulated contact area (a) without and (b) with discretization error compensation for a surface of size $N \times N$ with the well-represented surface spectrum already with $N = 128$, i.e. the higher frequency cutoff is set to $L/\lambda_s = 128$. It can be seen that with the compensation technique Eq. (1.11), the result almost does not depend on the discretization! The inset shows the distribution of the real contact area $A' \approx 22$ % found by the calculation.

Version française: Convergence de l'aire de contact mesurée (a) sans et (b) avec compensation d'erreur de discrétisation pour une surface de taille $N \times N$ avec le spectre de surface bien représenté déjà avec $N = 128$. On constate qu'avec la technique de compensation Eq. (1.11), le résultat ne dépend pas de la discrétisation ! La figure en insertion montre la distribution de l'aire réelle de contact $A' \approx 22$ % trouvée par le calcul.

References

- [9] V.A. Yastrebov, G. Anciaux, J.F. Molinari. "From infinitesimal to full contact between rough surfaces: evolution of the contact area". International Journal of Solids and Structures, 52:83-102 (2015) [doi] [arXIv] [pdf]
- [88] V.A. Yastrebov, G. Anciaux, J.F. Molinari. "On the accurate computation of the true contact area in mechanical contact of random rough surfaces". Tribology International, 114:161-171 (2017) [doi] [arXIv] [pdf]

1.7.2 MorteX method for tying, contact and wear

In PhD project of Basava Raju Akula (I could supervise this project in collaboration with Julien Vignollet (Safran tech) thanks to the trust of my thesis supervisor, Prof. Georges Cailletaud, who was the official supervisor), we have developed an original numerical method to deal with contact and sticking problems between virtual surfaces embedded in finite element mesh (cf. Fig. 1.46). The trick is to realize a combination of the X-FEM method [89] and the mortar method based on the monolithic augmented Lagrangian method; these two methods gave the name MorteX to our novel method. In addition to the purely technical difficulty related to the implementation of this coupling, there is a well-known theoretical obstacle in the world of extended finite elements: those are spurious oscillations that arise in the interface between bodies when the materials have a large difference in stiffness, or when the mesh densitis on tying sides contrast too much. We have proposed a *coarse-grained Lagrange multiplier* interpolation technique that avoids this problem [90]. The idea behind is to avoid over-constraint and adjust the number of available primal and dual DOFs in the interface. This technique has been successfully tested on classical patch tests as well as on the Eshelby inclusion problem; it has also proved useful for the classical Mortar method in the case of strong contrasts between the elastic properties or in presence of curvatures under-represented by FE discretization. Further the methodology was extended for *contact problems* between virtual surfaces [91].

The MorteX method is especially adapted to treat wear problems [92]. In this case, the evolution of contact surfaces resulting from material removal due to wear is modeled as a virtual surface evolution that propagates within the existing mesh. The use of the MorteX method therefore eliminates the need for complex remeshing techniques. Currently, we are working on the optimization of the space of interpolation functions used for Lagrange multipliers. Our preliminary results suggest that the use of the so-called dual shape functions for Lagrange multipliers permits to avoid some inconsistencis in pressure interpolation near contact edges, which are inevitable within the standard interpolation scheme.

Version française: Dans le cadre de la thèse de Basava Raju Akula (c'est une thèse que j'ai dirigée grâce à la confiance qui m'a été accordé par mon directeur de thèse, Prof. Georges Cailletaud, qui en était le directeur officiel), nous avons développé une méthode numérique originale qui permet de traiter des problèmes de contact et de collage entre des surfaces virtuelles embarquées au sein du maillage élément finis (cf. Fig. 1.46). L'astuce consiste à réaliser une combinaison de la méthode X-FEM [89] et de la méthode de mortar basée sur le Lagrangien augmenté monolithique ; ces deux méthodes ont donné le nom MorteX à la nôtre. En plus de la difficulté purement technique liée à la mise en œuvre de ce couplage, il existe un obstacle théorique bien connu dans le monde des élément finis étendus : il s'agit d'oscillations parasites qui surgissent dans l'interface entre des corps lorsque les matériaux présentent une grande différence de propriétés élastiques, ou bien lorsque les densités de maillage sont très élevées. Nous avons proposé une technique d'interpolation des multiplicateurs de Lagrange à grains grossiers qui permet d'éviter ce problème [90]. Cette technique a été testée avec succès sur des "patch-tests" classiques ainsi que sur le problème d'inclusion d'Eshelby ; elle s'est également avérée utile pour la méthode Mortar classique dans le cas de forts contrastes entre les propriétés élastiques. Ensuite la méthodologie a été étendue pour des problèmes de contact entre des surfaces virtuelles [91].

La méthode MorteX est sutout adaptée pour traiter des problèmes d'usure [92]. Dans ce cas, l'évolution des surfaces de contact qui résulte de l'enlèvement de matière dû à l'usure est modélisée comme une évolution de surface virtuelle qui se propage au sein du maillage existant. L'utilisation de la méthode MorteX élimine donc le besoin de recourir aux techniques complexes de remaillage. Actuellement, nous travaillons sur l'optimisation de l'espace des fonctions d'interpolations utilisées pour les multiplicateurs de Lagrange.

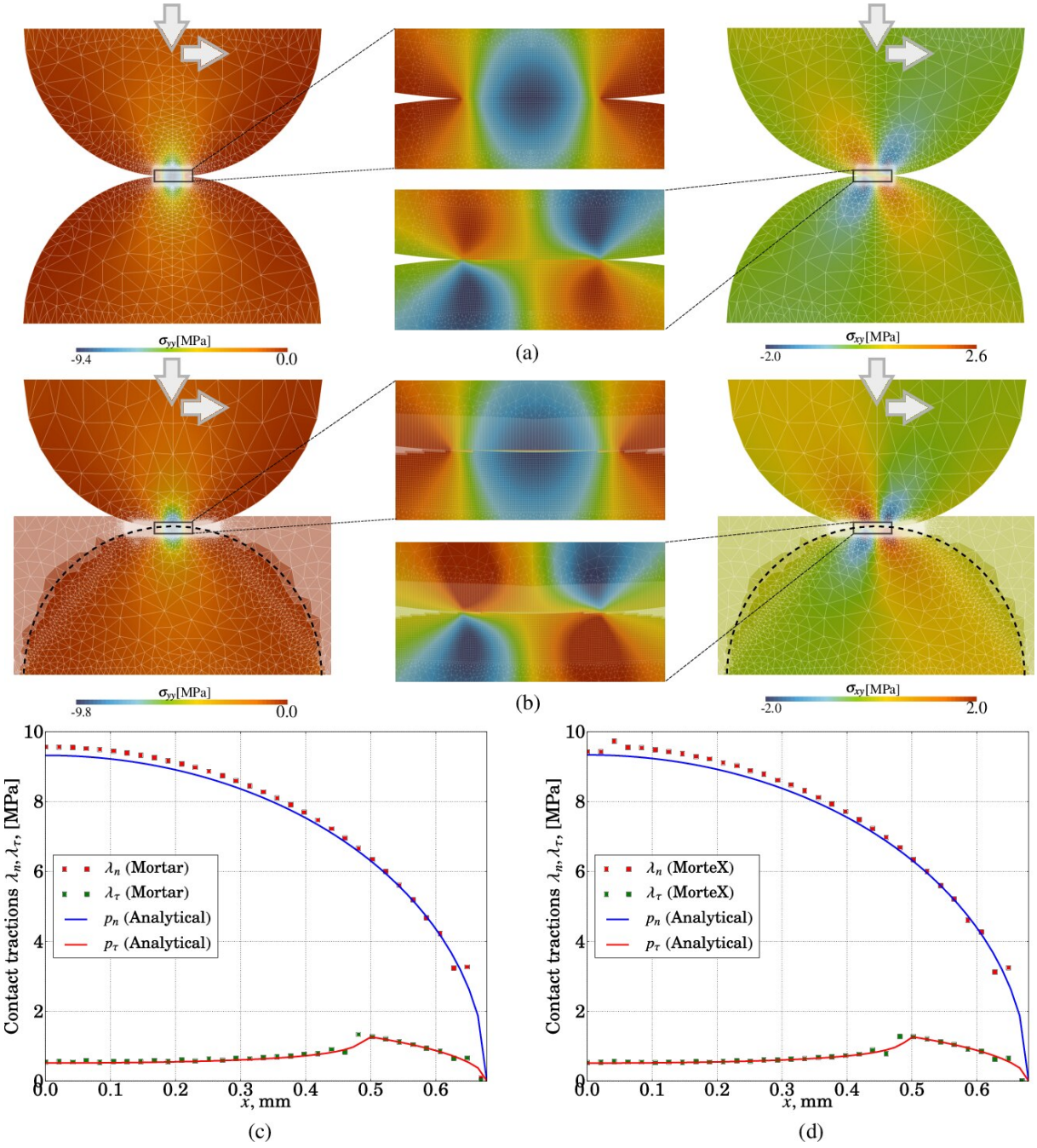

Figure 1.46: Problem of the frictional contact between two identical cylinders. Comparison of (a) the classical mortar method (which uses a boundary-fitted discretization) and (b) the MorteX method in which one of the cylinders is defined by a virtual surface passing through the mesh of a rectangle; (c) and (d) show normal and tangent traction distributions at the interface obtained by these two methods.

Version française: Problème du contact frottant entre deux cylindres. La comparaison de (a) la méthode classique de mortar avec la discrétisation conforme à la géométrie et (b) de la méthode MorteX dans laquelle un des cylindres est défini par un demi-cercle inseré dans le maillage d'un rectangle ; (c) et (d) montrent des distributions de contraintes à l'interface obtenues par ces deux méthodes.

References

- [90] B.R. Akula, J. Vignollet, V.A. Yastrebov (2019). "Stabilized MorteX method for mesh tying along embedded interfaces". Preprint is available [arXiv] [pdf]
- [91] B.R. Akula, J. Vignollet, V.A. Yastrebov (2019). "MorteX method for contact along real and embedded surfaces: coupling X-FEM with the Mortar method". Preprint is available [arXiv] [pdf]
- [93] B.R. Akula "Extended mortar method for contact and mesh-tying applications". PhD thesis defended on the 4th of February 2019 at Ecole des Mines de Paris, Paris, France. Supervisors: G. Cailletaud, J. Vignollet, V.A. Yastrebov. PhD committee: M.C. Baietto (president), A. Popp (reviewer), F. Lebon (reviewer), N. Moës, V. Chiaruttini. [HAL]
- [92] B.R. Akula, J. Vignollet, V.A. Yastrebov (2020). "MorteX method for the simulation of wear" submitted. Draft is available [encrypted pdf]
- Extended presentation "The MorteX method and its applications", World Congress on Computational Mechanics, Paris (virtually), France. January 2021 [youtube]

1.7.3 Computational framework for coupled thin flow in contact interfaces

In addition to the study of dry contact, we studied various effects resulting from the presence of a fluid in the contact interface. These studies were carried out in the context of normal contact in the absence of any effort or tangential movement. This problem is relevant for several applications, among others: static sealing of systems, lubrication in hot/cold-rolling and other types of metal forming, hydrogeology, extraction of shale oil and gas, tire/road contact in wet conditions, and a large number of biomechanical contact problems in presence of fluid.

As part of the thesis of Andrei Shvarts (I was allowed to supervise this thesis thanks to the trust that was granted to me by my thesis director, Prof. Georges Cailletaud, who was the official director), we built a coherent and monolithic finite element framework to address problems of viscous saturated flow in contact interfaces between solids [94]. This problem is not new, but we have been able to build an original framework which is more complete than existing ones. The novelty consists in a careful treatment of "lakes" of trapped fluid, i.e. the fluid regions completely surrounded by the contact areas. This mechanism was incorporated into the monolithic finite element framework which solves the global non-linear system for (1) the displacement field in the solid, (2) the pressure field in the thin film of fluid governed by the Reynold equation, (3) the field of Lagrange multipliers necessary to ensure the conditions of Hertz-Signorini-Moreau contact, and finally (4) the pressures in the trapped fluids obeying a non-linear behavior. In this framework, the Reynolds equation is solved on the updated geometry, and the fluid in the trapped zones and in the flow exerts surface forces on the solid Fig. 1.47. What is important is that we have used a model of compressibility of the fluid in the trapped zones which is sufficiently representative of the relevant physics of the phenomenon: the modulus of compressibility increases in an affine manner with the pressure in the fluid (liquid). This numerical framework allowed us to explore the system behavior under the strong coupling between solid and fluid equations, and to deduce some new theoretical results, for example, an empirical law for non-local permeability.

Version française: En complément de l'étude du contact sec, nous avons travaillé sur l'effet de la présence d'un fluide dans l'interface de contact. Cette étude est menée toujours dans le contexte du contact sous un effort normal, en absence de tout effort ou mouvement tangentiel. Ce problème est pertinent pour plusieurs applications, entre autres : l'étanchéité des systèmes, la lubrification dy laminage et formage, l'hydrogéologie, l'extraction d'hydrocarbures de couches de schiste, le contact pneu/chaussée en conditions humides, et un grand nombre de problèmes de contact anatomiques en présence de fluide.

Dans le cadre de la thèse d'Andrei Shvarts (c'est une thèse que j'ai dirigée grâce à la confiance qui m'a été accordéee par mon directeur de thèse, Prof. Georges Cailletaud, qui était le directeur officiel), nous avons construit un cadre élément-finis cohérent et monolithique pour aborder des problèmes d'écoulement visqueux et saturé dans l'interface entre des solides en présence du contact [94]. Ce problème n'est pas nouveau, mais nous avons pu construire un cadre qui nous semble plus complet que ceux qui existaient auparavant. La nouveauté consiste en un traitement soigneux des îlots (ou plutôt des flaques) de fluide piégé, i.e. le fluide complètement entouré par les zones de contact. Ce traitement a été intégré dans le cadre monolithique élément finis qui résout le système global non-linéaire pour

(1) le champ de déplacements dans le solide, (2) le champ de pression dans la couche mince de fluide gouverné par l'équation de Reynolds, et (3) le champ de multiplicateurs de Lagrange nécessaire pour assurer les conditions de contact de Hertz-Signorini-Moreau, et enfin (4) les pressions dans le fluide piégé à comportement non-linéaire. Dans ce cadre, l'équation de Reynolds est résolue sur la géométrie actualisée, et le fluide dans les zones piégées et dans l'écoulement exerce des efforts surfaciques sur le solide Fig. 1.47. Ce qui est important, c'est que nous avons utilisé un modèle de compressibilité du fluide dans les zones piégées qui est suffisamment représentatif de la physique du phénomène : le module de compressibilité augmente d'une manière affine avec la pression dans le fluide (liquide). Ce cadre numérique nous a permis d'explorer le comportement local fortement couplé entre solide et fluide, et de déduire quelques nouveaux résultats théoriques notamment sur la perméabilité non-locale.

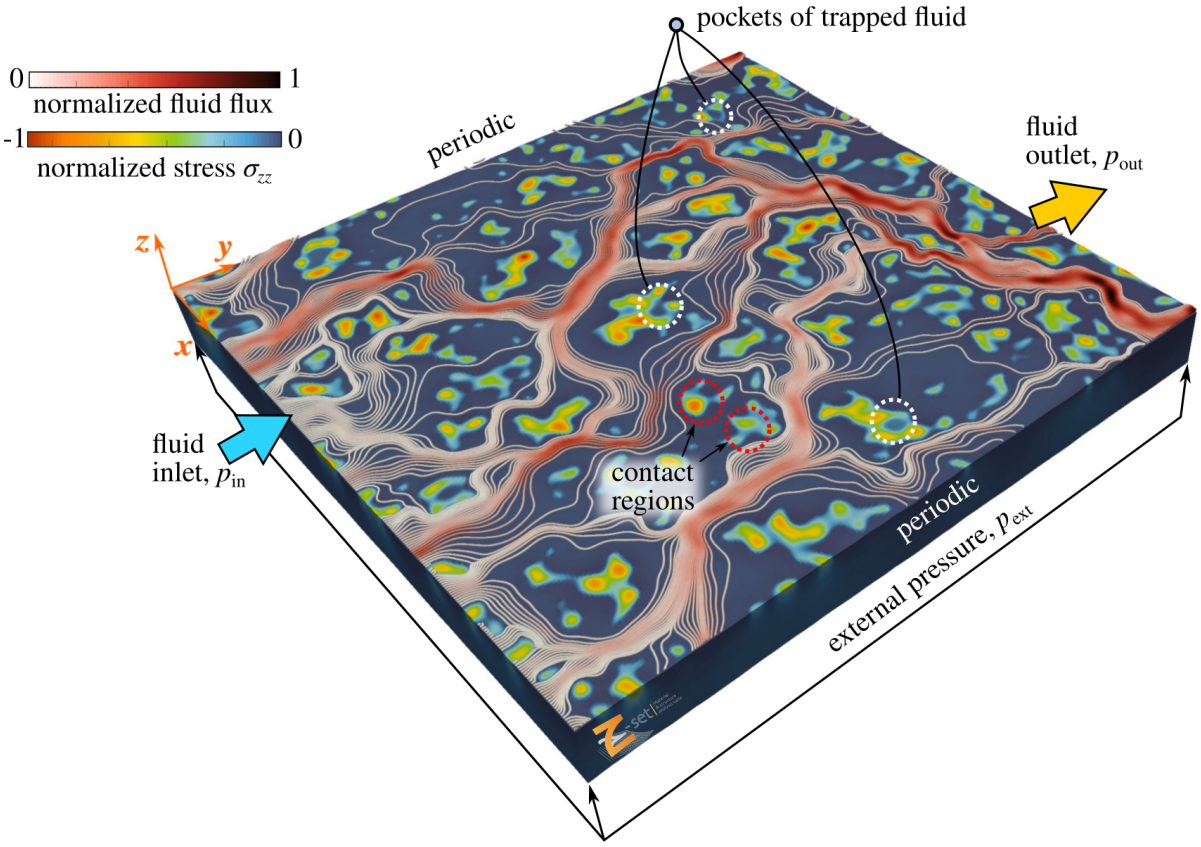

Figure 1.47: Strongly coupled simulation of thin flow in contact interface (couloured spots represents contact areas, flow lines represent direction and intensity of the main flux channels, lakes of trapped fluid are highlighted).

Version française: Simulation d'écoulement dans l'interface de contact : couplage fort

References

- [41] A.G. Shvarts, V.A. Yastrebov. "Fluid flow across a wavy channel brought in contact". Tribology International, 126:116-126 (2018). [doi] [arXiv] [pdf]
- [94] A.G. Shvarts, J. Vignollet, V.A. Yastrebov. "Computational framework for monolithic coupling for thin fluid flow in contact interfaces". Computer Methods in Applied Mechanics and Engineering, 379:113738 (2021) [doi] [arXiv] + Supplementary videos [zenodo]
- [26] A.G. Shvarts. "Coupling mechanical frictional contact with interfacial fluid flow at small and large scales" (2019). PhD thesis defended on March 20, 2019 at École des Mines de Paris in presence of the jury Res. Dir. D. Lasseux, Prof. M. Paggi, Prof. S. Stupkiewicz, Prof. J.A. Greenwood, Assist.

Prof. V. Rey, Assist. Prof. N. Moulin, Prof. G. Cailletaud, Dr. J. Vignollet, Dr. V.A. Yastrebov. This PhD thesis was awarded by a 🏆 CSMA award for one of two best theses in computational mechanics and by 🏆 Hirn award for the best thesis in tribology. [HAL] [pdf]

Chapter 2

Ideas & very preliminary results

During my academic career, occasionally I had time to touch upon (explore superficially, study and try to understand) various topics in science. Almost all of these attempts were stuck either because of lack of time, enthusiasm or because of technical difficulties which I could not overcome on the spur of the moment. Since I strongly believe that the work is not done if a paper is not written on the topic, almost all of these studies remain rather raw ideas and cannot be considered as scientific production. The only reason to mention these studies here is to leave a trace of these ideas with the hope to interest someone in taking a step forward with or without me. I would be happy to publish one day these raw ideas and first results in a kind of a small open access online book of ideas, but I am not sure that such a day will ever happen.

During last 10 years I touched upon the following topics and problems:

- Finite-speed gravity simulations of interacting galaxies.
- Surface-energy induced adhesion in finite element framework.
- Transmissivity of dilated conformal cracks.
- Coalescence of rain drops.
- River formation on a fractal landscape.
- Optimality of fractal characteristics of rough surfaces.
- Crystal plasticity modelling of Hadfield steels (high manganese-content austenitic steels).
- Creeping contact interfaces of rough cracks under strong hydrostatic compression.
- Hard third particles in rough contact interfaces.
- Viscoelasticity induced friction for tyre-road applications.
- Generation of bi-phase composites.
- Modified version of Persson's rough-contact model to deal with discrete spectra.
- Formalization of multi-dimensional tensorial structures S-structures.
- Random number generator takes part in review panel.
- Normal contact between multi-fractal rough surfaces.
- Static friction in presence of saturated pressurized fluid.
- Instability of thin structures in water.
- Analytical model for wear of a drilling insert with a rock.

Below I list some studies for which I have some illustrations.

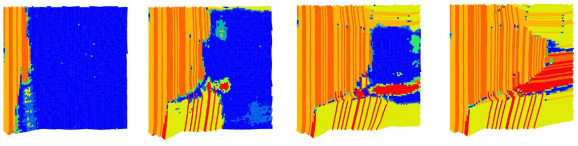

Martensitic transformations using special bi-stable potential [95] with my own molecular dynamics code, which I later used for teaching.

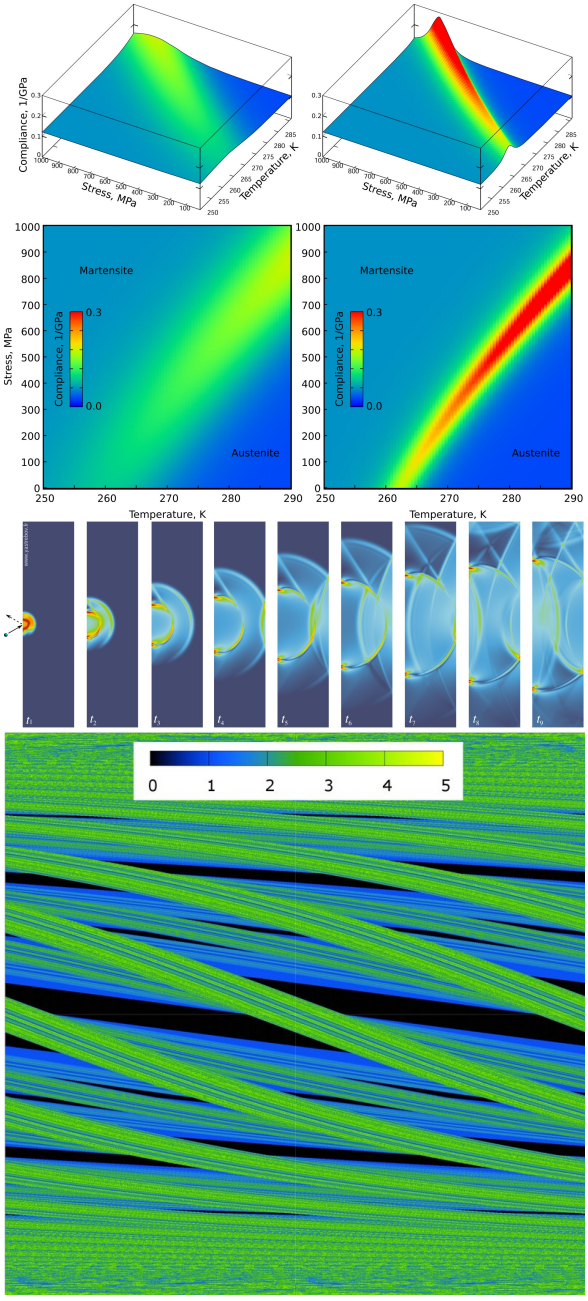

Martensitic transformations using multi-variant Ising-type model with interface energy; first 1D results were published [96]. Later, I obtained some closed form solutions for the probability of sates for the reference Hamiltonian of martensite/austenite including interface energy. I studied coarsening behavior in 2D.

Wave propagation in wave-guides and seismic waves simulations.

Crypto-billiard project: Lorentz gas simulation (elastic rebound of a point particle from a sphere) for various initial conditions could lead to complex chaotic patterns, here I show initial position – and angle map and the color corresponds to the number of rebounds on a finite size system.

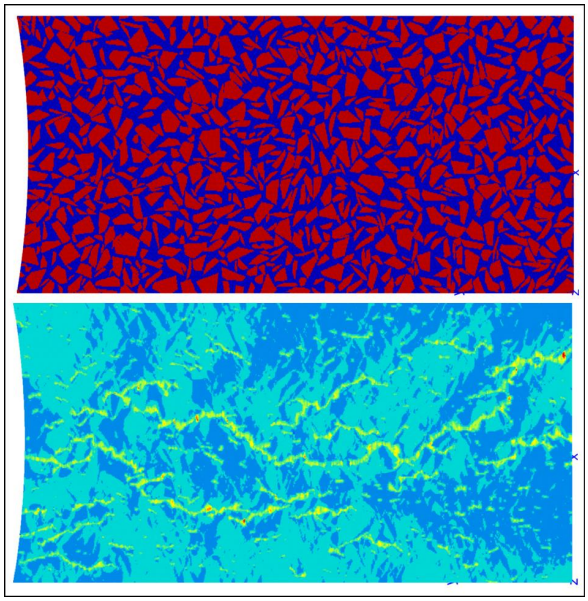

Models for heterogeneous concrete and brittle fracture of resulting microstructures.

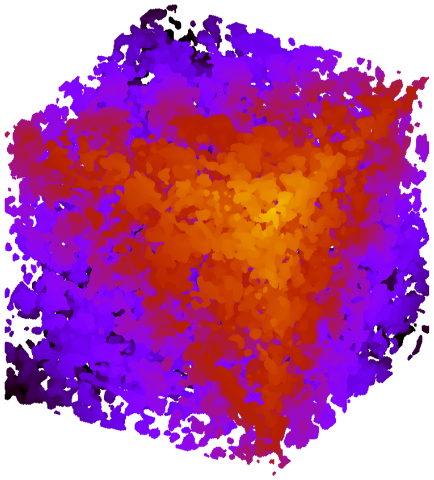

Porous media generator based on the self-affine (fractal-like) structure and filtering method for random noise that we use for generation of rough surfaces.

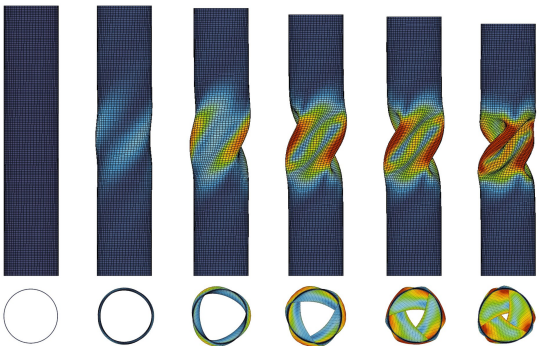

Plastic instabilities, post-buckling behavior with self-contact.

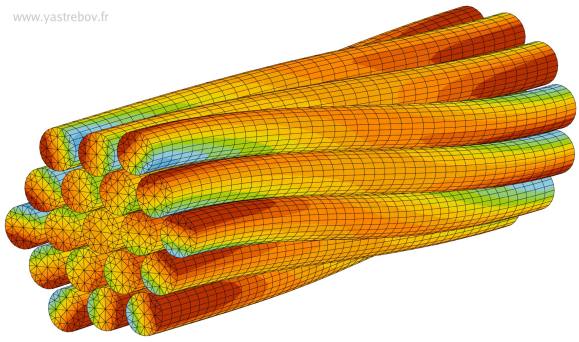

Multi-strand wires simulations.

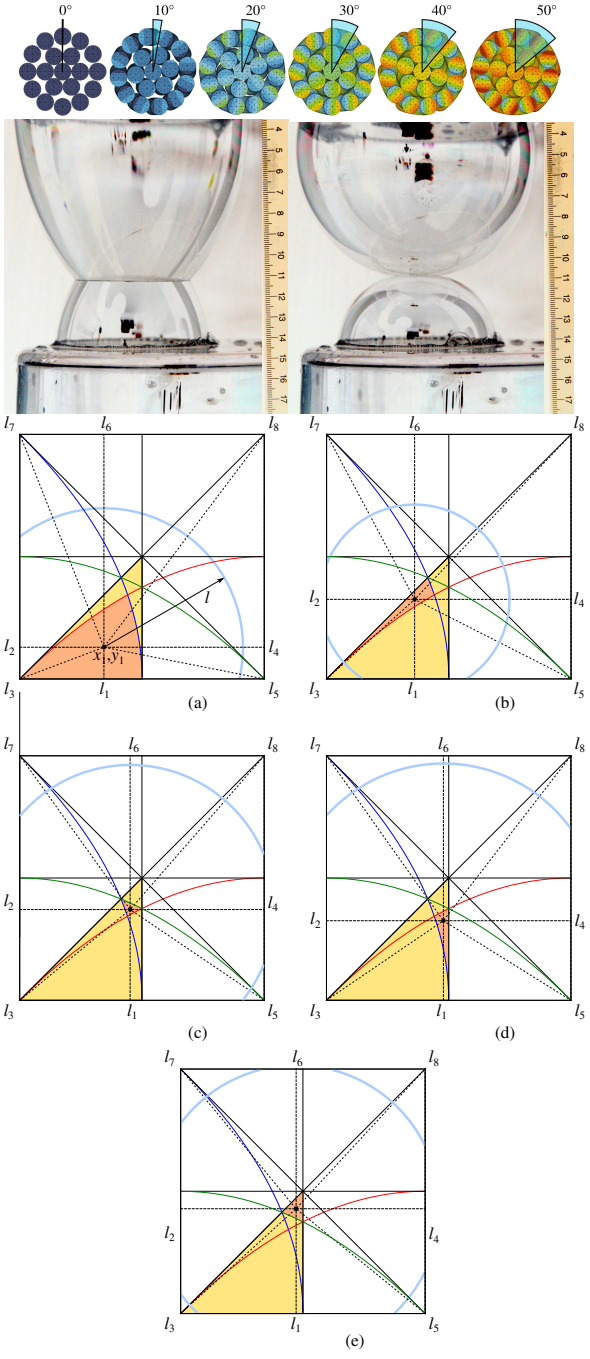

Contact between soap bubbles: home-made experiments and finite-element modelling.

Characterization of randomness of triangles in a circle and in a square domains.

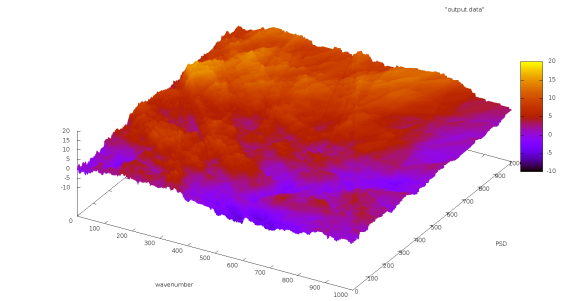

Shift induced rough surfaces and random surfaces on a sphere.

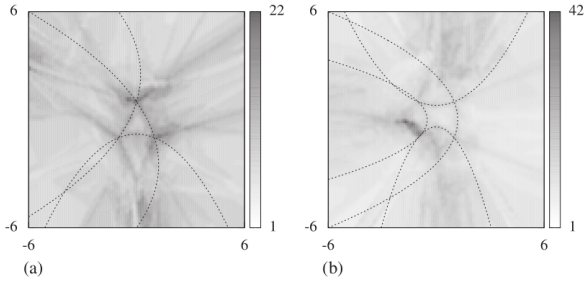

Constrained-optimization based contact detection and projection algorithms [97].

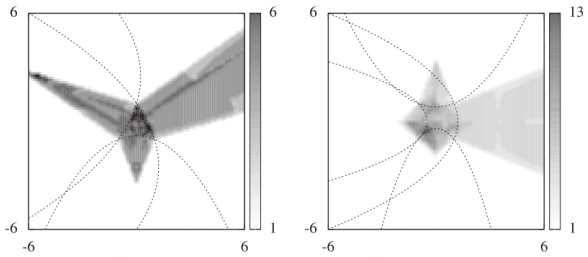

Collaborative study with Karim Inal and Brice Arrazat on accurate FE simulations reproducing micro-indentation experiments on electroplated gold on silicium substrate.

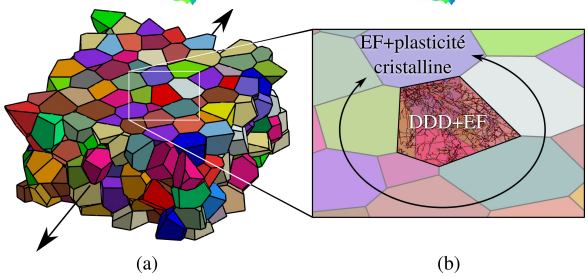

Coupling DDD (NumoDis) with FEM (Z-set), the topic of my postdoc at Centre des matériaux in the framework of AFGRAP ANR-funded project on the onset of fatigue cracks in steels.

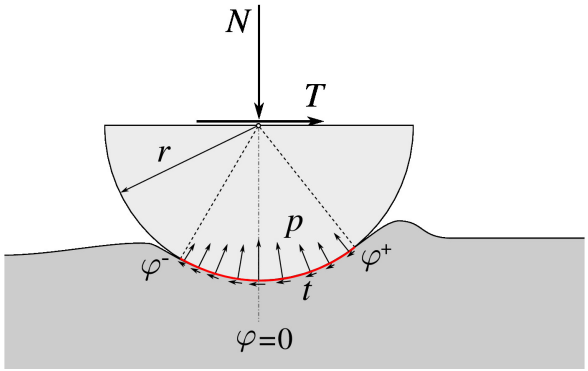

Geometrically induced difference in frictional contact for large penetrations.

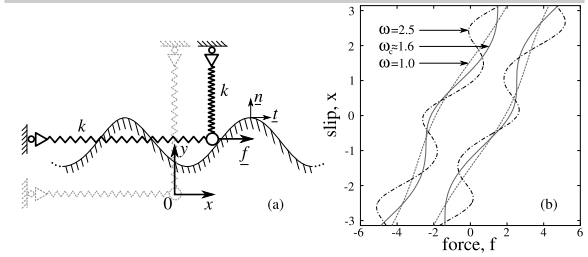

One-dimensional slip on a wavy surface, from simple analytical results to root-analysis and statistics of randomly rough profiles.

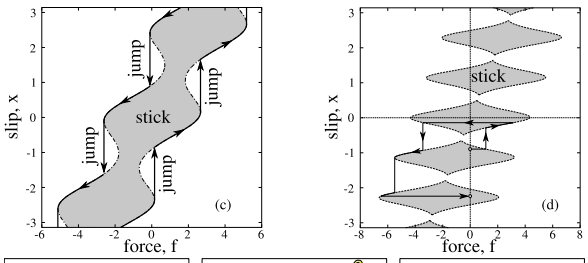

Topology and morphology of merging and splitting clusters in physics. In this figure I illustrate surgery cuts that restore manifolds from this topology.

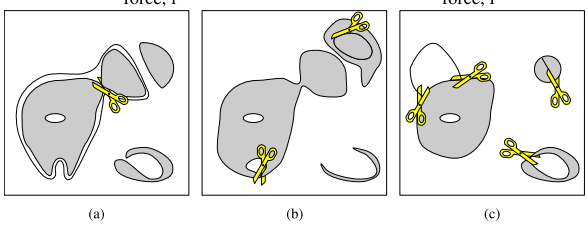

Onset of plastic core and its growth in smooth indentation (in this figure, a finite element simulation demonstrating the formation of an elastic layer under the indenter in absence of friction).

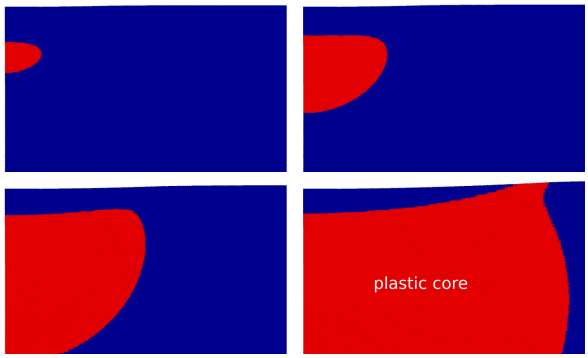

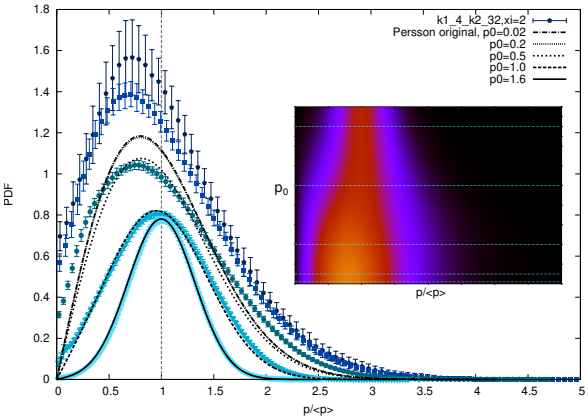

Statistics of contact pressure between contacting rough surfaces, the core quantity of Persson's rough contact model.

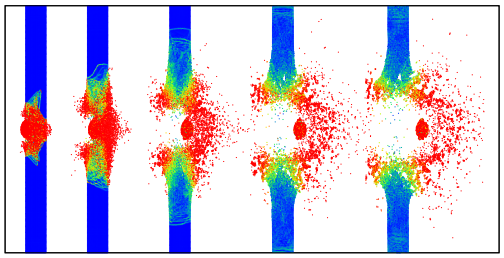

Molecular dynamics simulations of ultra high speed impacts with my MD code, which I also used for teaching during first few years of teaching Molecular Dynamics, later I switched to LAMMPS.

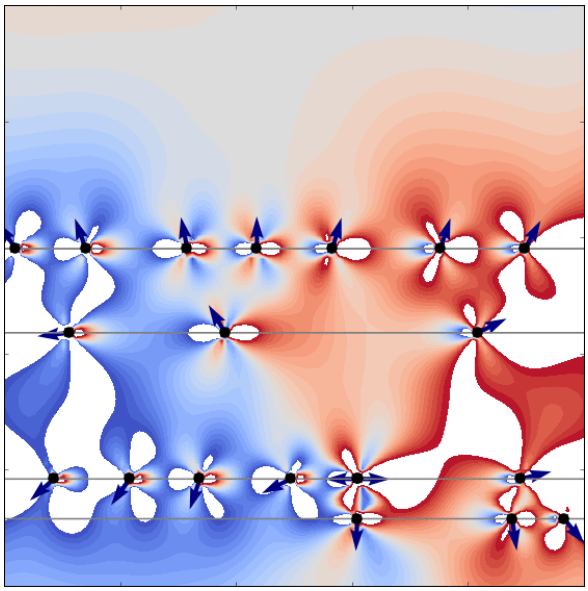

Simple 2D DDD solver for teaching needs.

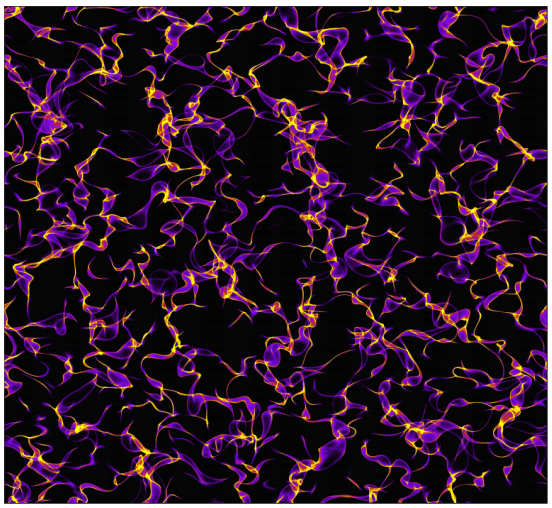

Density-caustic formation in early Universe using fractal perturbation of initial velocities inspired by Catastrophe Theory" by Vladimir Arnold.

Bibliography

[1] AI Vakis, VA Yastrebov, J Scheibert, L Nicola, D Dini, C Minfray, A Almqvist, M Paggi, Seunghwan Lee, G Limbert, et al. Modeling and simulation in tribology across scales: An overview. *Tribology International*, 125:169–199, 2018.

[2] Julian Durand. *Approche multi-échelles des problèmes de contact et d'étanchéité*. PhD thesis, Ecole des Mines, Paris, France, 2012. Advisers: H. Proudhon, G. Cailletaud.

[3] K.L. Johnson, J.A. Greenwood, and J.G. Higginson. The contact of elastic regular wavy surfaces. *Int J Mech Sci*, 27(6):383–396, 1985.

[4] Vladislav A. Yastrebov, Guillaume Anciaux, and Jean-François Molinari. The contact of elastic regular wavy surfaces revisited. *Tribology Letters*, 56:171–183, 2014.

[5] Vijaykumar Krithivasan and Robert L. Jackson. An analysis of three-dimensional elasto-plastic sinusoidal contact. *Tribol Lett*, 27(1):31–43, 2007.

[6] V. A. Yastrebov, J. Durand, H. Proudhon, and G. Cailletaud. Rough surface contact analysis by means of the finite element method and of a new reduced model. *Comptes Rendus Mécanique*, 339(7–8):473–490, 2011.

[7] Richard S Sayles and Tom R Thomas. Surface topography as a nonstationary random process. *Nature*, 271(5644):431, 1978.

[8] V. A. Yastrebov, G. Anciaux, and J.-F. Molinari. Contact between representative rough surfaces. *Physical Review E*, 86(3):035601(R), 2012.

[9] Vladislav A. Yastrebov, Guillaume Anciaux, and Jean-François Molinari. From infinitesimal to full contact between rough surfaces: evolution of the contact area. *International Journal of Solids and Structures*, 52:83–102, 2015.

[10] A. W. Bush, R. D. Gibson, and T. R. Thomas. The elastic contact of a rough surface. *Wear*, 35(1):87–111, 1975.

[11] G. Carbone and F. Bottiglione. Asperity contact theories: Do they predict linearity between contact area and load? *J Mech Phys Solids*, 56:2555–2572, 2008.

[12] B. N. J. Persson. Theory of rubber friction and contact mechanics. *J Chem Phys*, 115:3840–3861, 2001.

[13] BNJ Persson. Elastoplastic contact between randomly rough surfaces. *Physical Review Letters*, 87(11):116101, 2001.

[14] S. Hyun, L. Pei, J. F. Molinari, and M. O. Robbins. Finite-element analysis of contact between elastic self-affine surfaces. *Phys Rev E*, 70(2):026117, 2004.

[15] C. Campañá and M. H. Müser. Contact mechanics of real vs. randomly rough surfaces: A Green's Function Molecular Dynamics study. *Europhys Lett*, 77:38005, 2007.

[16] C. Putignano, L. Afferrante, G. Carbone, and G. Demelio. The influence of the statistical properties of self-affine surfaces in elastic contacts: A numerical investigation. *J Mech Phys Solids*, 60:973–982, 2012.

[17] Nikolay Prodanov, Wolf B. Dapp, and Martin H. Müser. On the contact area and mean gap of rough, elastic contacts: Dimensional analysis, numerical corrections, and reference data. *Tribol Lett.*, 53:433–448, 2014.

[18] Vladislav A. Yastrebov, Guillaume Anciaux, and Jean-François Molinari. The role of the roughness spectral breadth in elastic contact of rough surfaces. *Journal of the Mechanics and Physics of Solids*, 107:469 – 493, 2017.

[19] W. Manners and J. A. Greenwood. Some observations on persson's diffusion theory of elastic contact. *Wear*, 261:600–610, 2006.

[20] JA Greenwood, KL Johnson, and E Matsubara. A surface roughness parameter in Hertz contact. *wear*, 100(1-3):47–57, 1984.

[21] Jim A Greenwood and J Hl Tripp. The elastic contact of rough spheres. *Journal of Applied Mechanics*, 34(1):153–159, 1967.

[22] Lars Pastewka and Mark O Robbins. Contact area of rough spheres: large scale simulations and simple scaling laws. *Applied Physics Letters*, 108(22):221601, 2016.

[23] Vladislav A Yastrebov. The elastic contact of rough spheres investigated using a deterministic multi-asperity model. *Journal of Multiscale Modelling*, page 1841002, 2018.

[24] J. A. Greenwood. A simplified elliptic model of rough surface contact. *Wear*, 261:191–200, 2006.

[25] V. A. Yastrebov. *Numerical Methods in Contact Mechanics*. ISTE/Wiley, 2013.

[26] A. G. Shvarts. *Coupling mechanical frictional contact with interfacial fluid flow at small and large scales*. PhD thesis, PSL, MINES ParisTech, Paris, France, 2019.

[27] Fredrik Sahlin, Roland Larsson, Andreas Almqvist, PM Lugt, and Pär Marklund. A mixed lubrication model incorporating measured surface topography. part 1: theory of flow factors. *Proceedings of the Institution of Mechanical Engineers, Part J: Journal of Engineering Tribology*, 224(4):335–351, 2010.

[28] C. Vallet. *Fuite liquide au travers d'un contact rugueux: application à l'étanchéité interne d'appareils de robinetterie*. PhD thesis, Arts et Métiers ParisTech, 2008. PhD advisers: J.-R. Puiggali, D. Lasseux, HAL: https://tel.archives-ouvertes.fr/pastel-00004539/.

[29] Ye.A. Kuznetsov. Effect of fluid lubricant on the contact characteristics of rough elastic bodies in compression. *Wear*, 102(3):177–194, 1985.

[30] Andrei G Shvarts and Vladislav A Yastrebov. Trapped fluid in contact interface. *Journal of the Mechanics and Physics of Solids*, 119:140–162, 2018.

[31] JR Rice and George C Sih. Plane problems of cracks in dissimilar media. *Journal of Applied Mechanics*, 32(2):418–423, 1965.

[32] JR Rice. Elastic fracture mechanics concepts for interfacial cracks. *Journal of Applied Mechanics*, 55(1):98–103, 1988.

[33] David Anthony Hills. Mechanics of fretting fatigue. *Wear*, 175(1-2):107–113, 1994.

[34] Henry Proudhon, Siegfried Fouvry, and J-Y Buffière. A fretting crack initiation prediction taking into account the surface roughness and the crack nucleation process volume. *International Journal of fatigue*, 27(5):569–579, 2005.

[35] Vladislav A. Yastrebov, Guillaume Anciaux, and Jean-François Molinari. Permeability of the contact interface between rough surfaces. 2021. Draft version is available in appendix.

[36] Andreas Almqvist, C Campana, N Prodanov, and BNJ Persson. Interfacial separation between elastic solids with randomly rough surfaces: comparison between theory and numerical techniques. *Journal of the Mechanics and Physics of Solids*, 59(11):2355–2369, 2011.

[37] Vladislav A. Yastrebov, Guillaume Anciaux, and Jean-François Molinari. Gap distribution in contact interfaces between rough surfaces and transmissivity analysis. 2021. Draft version is available in appendix.

[38] Jané Kondev and Christopher L Henley. Geometrical exponents of contour loops on random gaussian surfaces. *Physical review letters*, 74(23):4580, 1995.

[39] Martin H Müser, Wolf B Dapp, Romain Bugnicourt, Philippe Sainsot, Nicolas Lesaffre, Ton A Lubrecht, Bo NJ Persson, Kathryn Harris, Alexander Bennett, Kyle Schulze, et al. Meeting the contact-mechanics challenge. *Tribology Letters*, 65(4):118, 2017.

[40] Joseph M Monti, Antoine Sanner, and Lars Pastewka. Distribution of gaps and adhesive interaction between contacting rough surfaces. *Tribology Letters*, 69(3):1–8, 2021.

[41] Andrei G. Shvarts and Vladislav A. Yastrebov. Fluid flow across a wavy channel brought in contact. *Tribology International*, 126:116 – 126, 2018.

[42] Vladislav A Yastrebov, Georges Cailletaud, Henry Proudhon, Frederick S Mballa Mballa, Sophie Noël, Philippe Testé, and Frédéric Houzé. Three-level multi-scale modeling of electrical contacts sensitivity study and experimental validation. In *Electrical Contacts (Holm), 2015 IEEE 61st Holm Conference on*, pages 414–422. IEEE, 2015.

[43] James A Greenwood. Constriction resistance and the real area of contact. *British Journal of Applied Physics*, 17(12):1621, 1966.

[44] J. Krim and G. Palasantzas. Experimental observations of self-affine scaling and kinetic roughening at sub-micron lengthscales. *Int J Mod Phys B*, 9:599–632, 1995.

[45] William D Nix and Huajian Gao. Indentation size effects in crystalline materials: a law for strain gradient plasticity. *Journal of the Mechanics and Physics of Solids*, 46(3):411–425, 1998.

[46] Gang Feng and William D Nix. Indentation size effect in mgo. *Scripta materialia*, 51(6):599–603, 2004.

[47] JG Swadener, EP George, and GM Pharr. The correlation of the indentation size effect measured with indenters of various shapes. *Journal of the Mechanics and Physics of Solids*, 50(4):681–694, 2002.

[48] R De Borst and LJ Sluys. Localisation in a cosserat continuum under static and dynamic loading conditions. *Computer Methods in Applied Mechanics and Engineering*, 90(1-3):805–827, 1991.

[49] Prajwal A. Sabnis, Samuel Forest, Nagaraj K. Arakere, and Vladislav A. Yastrebov. Crystal plasticity analysis of cylindrical indentation on a ni-base single crystal superalloy. *International Journal of Plasticity*, 51:200 – 217, 2013.

[50] Aurélien Fouque, Georges Cailletaud, Vladimir Esin, Romaric Landfried, Philippe Testé, Frédéric Houzé, Alexandre Bonhomme, Jean-Luc Ponthenier, François Chaudot, and Marina Lisnyak. Observation of metallurgical changes induced by an electric arc on ag-sno2-cuo electrodes. In *2019 IEEE Holm Conference on Electrical Contacts*, pages 239–244. IEEE, 2019.

[51] O. Ben-David, G. Cohen, and J. Fineberg. The dynamics of the onset of frictional slip. *Science*, 330(6001):211, 2010.

[52] D. S. Kammer, V. A. Yastrebov, P. Spijker, and J.-F. Molinari. On the propagation of slip fronts at frictional interfaces. *Tribology Letters*, 48(1), 2012.

[53] Yehuda Ben-Zion and Yueqiang Huang. Dynamic rupture on an interface between a compliant fault zone layer and a stiffer surrounding solid. *Journal of Geophysical Research: Solid Earth*, 107(B2):ESE 6–1–ESE 6–13, 2002.

[54] K. Ranjith and J. R. Rice. Slip dynamics at an interface between dissimilar materials. *J. Mech. Phys. Solids*, 49(2):341–361, 2001.

[55] A. Cochard and J. R. Rice. Fault rupture between dissimilar materials: Ill-posedness, regularization, and slip-pulse response. *J. Geophys. Res.*, 105(B11):25891, 2000.

[56] D. S. Kammer, V. A. Yastrebov, G. Anciaux, and J. F. Molinari. The existence of a critical length scale in regularised friction. *Journal of the Mechanics and Physics of Solids*, 63(0):40–50, 2014.

[57] V. Prakash and R. J. Clifton. Time resolved dynamic friction measurements in pressure-shear. In K.T. Ramesh, editor, *Experimental Techniques in the Dynamics of Deformable Solids, AMD-vol. 165*, pages 33–48, New York, 1993. ASME.

[58] JAC Martins, J Guimaraes, and LO Faria. Dynamic surface solutions in linear elasticity and viscoelasticity with frictional boundary conditions. *Journal of Vibration and Acoustics*, 117(4):445–451, 1995.

[59] DJ Andrews. Rupture propagation with finite stress in antiplane strain. *Journal of Geophysical Research*, 81(20):3575–3582, 1976.

[60] LB Freund. The mechanics of dynamic shear crack propagation. *Journal of Geophysical Research: Solid Earth (1978–2012)*, 84(B5):2199–2209, 1979.

[61] JRf Rice. Elastic fracture mechanics concepts for interfacial cracks. *Journal of applied mechanics*, 55(1):98–103, 1988.

[62] Robert C Viesca and James R Rice. Nucleation of slip-weakening rupture instability in landslides by localized increase of pore pressure. *Journal of Geophysical Research: Solid Earth*, 117(B3), 2012.

[63] Dmitry I Garagash and Leonid N Germanovich. Nucleation and arrest of dynamic slip on a pressurized fault. *Journal of Geophysical Research: Solid Earth*, 117(B10), 2012.

[64] Andrew Clennel Palmer and JR Rice. The growth of slip surfaces in the progressive failure of over-consolidated clay. In *Proceedings of the Royal Society of London A: Mathematical, Physical and Engineering Sciences*, volume 332, pages 527–548. The Royal Society, 1973.

[65] V. A. Yastrebov. Slip propagation along slip-weakening interfaces with a non-uniform contact pressure distribution. 2021. Draft version is available in appendix.

[66] Paul A Selvadurai, Steven D Glaser, and Jessica M Parker. On factors controlling precursor slip fronts in the laboratory and their relation to slow slip events in nature. *Geophysical Research Letters*, 44(6):2743–2754, 2017.

[67] Shmuel M Rubinstein, Gil Cohen, and Jay Fineberg. Detachment fronts and the onset of dynamic friction. *Nature*, 430(7003):1005–9, 2004.

[68] R. D. Mindlin. An introduction to the mathematical theory of vibrations of elastic plates, 1955. A monograph prepared for U. S. Army Signal Corps Engineering Laboratories, Fort Monmouth, N. J., Department of the Army Project 3-99-11-022, Signal Corps Project 142B, Signal Corps Contract DA-36-039 SC-56772.

[69] GG Adams. Radiation of body waves induced by the sliding of an elastic half-space against a rigid surface. *Journal of applied mechanics*, 67(1):1–5, 2000.

[70] Vladislav A. Yastrebov. Sliding without slipping under coulomb friction: Opening waves and inversion of frictional force. *Tribology Letters*, 62(1):1–8, 2016.

[71] Maria Comninou and J Dundurs. Elastic interface waves involving separation. *J. Appl. Mech.*, 44(2):222–226, 1977.

[72] LB Freund. Discussion: "elastic interface waves involving separation" (comninou, m., and dundurs, j., 1977, asme j. appl. mech., 44, pp. 222–226). *J. Appl. Mech.*, 45(1):226–227, 1978.

[73] Maria Comninou and J. Dundurs. Can two solids slide without slipping? *Int. J. Solids. Struct.*, 14(4):251 – 260, 1978.

[74] Eric Gerde and M Marder. Friction and fracture. *Nature*, 413(6853):285–288, 2001.

[75] Franck Moirot, Quoc-Son Nguyen, and Abdelbacet Oueslati. An example of stick–slip and stick–slip–separation waves. *European Journal of Mechanics - A/Solids*, 22(1):107–118, 2003.

[76] Dmitry Tkalich, Vladislav A Yastrebov, Georges Cailletaud, and Alexandre Kane. Multiscale modeling of cemented tungsten carbide in hard rock drilling. *International Journal of Solids and Structures*, 128:282–295, 2017.

[77] Georges Cailletaud and Philippe Pilvin. Utilisation de modèles polycristallins pour le calcul par éléments finis. *Revue européenne des éléments finis*, 3(4):515–541, 1994.

[78] Dmitry Tkalich, Alexandre Kane, Afaf Saai, Vladislav A. Yastrebov, Mikko Hokka, Veli-Tapani Kuokkala, Maria Bengtsson, Anna From, Carina Oelgardt, and Charlie C. Li. Wear of cemented tungsten carbide percussive drill-bit inserts: Laboratory and field study. *Wear*, 386:106–117, 2017.

[79] Dmitry Tkalich, Georges Cailletaud, Vladislav A. Yastrebov, and Alexandre Kane. A micromechanical constitutive modeling of {WC} hardmetals using finite-element and uniform field models. *Mechanics of Materials*, 105:166 – 187, 2017.

[80] V. A. Yastrebov. Wave propagation through an elastically-asymmetric architected material. 2021. arxiv.org/abs/1712.06294.

[81] Amandine Sergeant, Vladislav A Yastrebov, Anne Mangeney, Olivier Castelnau, Jean-Paul Montagner, and Eléonore Stutzmann. Numerical modeling of iceberg capsizing responsible for glacial earthquakes. *Journal of Geophysical Research: Earth Surface*, 123(11):3013–3033, 2018.

[82] Amandine Sergeant, Anne Mangeney, Vladislav A Yastrebov, Fabian Walter, Jean-Paul Montagner, Olivier Castelnau, Eléonore Stutzmann, Pauline Bonnet, Velotioana Jean-Luc Ralaiarisoa, Suzanne Bevan, et al. Monitoring greenland ice sheet buoyancy-driven calving discharge using glacial earthquakes. *Annals of Glaciology*, 60(79):75–95, 2019.

[83] Kurt Wendel. *Hydrodynamische Massen und hydrodynamische Massenträgheitsmomente*. PhD thesis, Hamburg, 1950. Translated in English by E.N. Labouvie and Avis Borden in 1956 "Hydrodynamic masses and hydrodynamic moments of inertia".

[84] Pauline Bonnet, Vladislav A Yastrebov, Patrick Queutey, Alban Leroyer, Anne Mangeney, Olivier Castelnau, Amandine Sergeant, Eléonore Stutzmann, and Jean-Paul Montagner. Modelling capsizing icebergs in the open ocean. *Geophysical Journal International*, 223(2):1265–1287, 2020.

[85] JC Burton, Jason M Amundson, DS Abbot, A Boghosian, L Mac Cathles, S Correa-Legisos, KN Darnell, N Guttenberg, DM Holland, and DR MacAyeal. Laboratory investigations of iceberg capsize dynamics, energy dissipation and tsunamigenesis. *Journal of Geophysical Research: Earth Surface*, 117(F1), 2012.

[86] Johannes Weertman. On the sliding of glaciers. *Journal of glaciology*, 3(21):33–38, 1957.

[87] V. A. Yastrebov, P. Bonnet, A. Mangeney, and O. Castelnau. Effect of iceberg's capsize on the deformation of marine-terminating glaciers. 2021.

[88] Vladislav A Yastrebov, Guillaume Anciaux, and Jean-François Molinari. On the accurate computation of the true contact-area in mechanical contact of random rough surfaces. *Tribology International*, 114:161–171, 2017.

[89] Natarajan Sukumar, David L Chopp, Nicolas Moës, and Ted Belytschko. Modeling holes and inclusions by level sets in the extended finite-element method. *Computer methods in applied mechanics and engineering*, 190(46-47):6183–6200, 2001.

[90] B.R. Akula, J. Vignollet, and V.A. Yastrebov. Stabilized mortex method for mesh tying along embedded interfaces. 2020. arxiv.org/abs/1902.04003.

[91] B.R. Akula, J. Vignollet, and V.A. Yastrebov. Mortex method for contact along real and embedded surfaces: coupling x-fem with the mortar method. 2020. arxiv.org/abs/1902.04000.

[92] B.R. Akula, J. Vignollet, and V.A. Yastrebov. Mortex method for the simulation of wear. 2020.

[93] B. R. Akula. *Extended mortar method for contact and mesh-tying applications*. PhD thesis, PSL, MINES ParisTech, Paris, France, 2019.

[94] Andrei G Shvarts, Julien Vignollet, and Vladislav A Yastrebov. Computational framework for monolithic coupling for thin fluid flow in contact interfaces. *Computer Methods in Applied Mechanics and Engineering*, 379:113738, 2021. Preprint is available arxiv.org/abs/1912.11292.

[95] Oliver Kastner. Molecular-dynamics of a 2d model of the shape memory effect. *Continuum Mechanics and Thermodynamics*, 15(5):487–502, 2003.

[96] V.A. Yastrebov, M. Fischlschweiger, G. Cailletaud, and T. Antretter. The role of phase interface energy in martensitic transformations: A lattice Monte-Carlo simulation. *Mechanics Research Communications*, 56:37 – 41, 2014.

[97] Alejandro M. Aragón, Vladislav A. Yastrebov, and Jean-François Molinari. A constrained-optimization methodology for the detection phase in contact mechanics simulations. *International Journal for Numerical Methods in Engineering*, 96(5):323–338, 2013.

Chapter 3

Perspective Research

My research program for the following years will be focused mainly on the topics which were initiated in recent years. Below, these topics are summarized with some details on concrete research questions and applications.

Physics and mechanics of contact at the roughness scale. Along this line of my research I plan to focus on the study of (1) heat transfer through contact interfaces (PhD project of P. Beguin 2020-2023) and (2) statistical properties of various characteristics: pressure, gap, fluid-pressure-terrace formation and morphological transformations (formation of non-simply connected clusters, joining of clusters, geometrical compactness and percolation). In addition, I obtained some preliminary results on (3) an original analytical model for the contact of rough surfaces inspired by Persson's model; (4) the normal contact between rough surfaces with different fractal dimensions, which in the simplest case results in bi-fractal composite surfaces; (5) permeability of dilated cracks with conformal faces, results are based on the phenomenological equations involving higher order moments; (6) presence of the third body in the contact interfaces which affects both macroscopic friction and permeability, this study has various applications in engineering and geotechnics; (7) effect of surface energy on the roughness characteristics. Finally, (8) I take part in research projects on non-local plasticity which will enable us to study, among other things, size effects in "rough contact".

Elasto-dynamics frictional sliding. I plan to finalize some preliminary analytical results (based on the analogy with the Linear Elastic Fracture Mechanics) on slip destabilization at frictional interfaces subject to non-uniform pressure distributions. The study of opening waves, standing and supersonic propagating slip pulses in finite size systems demonstrated numerically has not yet been published and fully explained analytically, I plan to finalize these findings. In addition, with David S. Kammer (ETH Zürich, Switzerland) we have restarted our collaboration on elasto-dynamic frictional instabilities and slip propagation. We have already accumulated some analytical results on potentially possible supersonic slip pulses propagating in frictional interfaces between a half-space and a rigid plane. We put recently in evidence such pulses for finite size systems and in the near future we hope to prove analytically and numerically the existence of supersonic pulses in infinite systems.

Contact-based architected materials. During last few years, I have been accumulating ideas and preliminary results on a novel class of contact-based architected materials. This multi-facet project has an ambitious to study static, vibrational and wave-propagation properties of these materials both theoretically and numerically. First prototypes of such materials have been tested numerically and also digitally fabricated. The particularity of such materials lies in the strong coupling of thermomechanical phenomena and in the fact that internal contact areas can be made arbitrary large, which can strongly enhance non-linear effects associated with contact and friction and thus it can endow the resulting materials with novel mechanical and physical properties. I plan to seek for a financial support and invest a large fraction of my time to this project which requires a really multi-disciplinary investigation combining theoretical, numerical and experimental research. In particular, I am interested in (1) the foundation of constitutive models for arbitrary asymmetric and anisotropic materials, (2) the formulation of homogenized models for history-dependent and dissipative behavior of such materials, and (3) in the study of bulk and surface wave propagation in such materials.

Chapter 4

Curriculum Vitae

4.1 Teaching

4.1.1 1. Contact Mechanics and Elements of Tribology (CMET)

This is a week-long master level course that I created from scratch has an ambition to cover main aspects of the contact mechanics and also introduce students to notions of tribology (lubrication, wear and fretting). Micromechanical contact, roughness, continuum mechanics of contact and friction, Reynolds equation for lubrication, computational contact mechanics, friction laws and also a link between contact, friction and material behavior are all covered. In addition, a large panorama of applications is provided. The course contains also some practical work dealing with integration of Flamant's solution for specific distributed loads to obtain stress state in the bulk, coding a simple penalty algorithm (residual vector and tangent matrix) in a basic finite element code and solving simple contact problems with Z-set software. The final day of the course is dedicated to seminars (cutting-edge research in tribology and contact mechanics) and to the 2h written exam. Within this course Henry Proudhon gives lectures on Wear and Fretting. All lectures, scripts for practical work and notes, are shared under CC BY 4.0 license on my web-page.

4.1.2 2. Multi-scale and multi-physics of materials and structures

In this collaborative course of Samuel Forest, Benoit Appolaire, Vladimir Esin, Kais Ammar and Victor de Rancourt, I give lectures on Molecular Dynamics (MD) and Dynamics of Dislocations and I also organize a 3h practical session on MD using LAMMPS, last years we study toughness of "porous crystal" playing with parameters of Lennard-Jones potential. All lectures, scripts for practical work and notes, are shared under CC BY 4.0 license on my web-page.

4.1.3 3. Non-Linear Computational Mechanics (NLCM)

This course initially created by Georges Cailletaud and Jean-Louis Chaboche for ATHENS (European students exchange week) introduces different aspects of nonlinear computational mechanics: from basics of nonlinear finite element method and material integrations up to large deformations, remeshing, localization and regularization. I give lectures on computational contact mechanics.

4.1.4 4. Continuum Mechanics (Mécanique des Milieux Continus)

This is a fundamental course on continuum mechanics of solids and fluids in which under the supervision of Samuel Forest, the lecturer of the course, a team of tutors ensures the link between the theory and practice solving with students a selection of problems from simple pressurized tank and tension/bending up to torsion, theorem of strain compatibility, stress concentrators, etc. ----------

4.2 Supervision

4.2.1 Internship students

- **Olga Trubienko** (MINES, 2008), Computational Contact Mechanics (master), with G. Cailletaud. Now, engineer in Total, France.
- **Olga Zinovieva** (MINES, 2012), Plasticity induced Roughness (master), with G. Cailletaud. Now, Assistant Professor in UNSW Canberra, Australia.
- **Fadoua Majid** (MINES & Schneider, 2015-2016), Electric contactors (master), with G. Cailletaud & V. Esin. Now, Engenineer in Akka Technologies.
- **Amine Saidi** (MINES & Safran Tech, 2018-2019), Simulation of fretting wear (master), with S. Basseville & J. Vignollet. Now, PhD student in LaMCoS, Lyon, France.
- **Yirun Zou** (MINES, 2019), Machine learning for non-linear dynamics (undegraduate).
- **Paul Beguin** (MINES, 2020), Iceberg-glacier dynamics (master). Now, PhD student in MINES ParisTech, France.

4.2.2 Co-supervision of graduate students

- **Julian Durand** (MINES, 2009-2010), Elasto-plastic rough contact, with G. Cailletaud & H. Proudhon. Now, engineer in Areva.
- **David S. Kammer** (EPFL, 2011-2012), Dynamic sliding, with J.F. Molinari & P. Spijker. Now, Assistant Professor in ETHZ, Switzerland.
- **Dmitry Tkalich** (MINES & NTNU, Norway, 2012-2016), Wear of drilling tools, with G. Cailletaud, Ch. C. Li, A. Kane.
- **Amandine Sergeant-Boy** (IPGP, Paris, 2013-2016), Glacial earthquakes, with A. Mangeney, O. Castelnau, J.P. Montagner, E. Stutzmann. Now, postdoc at LMA, Marseille, France
- **Matti Lindroos** (TUT & TWC, Finland, 2014), Thermo-mechano-metallurgical wear model, with G. Cailletaud. Now, research engineer at VTT, Finland.
- **Basava R. Akula** (MINES & Safran, 2015-2018), Parallel mortar-based contact algorithms, with J. Vignollet. Now, engineer at Transvalor.
- **Robin Lethiecq** (MINES & CEA-Leti, 2015-2018), Textile embedded chip on wire, with H. Proudhon & V. Mandrillon.
- **Takahiro Sakimoto** (MINES, 2015-2017), Modeling DWTT for high-strength steels, with J. Besson & Y. Madi. Now, senior researcher in JFE Steel corporation, Japan.
- **Andrei Shvarts** (MINES, 2015-2018), Fully coupled FE framework for fluid/contact interface, with J. Vignollet. Now, lecturer at Univesity of Glasgow, UK.
- **Paolo Cinat** (IMT Lucca, Italy, 3 months stay, 2016), Sealing problems. Now, engineer in Leonardo, Italy.
- **Aurélien Fouque** (MINES & SUPELEC & Schneider Electric, 2016-2020), Electric arc, with G. Cailletaud, V. Esin, F. Houzé, Ph. Testé. Now, engineer at Siemens, Berlin, Germany.
- **Pauline Bonnet** (IPGP & ENSAM & MINES, 2017-2021), Glacial earthquakes, with A. Mangeney, O. Castelnau, A. Leroyer, P. Queutey.
- **Vikram Phalke** (MINES, 2018-2021), Size effect in single crystal indentation, with S. Forest.
- **Paul Beguin** (MINES, 2020-2023), Thermomechanical contact, with S. Forest, C. Ovalle-Rodas, J. Vignollet.

4.2.3 Co-supervision of postdoctoral fellows

- **Ming Liu** (MINES, 2012-2013), Indentation analysis, with H. Proudhon. Now, Professor, Fuzhou University, China.
- **Ayaovi Dzifa Kudawoo** (MINES, 2012-2013), Computational contact, with G. Cailletaud. Now, engineer at EDF, Manchester, UK.

- **Frederick S. Mballa Mballa** (LaSIPS: MINES & SUPELEC, 2013-2015), Electric contact, with G. Cailletaud, H. Proudhon, F. Houzé, S. Noël. Now, engineer at Vitrociset, Italy.
- **Dmitry Tkalich** (MINES, 2016-2017), Microstructural mechancis of cemented tungsten carbides, with G. Cailletaud.

4.3 Software/code development

4.3.1 Z-set

With students and collaborators we implemented some new features in our in-house finite element software Z-set:

- Simple Fluid-Solid Interaction algorithm
- Mortar contact and tying algorithms
- Viscous friction law
- WC/binder β-model
- Strongly coupled Reynolds equation for interfacial viscous flow in contact interfaces
- Penalty and Augmented Lagrangian algorithms
- Surface tension
- Bezier smoothing for meshed surfaces
- Fast contact detection

4.3.2 Roughness generator + spectral BEM

In collaboration with Guillaume Anciaux we created simultaneously two codes for roughness generation and spectral BEM, which enabled us to fix bugs in both and have a converged results. Both codes for roughness generation and the spectral BEM are **C++** ensuring the best performance.

4.3.3 MD code

During my PhD thesis I created a simple Molecular Dynamics **C++** code, which I further improved by adding different potentials. This code I successfully used for teaching Molecular Dynamics, the students were invited (1) to code some simple algorithms for gas atom placing to avoid too high forces which would require excessively small time steps and (2) to study solidification of argon under soft temperature control. Tracing internal energy as a function of temperature allowed to determine heat capacity and its change under phase transition. Difference between ideal gas model (non-interacting particles) and interacting gas were highlighted.

4.3.4 DDD code

Over few years of teaching DDD I crafted a simple explicit 2D **Python** code for simulation of interacting dislocations in a finite size box, mainly used to demonstrate dipole interactions and work-hardening of dislocation pile-ups.

4.3.5 WC/binder microstructure and CAD generator

This is an add-on written as a separate **C++** class for voro++ which allows (1) to generate gmsh CAD model for further meshing in gmsh, with some extra possibilities to simply embed the CAD in a host structure, (2) generate realistic WC/binder microstructures. Regardless the seeming simplicity of the algorithm its implementation took me really a lot of time.

4.3.6 Wave dynamics in asymmetric Materials

C++ code for simulation of wave propagation in one-dimensional bars of asymmetric materials which uses absorbing boundary conditions and smart measurement of input and output energies. The code is clean and made publicly available under BSD-3-Clause at Zenodo DOI.

4.3.7 Semi-Analytical Floating Iceberg Models (SAFIM)

Python script for 2D simulation of capsizing/floating rectangular objects (for example, icebergs) which takes into account hydrostatic and hydrodynamic pressures as well as added mass matrix. The code is made publicly available under CC BY 4.0 license at Zenodo DOI

4.4 The First Overlay Journal in Mechanics

Started with Vincent Acary, Mathias Legrand and later with Maurine Montagnat & François Gibier we created the very first **overlay** journal in Mechanics Journal of Theoretical, Computational and Applied Mechanics (JTCAM). Now, all of us serve Technical Editors at JTCAM and we deal with all organizational and technical questions, we also ensure copy-editing work. For today (July 2, 2021) the journal published 4 articles, and has 12 more in review process.

4.4.1 Description

The Journal of Theoretical, Computational and Applied Mechanics (JTCAM) is a scholarly overlay journal covering all main branches of the solid mechanics, mechanical engineering and numerical methods in mechanics.

Papers can be submitted either via arXiv or HAL (open archive). The review process is managed by the board of at least eight Associate Editors. The journal promotes the Diamond Open Access (free for authors and readers) and Open science principles: sharing of data, code source and open peer review. The articles are published under Creative Commons BY licence. In journal's open peer review model: the reviewers are invited to reveal their identity and their reports as well as the authors' rebuttal letter are made publicly accessible as a separate document. The journal operates without Editor in chief, and is governed by the Board of the Journal composed of the Editorial Board (Associate Editors), the Scientific Advisory Board, and the Technical Board (Technical Editors).[1]. The copy-editing is ensured internally by the Technical Board in a close collaboration with the authors.

4.4.2 History

- JTCAM was launched in August 2020 on the dedicated platform for overlay journals Episciences.org.
- The first paper of JTCAM was published on March 16, 2021.
- In April 2020 JTCAM signed San Francisco Declaration on Research Assessment.
- The first open peer review was published on April 16, 2021.

4.5 Scientific production

4.5.1 Book & book chapter

1. V.A. Yastrebov. "Numerical Methods in Contact Mechanics", WILEY-ISTE (2013). [url]
2. V.A. Yastrebov. "Méthodes numériques en contact micromécanique". in book "Mécanique Numérique du Contact", ISTE, in press (2020) [HAL]

4.5.2 Publications in peer-reviewed journals

2011

1. V.A. Yastrebov, G. Cailletaud, F. Feyel. **"A local contact detection technique for very large contact and self-contact problems: sequential and parallel implementations"**. in G. Zavarise and P.Wriggers, ed., Trends in Computational Contact Mechanics ser. Lecture Notes in Applied and Computational Mechanics, 58:227-251 (2011).
2. V.A. Yastrebov, J. Durand, H. Proudhon, G. Cailletaud. **"Rough surface contact analysis by means of the Finite Element Method and of a new reduced model"**. Comptes Rendus Mecanique, 339:473-490 (2011).

2012

3. D.S. Kammer, V.A. Yastrebov, P. Spijker, J.F. Molinari. **"On the propagation of slip fronts at frictional interfaces"**. Tribology Letters, 48(1):27-32 (2012).

4. V.A. Yastrebov, G. Anciaux, J.F. Molinari. **"Contact between representative rough surfaces"**. Physical Review E, 86(3):035601 (2012). [pdf]

2013

5. P. A. Sabnis, S. Forest, N. K. Arakere, V.A. Yastrebov. **"Crystal plasticity analysis of cylindrical indentation on a Ni-base single crystal superalloy"**. International Journal of Plasticity, 51:200-217 (2013).

6. A.M. Aragon, V.A. Yastrebov, J.F. Molinari. **"A constrained-optimization methodology for the detection phase in contact mechanics simulations"**. International Journal for Numerical Methods in Engineering, 96(5):323-338 (2013).

2014

7. D.S. Kammer, V.A. Yastrebov, G. Anciaux, J.F. Molinari. **"The existence of a critical length scale in regularised friction"**. Journal of the Mechanics and Physics of Solids, 63:40-50 (2014).

8. V.A. Yastrebov, M. Fischlschweiger, G. Cailletaud, T. Antretter. **"The role of phase interface energy in martensitic transformations: a lattice Monte-Carlo simulation"**. Mechanics Research Communications, 56:37-41 (2014).

9. V.A. Yastrebov, G. Anciaux, J.F. Molinari. **"The contact of elastic regular wavy surfaces revisited"**. Tribology Letters, 56:171-183 (2014).

2015

10. V.A. Yastrebov, G. Anciaux, J.F. Molinari. **"From infinitesimal to full contact between rough surfaces: evolution of the contact area"**. International Journal of Solids and Structures, 52:83-102 (2015).

11. V.A. Yastrebov, G. Cailletaud, H. Proudhon, F.S. Mballa Mballa, S. Noël, Ph. Testé, F. Houzé. **"Three-level multi-scale modeling of electrical contacts: sensitivity study and experimental validation"**. In Proceedings of the Holm 2015 61st IEEE Holm Conference on Electrical Contacts, 414-422 (2015).

2016

12. V.A. Yastrebov. **"Sliding without slipping under Coulomb friction: opening waves and inversion of frictional force"**. Tribology Letters, 62(1):1-8 (2016)

13. B.L. Boyce, S.L.B. Kramer, T.R. Bosiljevac, E. Corona, . . . , V. Chiaruttini, M. Mazière, S. Feld-Payet, V.A. Yastrebov, J. Besson, J.L. Chaboche, . . . **"The Second Sandia Fracture Challenge: Predictions of Ductile Failure under Quasi-Static and Moderate-Rate Dynamic Loading"**. International Journal of Fracture, 198(1):5-100 (2016).

2017

14. D. Tkalich, G. Cailletaud, V.A. Yastrebov, A. Kane. **"A micromechanical constitutive modeling of WC hardmetals using finite-element and uniform field models"**. Mechanics of Materials, 105:166-187 (2017).

15. V.A. Yastrebov, G. Anciaux, J.F. Molinari. **"On the accurate computation of the true contact area in mechanical contact of random rough surfaces"**. Tribology International, 114:161-171 (2017).

16. D. Tkalich, A. Kane, A. Saai, V.A. Yastrebov, M. Hokka, V.T. Kuokkala, M. Bengtsson, A. From, C. Oelgardt, Ch. C. Li. **"Wear of cemented tungsten carbide percussive drill-bit inserts: laboratory and field study"**. Wear, 386:106-117 (2017).

17. V.A. Yastrebov, G. Anciaux, J.F. Molinari. **"The role of the roughness spectral breadth in elastic contact of rough surfaces"**. Journal of the Mechanics and Physics of Solids, 107:469-493 (2017).

18. D. Tkalich, V.A. Yastrebov, G. Cailletaud, A. Kane. **"Multiscale Modeling of Cemented Tungsten Carbide in Hard Rock Drilling"**. International Journal of Solids and Structures, 128:282-295 (2017).

2018

19. A.I. Vakis, V.A. Yastrebov, J. Scheibert, L. Nicola, D. Dini, C. Minfray, A. Almqvist, M. Paggi, S. Lee, G. Limbert . . . M. Mueser, M. Ciavarella. **"Modeling and simulation in tribology across scales: An overview"**. Tribology International, 125:169-199 (2018).

20. A.G. Shvarts, V.A. Yastrebov. **"Fluid flow across a wavy channel brought in contact"**. Tribology International, 126:116-126 (2018).

21. A.G. Shvarts, V.A. Yastrebov. **"Trapped fluid in contact interface"**. Journal of the Mechanics and Physics of Solids, 119:140-162 (2018).

22. A. Sergeant, V.A. Yastrebov, A. Mangeney, O. Castelnau, J.P. Montagner, E. Stutzmann. **"Numerical modeling of iceberg capsize responsible for glacial earthquakes"**. Journal of Geophysical Research: Earth Surface, 123:3013-3033 (2018).

2019

23. V.A. Yastrebov. **"The Elastic Contact of Rough Spheres Investigated Using a Deterministic Multi-Asperity Model"**. Journal of Multiscale Modelling (2019), 10(1):1841002.

24. A. Sergeant, A. Mangeney, V.A. Yastrebov, F. Walter, J.-P. Montagner, O. Castelnau, E. Stutzmann, P. Bonnet, V.J.L. Ralaiarisoa, S. Bevan, A. Luckman. **"Monitoring Greenland ice-sheet buoyancy-driven calving discharge using glacial earthquakes"**. Annals of Glaciology, 60(79):75-95 (2019). Open access.

2020

25. P. Bonnet, V.A. Yastrebov, P. Queutey, A. Leroyer, A. Mangeney, O. Castelnau, A. Sergeant, E. Stutzmann, J.-P. Montagner. **"Modeling iceberg capsize in open ocean"**. Geophysical Journal International, 223(2):1265-1287 (2020).

2021

26. A.G. Shvarts, J. Vignollet, V.A. Yastrebov. **"Computational framework for monolithic coupling for thin fluid flow in contact interfaces"**. Computer Methods in Applied Mechanics and Engineering, 379:113738 (2021), supplementary videos DOI

Preprints

27. V.A. Yastrebov. **"Wave propagation through an elastically-asymmetric architected material"**. submitted (2021) [arXiv], supplementary data, scripts and figures DOI

28. B.R. Akula, J. Vignollet, V.A. Yastrebov. **"Stabilized MorteX method for mesh tying along embedded interfaces"**. in submission process (2019) [arXiv] [pdf].

29. B.R. Akula, J. Vignollet, V.A. Yastrebov. **"MorteX method for contact along real and embedded surfaces: coupling X-FEM with the Mortar method"**. in submission process (2019) [arXiv] [pdf].

4.5.3 Presentations at conferences/workshops

2007

1. 38th Conference Control Processes and Stability 2007, Saint-Petersburg, Russia, 9-12 April (2007), oral presentation

2009

2. 9e Colloque National en Calcul des Structures, Giens, France, 25-29 May (2009), poster presentation
3. 1st International Conference on Computational Contact Mechanics, Lecce, Italy, 16-18 September (2009), oral presentation

2010

4. IV European Conference on Computational Mechanics, Paris, France, 16-21 May (2010), oral presentation

2011

5. 10eme Colloque National en Calcul des Structures, Giens, France, 9-13 May (2011), oral presentation

6. CECAM: Brittle Fracture at the Atomic Scale, EPFL Lausanne, Switzerland, 16-19 May (2011)

2012

7. Materials Deformation: Fluctuations, Scaling, Predictability, Les Houches, France, 22-27 January (2012), poster presentation

8. EuroMech: New trends in Contact Mechanics, Cargèse, France, 26-31 March (2012), oral presentation

9. ECCOMAS Young Investigators Conference, Aveiro, Portugal, 24-27 April (2012), invited talk

10. 24 Journées Internationales Francophones de Tribologie, Aix-en-Provence, France, 9-11 May (2012), oral presentation

2013

11. Colloque Plasticité, Paris, France, 17-19 April (2013), poster presentation
12. 11e Colloque CSMA, Giens, France, 13-17 May (2013), oral presentation + invited talk
13. 3rd International Conference on Computational Contact Mechanics, Lecce, Italy, 10-12 July (2013), oral presentation
14. 20e Congrès Français de Mécanique, Bordeaux, France, 27-30 August (2013), oral presentation
15. 40th Leeds-Lyon Symposium on Tribology, Lyon, France, 4-6 September (2013), oral presentation

2014

16. Contact Mechanics International Symposium (CMIS), Abu-Dhabi, United Arab Emirates, 3-5 February (2014), not present.
17. 20th European Conference on Fracture, Trondheim, Norway, 30 June-4 July (2014), oral presentation.
18. 11th World Congress on Computational Mechanics, Barcelona, Spain, 20-25 July (2014), oral presentation.
19. 7th International Conference on Multiscale Materials Modeling, Berkeley, USA, 6-10 October (2014), not present.
20. Predictive approach of sealing, Paris, France, 13 October (2014), invited talk.
21. International Workshop on Dislocation Dynamics Simulations, Saclay, France, December 10-12 (2014), poster presentation.

2015

22. 18e Rencontre du Non-Linéaire, Paris, France, 17-19 March (2015), poster presentation.
23. Contact mechanics and coupled problems in surface phenomena, Lucca, Italy, 30 March - 2 April (2015), oral presentation.
24. IV International Conference on Computational Contact Mechanics, Hannover, Germany, 27-29 May (2015), oral presentation.
25. 9th European Solid Mechanics Conference, Madrid, Spain, 6-10 July (2015), oral presentation.
26. 42nd Leeds-Lyon Symposium on Tribology, Lyon, France, 7-9 September (2015), oral presentation.
27. 52nd Annual Technical Meeting of the Society of Engineering Sciences (SES), Texas A&M University, USA, 26-28 October (2015), invited presentation.

2016

28. CMIS 2016: Contact Mechanics International Symposium, Warsaw, Poland, 11-13 May (2016), oral presentation.
29. ICTAM 2016: 24th International Congress of Theoretical and Applied Mechanics, Montreal, Canada, 21-26 August (2016), invited presentation.
30. Journées annuelles du GDR DYNOLIN (Dynamique Non Linéaire), ENSTA-ParisTech, Palaiseau, France, 10-11 August (2016), opening lecture.

2017

31. Micro/Nanoscale Models for Tribology, Lorentz Centre, Leiden, The Netherlands, 30 Jan - 3 Feb (2017), organizer, presenter of day summary & round table animator.
32. GDR MéPhy, Workshop on "Programmable Matter", ESPCI, Paris, France, 7 June (2017), oral presentation.
33. 6th Biot Conferences on Poromechanics, Ecole des Ponts ParisTech and IFSTTAR, Paris, France, 9-13 July (2017), oral presentation.
34. Leeds-Lyon Symposium on Tribology, Lyon, France, 4-6 September (2017), two oral presentations.
35. 7th GACM Colloquium on Computational Mechanics, Stuttgart, Germany, 11-13 October (2017), invited presentation.
36. Computational Modeling of Complex Materials Across the Scales, ECCOMAS Thematic Conference, Paris, France, 7-9 November (2017), oral presentation.

2018

37. 21e Rencontre du Non-Linéaire, Paris, France, 27-29 March (2018), poster presentation.
38. Contact Mechanics International Symposium, Sanctuary of Oropa, Italy, 16-18 May (2018), oral presentation.
39. 10th European Solid Mechanics Conference, Bologna, Italy, 2-6 July (2018), oral presentation.
40. 13th World Congress in Computational Mechanics, New York, USA, 22-27 July (2018), oral presentation.

2019

41. CECAM Workshop "Modeling tribology: friction and fracture across scales", Lausanne, Switzerland, 28-30 January (2019), oral presentation and round table.
42. 14e Colloque CSMA, Giens, France, 13-17 May (2019)
43. VI International Conference on Computational Contact Mechanics, Hannover, Germany, 3-5 July (2019), keynote lecture.
44. Congres Français de Mecanique, Brest, France, 26-30 August (2019), oral presentation.

2021

45. World Congress of Computational Mechanics, January, Paris, France (virtually) (2021), oral presentation.
46. 24e Rencontre du Non-Linéaire: Mini-colloque "Géométrie et élasticité". Paris, France (virtually), 24-26 March (2021), Zoom presentation.

4.5.4 Invited presentations

- "Scientific Publications". Junior Workshop at WCCM-ECCOMAS 2020/2021, Paris, France (virtually), January 8, 2021.
- "Weakly and strongly coupled simulations of interfacial fluid flow at roughness scale" at Workshop "Predictive approach of sealing", Maestral lab 50th anniversary, Pont du Garde, Oct 2-3 2019.
- "Contact Mechanics at the Roughness Scale". VI International Conference on Computational Contact Mechanics, Leibnizhaus Hannover, Germany, July 3-5 2019.

- "The role of surface roughness in contact and transport phenomena". School of Civil & Environmental Engineering, Cornell University, Ithaca, USA, October 4, 2018.
- "The role of surface roughness in contact and transport phenomena". Sullivan Park, Corning Inc, Corning, USA, October 2, 2018.
- "Contact along virtual interfaces: coupling the X-FEM with the mortar discretization". 7th GACM Colloquium on Computational Mechanics, Stuttgart, Germany, October 12, 2017.
- "The role of surface roughness in contact and transport phenomena". Institut Jean le Rond d'Alambert, Paris, France, September 28, 2017.
- "Micromechanical and transport properties of contact interfaces between rough surfaces". Laboratoire Modélisation et Simulation Multi Echelle (MSME), Université Paris-Est, Marne-la-Vallée, France, April 20, 2017.
- "Contact and sealing between solids with rough surfaces: numerical approach" Institute of Mechanics, Lomonosov State University, Moscow, Russia, November 21, 2016.
- "Quelques exemples de dynamique non-linéaire dans la mécanique du contact / frottement". Manifestation du GDR DYNOLIN, DYnamique NOn LINéaire, ENSTA ParisTech, Palaiseau, France, October 11, 2016, opening lecture.
- "Contact between rough surfaces: mechanical and transport phenomena at small scales". ICTAM 2016: 24th International Congress of Theoretical and Applied Mechanics, Montreal, Canada, August 26, 2016.
- "Contact between rough surfaces: mechanical and transport phenomena". Department of Engineering Sciences and Mathematics, Luleå University of Technology, LTU, Luleå, Sweden, April 13, 2016.
- "Mechanical contact between rough elastic-plastic solids: scale effect in deformation of asperities". Society of Engineering Science (SES) Technical Meeting, Texas A&M University, USA, October 27, 2015.
- "Mechanics and physics of rough contact". Fédération Francilienne de Mécanique, Arts et Métiers ParisTech, Paris, France, May 7, 2015.
- "Computational contact mechanics: engineering approach". Centre de Mise en Forme des Matériaux, MINES ParisTech, Sophia-Antipolis, France, April 21, 2015.
- "A numerical study of the contact between rough surfaces: mechanical and transport phenomena at small scales." Seismology lab, Institut de Physique du Globe de Paris, France, November 25, 2014.
- "Sealing and percolation of rough surfaces: focus on contact mechanics". Workshop "Predictive approach to sealing", Paris, France, October 13, 2014.
- "Mechanics of contact between rough surfaces". Laboratoire de Mécanique des Structures Industrielles (LaMSID), CNRS-EDF-CEA, Clamart, France, March 20, 2014.
- "Mechanics of elastic and elasto-plastic contact between rough surfaces", TriboLab, Politecnico di Bari, Italy, January 29, 2014.
- "Computational contact mechanics with finite elements". Laboratoire de Mécanique et Technologie (LMT), ENS Cachan, France, December 5, 2013.
- "Some recent developments in computational contact mechanics". Colloquium of the French Computational Structural Mechanics Association (CSMA), Giens, France, May 16, 2013.
- "Computational Contact Mechanics: geometry, detection and numerical techniques". PhD Olympiad, ECCOMAS Young Investigators Conference, Aveiro, Portugal, April 25, 2012.
- "Parallel treatment of contact problems". Laboratoire de Mécanique des Structures Industrielles (LaMSID), CNRS-EDF-CEA, Clamart, France, June 28, 2011.

Acknowledgements

Thank you Russia, FML 239 & Polytech for a great start, Switzerland and France for such a welcoming attitude to me and for the take-off! The MINES ParisTech for a great environment and the CNRS for a dream post!

In my heart or/and in my research I have a souvenir of our interaction and/or collaboration! **Thank you:**

Bachelor and thesis supervisors and much more that that: Boris E. Melnikov, Artem S. Semenov

PhD supervisors and much more that that: Georges Cailletaud, Frédéric Feyel

CdM of my "youth": Olga Klinkova, Fanny Jambon, Djamel Missoum-Benziane, Yoann Guilhem, Julien Frachon, Julian Durand, Lingtao Sun, Sophie Cartel, Nikolay Osipov, Stéphane Quilici, Kais Ammar, Olga Zinovieva, Olga Trubienko, André Pineau, Yves Bienvenu, Liliane Locicero, Anne Piant, Odile Adam, Isabelle Olzenski, Delphine Reche, Bahram Sarbandi, Nicolas Cordero, Clémence Devilliers, Guillaume Abrivard, Ozgur Aslan, Justin Dirrenberger, Florine Maes, Thibault Herbland, Laurent Maze, Jianqiang Chen, Thomas Villaro, Angélique Consil, Aurélie Jean, Céline Gérard, Esteban Busso, Matthieu Mazière, Siarhey Dubouski, Michael Fischlschweiger, Thomas Dick, Françoise Di Rienzo

"Modern" CdM: Georges Cailletaud, Samuel Forest, Henry Proudhon, Jacques Besson, Jérôme Crépin, Pierre Kerfriden, David Ryckelynck, Vladimir Esin, Stéphanie Basseville, Alain Thionnet, Claudine Devemy, Ziradjoudine Akber, Catherine Rouil, Véronique Matos, David Ryckelynck, Franck N'Guyen, Loïc Nazé, Thilo Morgeneyer, François Willot, Moubine Al Kotob, Laurent Corté, Anna Ask, Farida Azzouz, Vincent Maurel, Lucien Laiarinandrasana, Cristian Ovalle-Rodas, Sabine Cantournet, Sarojinee Bonneville, Alain Koster†, René Cluzet, Anne-Françoise Gourgues, Chantal Cocain, Michel Boussuge, Victor de Rancourt, Julie Heurtel, Jean-François Hochepied, Harris Farouk, Sébastien Joannès, Sandrine Laurent-Fontaine, Yazid Madi, Abdennour Meddour, Aurélien Villani, Francesco Delloro, Jonathan Ricard, Marie-Hélène Berger, Gregory Saint-Luce, Nicolas Gueninchault, Maria Simoes, Basile Marchand, Laurent Lacourt, Sylvain Gailliegue, Fabrice Gaslain, Franck Bluzzat, Cédric Toussaint, and all-all-all

EPFL Family: Guillaume Anciaux, Dave Kammer, Jean-François Molinari, Mathilde Radiguet, Daniel Pino-Munoz, Cyprien Wolff, Philippe Geubelle, Demir & Duygu Onay Coker, Lucas Frerot, Nicolas Richart, Fabien Barras, Alejandro Marcos Aragon, Ramin Aghababaei, S. Mohadeseh Taheri-Mousavi

DDD part of my life: Laurent Dupuy, Marc Bletry, Marc Fivel, Patrick Villechaise

Electricity GeePS & Scheinder: Sophie Noël, Frédéric Houzé, Philippe Testé, Marina Lisnyak, Alexander Bonhomme

External (and very important for me) support: Claude Stolz, Benoît Appolaire, Djimédo Kondo, Lev Truskinovsky, Oliver Allix, Kostas Danas, Mickael Abbas, Laurent Ponson, Michel Raous

Inspiration: James R. Rice, Jim A. Greenwood

Onera team: Johann Rannou, Jean-Didier Garaud, Vincent Chiaruttini, Jean-Louis Chaboche, Noémie Rakotomalala, Sylvia Feld-Payet, Eva Borakiewicz

Deutschland: Peter Wriggers, Alexander Popp, Martin Müser, Valentin Popov, Lars Pastewka, Alexander Konyukhov, Karl Schweizerhof, Anton Tkachuk

JTCAM team: Vincent Acary, Mathias Legrand, Maurine Montagnat, François Gibier

CSMA Juniors team: Régis Cottereau, Ludovic Chamoin, Thomas Heuzé, Valentine Rey, Cédric Giry, Jérémie Girardot, Andrea Barbarulo, Aline Bel-Brunon, Robin Bouclier, Mohamed Jebahi, Azdine Nait-Ali, Etienne Prulière

"Padawans": Fadoua Majid, Amine Saidi, Yirun Zou, Andrei G. Shvarts, Basava Raju Akula, Julian Durand, Dmitry Tkalich, Amandine Sergeant-Boy, Pauline Bonnet, Paul Beguin, Matti Lindroos, Robin Lethiecq, Takahiro Sakimoto, Paolo Cinat, Aurélien Fouque, Vikram Phalke, Ming Liu, Ayaovi Dzifa Kudawoo, Frederick S. Mballa Mballa, Guillaume Burgaud

Lorentz centre team: Lucia Nicola, Antonis Vakis, Julien Scheibert, Michele Ciavarella + Daniele Dini

Safran tech: Julien Vignollet, Arjen Roos, Augustin Parret-Fréaud

Happy to meet you (for some, only virtually): Aydar Akchurin, Karin Saavedra, Laura de Lorenzis, Mathias Wallin, Alexandre Dufour, Alex Thevenot, Matt Wilkin, Ivan Argatov, Kunnath Ranjith, Loic Serra, Stanisław Stupkiewicz, Jakub Lengiewicz, Margarita Akterskaya, Mark Robbins†, Robert Jackson, Serguei Potapov, Stefan Jacobsen, Guzel Shamsutdinova, Antoine Chateauminois, Anton Manoylov, Yang Xu, Manuel Petersmann, Thomas Antretter, Sinisa Mesarovic, Marc G.D. Geers, Ajay B. Harish

Glacial earthquakes team: Anne Mangeney, Olivier Castelnau, Jean-Paul Montagner, Eléonore Stutzmann, Alban Leroyer, Patrick Queutey

Luleå: Andreas Almqvist, Francesc Perez-Rafols

CEMEF team: Charbel Moussa, Pierre-Olivier Bouchard, Eli Hachem, Elisabeth Massoni, Karim Inal, Yannic Tillier, Florence Morcamp, Jean-Luc Bouvard

NEXT Drill team: Alexander Kane, Marion Fourmeau, Charlie Ch. Li, Afaf Saai, Mikko Hokka

Italy & Bari: Marco Paggi, Mauro Corrado, Giorgio Zavarise, Giuseppe Carbone, Michele Ciavarella, Nicola Menga, Carmine Putignano, Antonio Papangelo, Luciano Afferrante, Michele Scaraggi

MSME team: Nicolas Auffray, Guiseppe Rosi, Julien Yvonnet, Qi-Chang He

From Russia with love: Irina Goryacheva, Olga Antonova, Fedor Stepanov, Alexander Freidin, Ivan Ryndin, Sergey Semenov, Andrey & Anya Levandovsky, Misha Chevilikhin, Sergey Lobanov†, Kolya Panin, Lesha & Manya & Valya Shalygin, Andrey & Natacha Tolmachev, Leha Malyugin, Julia Zastavnaya, Jenya & Gleb Grigoriev

France: Siegfried Fouvry, Didier Lasseux, Benoit Roman, Basile Audoly, Florent Ledrappier, Marie-Christine Baietto, Yves Berthier, Melaine Guillou, Arina Marchenko, Brice Arrazat, Vincent Mandrillon, Emile Renner, Jean-François Rit, Quentin Pujol d'Andrebo, Cyril Touzé

CNRS: Pierre-Yves Bouf, Yves Remond, Section 9

Ma petite famille: Alexandra, Andrey, Daniel & Nicole

My bigger family: Mom, Dad, Iga, Nanay†, Babakay† and vse-vse-vse!

To all people who supported me and trusted in me, un grand merci!